UC Berkeley
UC Berkeley Electronic Theses and Dissertations

Title
Robustness of Biological and Bio-inspired Exoskeletons

Permalink
https://escholarship.org/uc/item/5g91f94t

Author
Jayaram, Kaushik

Publication Date
2015

Peer reviewed|Thesis/dissertation

Robustness of Biological and Bio-inspired Exoskeletons

by

Kaushik Jayaram

A dissertation submitted in partial satisfaction of the
requirements for the degree of
Doctor of Philosophy

in

Integrative Biology

in the

Graduate Division

of the

University of California, Berkeley

Committee in charge:

Professor Robert J Full, Chair
Professor Robert Dudley
Professor Ronald Fearing

Summer 2015

Robustness of Biological and Bio-inspired Exoskeletons

Abstract

Robustness of Biological and Bio-inspired Exoskeletons

by

Kaushik Jayaram

Doctor of Philosophy in Integrative Biology

University of California, Berkeley

Professor Robert J Full, Chair

The single greatest difference between biological organisms and human technologies today is perhaps robustness. Robustness is broadly defined as a system's ability to maintain performance despite disturbances. Qualitatively, a complex system may be called robust if it exhibits some or all of the following properties - multi-functionality, fault tolerance, damage resistance, modularity and redundancy. However, even the best engineering approaches that have attempted to consider some of these aspects find themselves 'fragile', slow and computationally intensive. On the other hand, I contend that biological systems are truly robust and capable of a plethora of complex activities such as locomotion, reproduction, respiration etc. In addition, animals constantly overcome challenges of growth and perform self-repair and learning, still a challenge for even the best engineered systems today. Using the cockroach as my model organism, I have investigated the role of exoskeletons in enabling robust high-speed locomotor behavior in cockroaches. Specifically, I have discovered that the cockroach exoskeleton (1) is effective at dealing with external loads/impulses through body reconfiguration, (2) facilitates (or enhances) rapid horizontal to vertical transitions during high-speed running, and (3) compensates for damage (loss of appendages (or its parts)) undergoing a limited decrement in high-speed running performance. Based on the impressive locomotion performance by cockroaches despite perturbations, internal and external to the animals, we propose that robustness is a crucial measure of the effectiveness of a system's performance.

To my family

Contents

List of Figures

List of Tables

Acknowledgments

I am truly indebted to everyone who have contributed to my journey towards a doctorate degree. This dissertation would not be possible without the countless individuals who have directly or indirectly contributed to this work and to those, I am sincerely and heartily grateful.

I am extremely grateful to my dad, Jayaram Channaiah, my mom, Vijayalakshmi Ramu and my brother, Bharath Jayaram for always being there for me and acting as a constant source of encouragement through out my program. It has been incredibly hard staying away from all of you, particularly you Bharath, and your compassion and understanding has made me strong to undertake and succeed at this challenge.

I want to thank my advisor, Robert Full for providing me this opportunity to pursue research at Berkeley and get closer towards achieving my dreams. I am very grateful to Bob for inspiring me constantly and mentoring me to always think about the bigger picture without compromising on any of the small details. I am very thankful for the world-class resources in the lab including access to the Center for Interdisciplinary Bio-inspiration in Education and Research (CiBER). It has been an incredible experience being your student for the last six years and there was never a time that I did not feel cared for. Thank you Bob, for your constant support and guidance.

I have had the wonderful opportunity of collaborating with a number of people and each one of those collaborations have added a new piece to my research and scientific thinking. In particular, I want to thank Dan Goldman who has been helpful in adding a physics based modeling approach to my work. Dan has been extremely approachable and is always willing to make time for reviewing a manuscript, talk about interesting experiments or advice about career options. I want to thank Ron Fearing for exposing me to the world of novel manufacturing techniques and letting me use his lab facilities. I want to thank Noah Cowan for advising with antenna research. I have benefitted tremendously from discussions with a number of researchers outside Berkeley including Dan Koditschek, Mark Cutkowsky, Tom Daniel and Simon Sponberg during scientific meetings and I am grateful to all of them.

I want to thank all my lab mates - Jean-Michel Mongeau, Chen Li, Pauline Jennings, Tom Libby, Dwight Springthorpe, Nate Hunt, Sam Burden, and Ardian Jusufi for showing their unwavering support though out my time. In particular, I owe a great deal to Jean for mentoring me during my early days in the lab. He not only made my transition to new field of research and new country very easy, but also a lot of fun. Chen has been very helpful in navigating the final stages of my PhD and preparing for the next phase of my research career. Even without her physical presence, Pauline has made my life in the lab simpler in innumerable ways, from assisting with administrative chores to helping me make pretty scientific illustrations. Tom has been an irreplaceable source of knowledge of everything related to the lab and great person to brainstorm my ideas with.

I thank all my undergraduate students, in particular, Andy Mahopatra, Brian McRae, Cody Merritt, Debbie Li, Yung-En Perng and Andy Li for their laboratory assistance and enthusiasm for doing research.

Chapter 1

Crawling into Crevices and in Confined Spaces

1.1 Summary

Cockroaches do not compromise speed and agility for the capability of conforming to environments, as do many soft-bodied animals. Exoskeletal compliance enabled cockroaches to rapidly traverse crevices that were smaller than a quarter of their standing height in 300-800 ms by compressing body segments 40-60%. High-speed video revealed that crevice negotiation was a complex, discontinuous maneuver whose probability of failure and duration increased with decreasing crevice height. After traversing crevices to enter vertically confined spaces, cockroaches crawled at velocities approaching 60 cm s^{-1}, despite body compression and postural changes. Running velocity, stride length and stride period only decreased at the smallest crevice height (4 mm), while slipping and the probability of zigzag paths increased. By altering kinetic friction, we describe an unexplored mode of locomotion - *frictional legged crawling* with body drag and friction dominated leg thrust, but no media flow as in air, water or sand. Increased ceiling friction decreased velocity by decreasing stride length and increasing slipping. Increased ground friction resulted in velocity and stride length attaining a maximum at intermediate friction levels supporting a model confirming a trade-off between increasing leg thrust and reducing body drag. Dynamic compressive cycle tests on living animals demonstrated non-linear, viscoelastic behavior. Exoskeletal toughness allowed cockroaches to withstand body compressive forces three hundred times body weight when traversing the smallest crevices and up to nearly nine hundred times body weight without injury. Cockroach exoskeletons provided biological inspiration for the manufacturing of an origami-style, soft legged robot that can locomote rapdily in confined spaces.

1.2 Challenges of confined locomotion

The emergence of terradynamics [1] has advanced the study of terrestrial locomotion by further focusing attention on the quantification of complex and diverse animal-environment interactions as has been the approach for over a century in hydro- and aero-dynamics research [2]. Studies of locomotion over rough terrain [3], compliant surfaces [4], mesh-like networks [5], sand [6][7][8][9] and through cluttered, three-dimensional terrain [10] have resulted in the discovery of new behaviors and novel theory characterizing environments [11]. The study of climbing has led to undiscovered templates [12] that define physical interactions through frictional van der Waals adhesion [13][14] and interlocking with claws [15] and spines [16]. Burrowing [17][18], sand swimming [6], and locomotion in tunnels [19] have yielded new findings determining the interaction of bodies, appendages and the substratum.

In particular, locomotion in confined environments offers considerable challenges for animals [19] that include limitations due to body shape changes [20][21], restricted limb mobility [22], increased body drag, and reduced thrust development [7]. Examining the motion repertoire of soft-bodied animals [23], such as annelids [20], insect larvae [24] and molluscs [25], has offered insight into a range of design strategies used to move in confined spaces. Inspiration from soft-bodies animals has fueled the explosive growth in soft robotics [26][27][28][29][30] which is not only creating new perspectives in robot design and control, but also aids in more sharply defining the advantage and disadvantages of soft systems capable of maneuvering in constrained environments. Certainly, as pointed out by Kim et al., [26] "soft materials also lend themselves to highly flexible and deformable structures, providing additional functional advantages to animals, such as enabling entrance into small apertures for shelter or hunting." However, disadvantages include weight support against gravity, body/appendage control and "high deformability and energy-absorbing properties of soft tissues prevent them from exerting large inertial forces and limit how fast soft animals can move from place to place [26]."

Here, we explore the capability of cockroaches to not only exploit the advantages of appendages with structures that allow effective interaction with diverse terradynamic surfaces, but also permit them to function as exceptional soft-bodied locomotors in confined spaces. Agile and elusive cockroaches use rigid, jointed exoskeletons to run rapidly at speeds approaching 1.5 m s^{-1} [31], climb up walls [32][33], race along ceilings [34], and swing stealthily under ledges out of sight [35]. Yet, materials science has revealed that the stiffness of exoskeletal tissue can differ by eight orders of magnitude [36][37][38][39] permitting the possibility that cockroaches with powerful propulsive appendages might also possess the advantages of soft-bodied animals capable of conforming to their environment [40]. As yet, no study has quantified cockroaches' capacity to traverse crevices and crawl in confined spaces.

We selected the American cockroach, Periplaneta americana, because of its high speed (31), maneuverability (34, 40), robustness (41), and tenacity to ingress and egress spaces. To determine the smallest crevice that a cockroach could traverse, we challenged animals with a series of decreasing crevice heights. Using high-speed video, we measured their traversal success rate and how frequently they turned back or became stuck. We characterized the

stages of their traversal behavior along with the duration of each stage.

Once cockroaches entered the confined space, we used high-speed video to quantify the kinematics of crawling, postural changes of sprawl angle, and foot or tarsal position relative to free running [31][41]. As animals became more sprawled, we hypothesized that running velocity, stride length, and stride period would decrease with crevice height, while slipping and the probability of a zigzag path would increase. Motivated by studies of the role of body friction during undulatory swimming in frictional fluids by sandfish lizards [6][42] and the thrust produced by flipper-driven surface locomotion by sea turtle hatchlings [9], we varied ceiling and ground friction to determine their effect on confined space crawling performance. Given these results, we created the first model of this unexplored mode of locomotion where drag acts on an animal's dorsal and ventral surface, but the media does not flow around the animal. As a first step towards quantifying the exoskeletal material properties [43] and shape changes that enable cockroaches to traverse crevices and crawl in confined spaces, we measured the compression of selected head and body segments by adding loads to anesthetized animals. In addition, we performed a series of dynamic compressive cycle tests on living animals. We hypothesized that compression of the body and legs would demonstrate non-linear, viscoelastic behavior suggesting crevice crossing might be affected by rate and that the magnitude of peak compression forces would reveal the extent of exoskeletal robustness.

Inspired by the data on cockroach segment and body compression, postural change, and kinematics, we designed a legged robot using the Smart Composite Microstructure manufacturing [44][45][46] approach involving laser-cutting, laminating and the folding of exoskeletal-like plates. We see this robot useful both as a physical model to test future hypotheses of the mechanisms permitting confined space locomotion, as well as a first step toward the development of a soft search-and-rescue robot that can penetrate the rubble left by tornados, earthquakes or terrorist bombings.

1.3   Methods and Materials

Animals

We used a total of twenty one male cockroaches (*Periplaneta americana*; Carolina Biological Supply, Burlington, NC, USA) distributed among our six experiments with an average mass of 0.76±0.16 g (mean ± s.d.) and body length of 31.10±2.16 mm. Prior to experimentation, cockroaches were kept in communal plastic containers at room temperature (22^0C) on a 12h:12h light dark cycle and provided water and food (fruit and dog chow) ad libitum.

Animal Experimental Design and Protocol

All experiments were performed at 28 ± 2^0C (mean ± s.d.). Before starting any experiment, each cockroach was marked with retro-reflective paint on the dorsal surface - two on the pronotum, one at the base of the abdomen, one at the tip of tibia-tarsus joint of each

hind leg to aid tracking. The dorsal body markers were used to calculate crawling velocity and tortuosity, whereas the leg markers were used to estimate gait, tarsus midline distance, stride success ratio, stride length and period. We attained a balanced experimental design by running the same animal across each of the different conditions for a minimum of five (and a maximum of eight) trials. Thus, each individual served as its own control allowing us to use paired statistics.

Kinematics

We recorded videos of cockroaches at 500 frames s^{-1} with a resolution of 1280 by 1024 pixels using synchronized high-speed video cameras. One camera was positioned directly above the track, capturing the top view, and the other recorded the side view. Images were buffered through the camera memory until post-triggering, after which a video clip (4 s) from each camera was reviewed and cropped to the relevant time segment. All video capture, downloading, and conversion were done with a proprietary software program. We determined the kinematics of the behavior from the videos using custom motion tracking software.

Statistics

We used repeated measures analysis of variance (ANOVA) and Cochran-Mantel-Haenszel tests for continuous and nominal variables respectively with Tukey HSD for post-hoc contrast analyses in JMP software (*SAS Inc.*). A repeated measures design with a mixed model was used to determine the effect of condition. In our model, the condition (crevice size/ceiling height as the case may be) was included as a fixed effect while the animal was included as random effect. The response was our performance metric (running velocity, stride period, stride length etc.). We used a standard least squares personality with reduced maximum likelihood (REML) as our method to fit our data. We report the P-value, F-ratio in American Psychological Association (APA) format to support/reject our hypothesis as appropriate. For categorical responses (success), we report the chi2 value.

Exoskeletal Compression

We directly measured the sagittal plane deformation of the cockroach exoskeleton for freshly anesthetized animals at 10, 25, 37, 50 and 75 % along the body from head to cerci upon a flat ground surface (Fig. 1.5; Table 1.1; Fig. 1.3). The lengths along the body correspond to the head-pronotum junction, front leg, middle leg, and hind leg coxa sections, and middle of the abdomen, respectively. To determine body compressibility, we obtained sagittal view measurements under two conditions - unloaded with an intact, undisturbed animal and loaded by suspending a 100 g load with a light string across the body segment at the given length. Five sets of loading and unloading cycles were performed at each of the five cross-sections.

Crevice Traversal

To measure crevice traversal performance, we constructed a chamber consisting of clear acrylic tube (square cross-section, 2.54 cm x 2.54 cm) with an opening at one end and a vertically adjustable gate also made of clear acrylic at the other (Fig. 1.1). The gate was mounted on a precision miniature linear stage (Model 422-1s, Newport Corporation) that allowed fine control (± 0.05 mm) in the range of 2-10 mm. The insides of the acrylic chamber, with the exception of video recording ports on the front and top, were lined with 40-grit sandpaper to ensure effective footholds. Our exoskeletal compression measurements led us to test performance at three different crevice heights - 3.2, 4.4 and 6.1 mm.

To encourage the animals to traverse the crevice, we evoked an escape response by light stimulation of their cerci or by gently blowing until they entered the apparatus. The open end was then sealed off leaving the crevice under the gate as the only escape outlet. In addition, we shined bright light from the sealed direction dissuading the animals from turning around. Animals typically searched and explored the opening using their antenna [47] and then rushed through. Successful trials were operationally defined as those where the animals were able to pass through the gate completely without stopping as determined by their cycling of the legs. Failures included both turning back away from the crevice as well as getting their body stuck or wedged within the crevice (Fig. 1.5).

Confined Space Crawling

To quantify confined space crawling, we constructed a closed horizontal clear acrylic chamber - 25 cm long and 10 cm wide with a vertically adjustable ceiling (Fig. 1.2). The ceiling was mounted on precision miniature linear stages (Model 422-1s, Newport Corporation) that allowed fine control (± 0.05 mm) in the range of 4-12 mm.

To encourage the animals to crawl rapidly through the confined space, we evoked an escape response by light stimulation of their cerci or by gently blowing. We accepted trials when the animal crawled within the confined space for a minimum of 15 cm. We rejected trials where: 1) the cockroaches stopped or tried to climb the side-wall, 2) their body (excluding their legs) collided with the side-wall, or 3) they exhibited turns of more than 150^0.

Ceiling Height Variation

We tested animals under four different ceiling heights - 4, 6, 9 and 12 mm, respectively (Fig. 1.2) and used 40-grit sandpaper for the track bottom surface and acrylic for the inside top surface (Fig. 1.8). We selected these particular sizes for the following reasons.

12 mm (Free Running Height) - the typical height of the dorsal surface of the cockroaches during unconstrained running. We used this as the control condition.

9 mm (Crouched Height) - the maximum height that the animals could locomote without making continuous contact with the ceiling. They adopted a suitable crouched posture by adjusting their leg joint angles and lowered their center of mass.

6 mm (Body Compression Height) - the mean height of the thickest abdominal section measured without compression. The height represented the smallest size before which the animal was forced to necessarily deform its body in compression to successfully negotiate the confined space.

4 mm (Minimum Ceiling Height) - the smallest ceiling height that cockroaches could successfully complete at least five trials based on our operational definition.

To evaluate confined space crawling performance, we calculated velocity, stride length, period, sprawl angle, tarsus centerline distance, stride success ratio and tortuosity (Fig. 1.10). We defined sprawl angle as the average angle of the vector from the tip of the tarsus when in contact with the ground to the cockroach's center of mass relative to the sagittal plane. We calculated the tarsus midline distance as the perpendicular distance of the meta-thoracic leg tarsus-ground contact point to the midline of the cockroach body approximated as the line joining the mid-point of the two pronotum markers with the one at the base of the abdomen. We defined stride success ratio as the ratio of successful strides (with no foot slipping) to the total number of strides. We determined tortuosity index to be the ratio of the forward displacement of the cockroach in the chamber relative to the length of the actual path taken.

Surface Friction Variation

We tested the effect of varying contact surface friction on cockroach performance across the four ceiling heights. We varied ceiling and ground kinetic friction with respect to the animal independently across three kinetic friction levels in two separate sets of experiments. For variation in ceiling kinetic friction, we used graphite powder over acrylic, uncoated acrylic and 40-grit sandpaper as dorsal contact surface for a low, medium and high condition, respectively, while 40-grit sandpaper served as the ground contact surface. For variation in ground kinetic friction, we used 100-grit, 40-grit and 20-grit sandpaper as ground contact surface for a low, intermediate and high condition, respectively, while uncoated acrylic served as the ceiling contact surface.

To quantify friction on body (drag), freshly anesthetized animals were mounted onto a six-axis force-torque sensor (Nano17, ATI Inc.). A flat plate mounted on a linear stage (Model 422-1s, Newport Corporation) at 4mm vertical offset to the sensor top was coated with the test material and dragged along horizontally at a constant speed that matched the animal's mean running speed. Data were recorded at 1000 Hz. We noted the mean normal force, maximum (peak drag) and settling value (sliding drag) of the horizontal force for each trial. The ratios of the peak drag and sliding drag to the mean normal force were defined as the coefficients of static and kinetic friction, respectively. Compressed animals appeared to be using their tibia spines for thrust, so to determine the friction coefficient with feet (lower bound) on the ground surface, we ablated the animal's tarsus, ran the animals on a semi-circular track of radius 60 cm and measured the critical angle of failure (falling off or sliding down the track) and quantified the tangent of failure angle as leg friction coefficient (Table 1.2).

We used the aforementioned friction measurements to set a range for kinetic friction. Assuming that our cockroaches have force production capabilities similar to that measured in a related species [48], we estimate the maximum force produced by each leg to be approximately 38.0 mN (5.1 times mean body weight of 0.76 g). This suggests that maximum forward thrust estimate (227.9 mN) can overcome the estimated body drag (24.71 - 224.80 mN) and likely pushes the animal to near maximal performance (comparable to burrowing performance in razor clams [25], earthworms [49] and ocellated skinks [50].

Dynamic Compressive Forces

To measure the material properties using a universal testing machine (Instron Industrial Products, 5900 series), we constructed a clear acrylic cylindrical chamber of diameter 5.08 cm with a freely sliding ceiling (Fig. 1.17). The chamber was mounted directly onto the lower fixture of the machine, while the ceiling was mounted onto the movable fixture comprising the load cell. A mechanical stop was added at 2 mm chamber height to prevent fatal damage to the animal.

We placed a live animal in the custom chamber with the initial ceiling height set to 15 mm. Using a triangular wave profile set, we performed cyclic compression tests on the animal by moving the ceiling between 15 mm and 3 mm at two speeds, 0.5 and 4 mm s^{-1}, over a range of compression values matching what animals experienced in crevice traversal and confined space crawling. We measured force - compression curves, recorded maximum net force, estimated stiffness as a function of compression distance and calculated resilience as the percentage of energy returned during relaxation to the energy input during compression. Before and after performing the test, we measured each animal's average straight-line speed over 25 cm and their ability to fly.

Robot Design - CRAM (Compressible Robot with Articulated Mechanisms)

Using a combination of postural adjustment from leg reorientation and body compression, cockroaches traversed and locomoted in vertically confined spaces. With this inspiration, we designed a robot that uses the above two principles to passively adjust its sprawl angle by reducing its vertical height and thus conforms to the confined space. The key to robot performance is a flexible back spine (along the longitudinal axis) and a deformable shell made of overlapping plates similar to the exoskeletal plates of a cockroach abdomen (Fig. 1.19; Movie S4; Fig. 1.4). The design of the robot is realized using the Smart Composite Microstructures (SCM) manufacturing technique. The rigid elements of the robot are made of a posterboard (*4-ply Railroad board, Peacock Inc.*) composite laminate with 125 μm polyester sheet (*Dura-lar, Grafix Inc.*) serving as the flexure layer. To construct the low friction, deformable shell, we used 0.005 inch polyester sheet (*Dura-lar, Grafix*) as the stiffer material. The legs of the robot are L-shaped to allow good ground contact in the standing and maximally sprawled

configurations and is 3D printed (*ProJet3500, 3DSystems Inc.*). The drive mechanism comprises of two miniature DC motors (*MK-07, Didel Inc.*) with custom 3D printed gearing operating independently to control the left and right side of the robot. We used commercially available electronics (*Dashboard, Dash Robotics Inc.*) to control the robot dynamics in open loop over Bluetooth 4.0. The resulting robot prototype is small (18 cm long, 75 mm high (unrestricted)), lightweight (46 g, with on-board control electronics and battery) and capable of crawling in vertical confinements as small as 35 mm in height.

The robot's maximum percentage vertical compression was $\approx 54\%$ (75 to 35 mm). Maximum load bearing capacity of exoskeleton was approximately 1000 g, greater than twenty times body mass. The robot's sprawl angle when unconfined was $\approx 50^0$ whereas in the unconfined at 35 mm it was as great as 81^0. The robot's unconfined speed at 75 mm ceiling height was approximately 27 cm s^{-1} (≈ 1.5 bl s^{-1}), whereas its confined speed compressed at 35 mm was ≈ 14 cm s^{-1} (≈ 0.75 bl s^{-1}) (Fig 1.20). The robot's maximum stride frequency was ≈ 25 Hz with a mean stride length unconfined at 75 mm of ≈ 1.1 cm and confined at 35 mm of approximately 0.6 cm.

1.4 Crevice Traversal

The American cockroach (0.76 ± 0.16 g; 31.10 ± 2.16 mm), *Periplaneta americana*, traversed crevices as small as 3 mm, the height of two stacked pennies (Fig. 1.5). A vertically adjustable acrylic gate mounted on a precision linear stage permitted control of crevice height (± 0.05 mm; Fig. 1.5; SI Methods and Fig. 1.1). To set experimental crevice height, we directly measured body compression of freshly anesthetized animals from their abdomen to head while positioned on a flat surface by suspending a load greater than one hundred times body weight across each section (Fig. 1.5; Fig. 1.3; Table 1.1). Exoskeletal sections were all highly compressible, ranging from 41 - 57% of normal with the load resulting in no injury.

Crevice traversal was rapid (288-821 ms interquartile range) and, to the naked eye, appeared continuous. High-speed videography revealed crevice traversal to be a complex behavior involving several stages (Fig. 1.5; Movie S1). We defined these stages to enable measurement of the time taken to progress through each stage at the three crevice heights. 1) Exploration and crevice detection. Once placed within the apparatus (Fig. 1.5), the animals used their antennae to explore their surroundings and searched for escape openings. If one or both antennae passed through the crevice, the animal reoriented itself to ensure both antennae were extending out of the crevice and continued tactile exploration. We suspect this searching behavior enabled the cockroaches to estimate the size of the crevice and to determine if the other side was safe for escape. 2) Head traversal with entry and body orientation. On completion of crevice detection, the cockroach typically paused briefly and rammed into the crevice head-first multiple times, often hitting the gate, before pitching downward to the enter the crevice. For larger crevice sizes (6 mm and above), this would be immediately be followed by abdominal traversal with little body compression. During this phase, the legs rapidly cycled attempting to grip surfaces and generate sufficient friction. In

concert with head entry, the front legs stretched outside the crevice attempting to pull the body through. At the same time, the remainder of body pitched upwards allowing the middle and hind legs to push off the side/ top walls of the chamber. 3) Pronotum traversal. As the leg movements began getting restricted (especially the front legs), the body rapidly rolled from side to side accompanied by leg pushing. The rapid body rotations possibly helped to increase the moment arms for the thrust generation [51] from the middle and hind legs and to potentially passively align the body with respect to the crevice opening. 4) Thorax traversal. We hypothesized this to be one of most challenging stages with the highest chance of failure by getting stuck due to the body morphology (Table 1.1). The movement of the legs was severely restricted and the animal was likely experiencing large normal forces. Animals made forward progress primarily by thrusting their hind legs. 5) Abdomen traversal. After thorax traversal, the body was again reoriented into a 'flat' position (body pitch of 0^0). The front legs and middle legs were free to operate, while hind leg movement was restricted making progression difficult. The compressibility of the abdomen appeared to reduce the normal load on the body enabling the animal to generate thrust sufficient to successfully negotiate the crevice. The time taken from head entry until abdomen tip exit increased with a decrease in crevice height from 6.1 to 3.2 mm (ANOVA, P< 0.001, F2,94 = 88.9; Fig. 1.6). Traversal time was similar for 6.1 and 4.4 mm crevices (0% and 27% abdomen compression, respectively; post-hoc analysis, Tukey HSD), but significantly longer at 3.2 mm (47% abdomen compression), approaching the limit of performance. Consistent with this conclusion, the probability of successful crevice traversal decreased significantly with a decrease in crevice height from 72% at 6.1 mm to just 17% at 3.2 mm (Cochran-Mantel-Haenszel, P< 0.001, $\chi^2(2)$= 44.8; Fig. 1.7). Turning back during a trial was the dominant failure mode suggesting that animals seek alternate routes if crevices are too small using sensory feedback [47]. Animals were never trapped in the largest crevices, but occasionally became stuck at the smallest crevice heights (9%) during thorax traversal, a potentially fatal event in nature if exposed to predators.

1.5   Confined Space Crawling

After traversing narrow crevices, cockroaches crawled rapidly in spaces confined vertically by two stacked horizontal plates (SI Methods and Fig. 1.2) at velocities approaching 60 cm s^{-1}, despite body compression and large postural changes such as sprawl angle (Movie S2). High-speed kinematic analysis of marked animals at four ceiling heights (Fig. 1.8 and 1.9) revealed that velocity (58.05±2.33 cm s^{-1}) remained statistically similar for the three greatest ceiling heights, and only decreased at the smallest height where animals experienced the greatest body compression and friction (4mm; 14.52±0.98 cm s^{-1}; ANOVA, P< 0.001, F3,96=14.72; Fig. 1.10). Effective stride length explained the changes in velocity, whereas stride period remained constant across all crevice sizes (61.05±6.06 ms, P=0.34, F3,96=1.28). Ceiling height constrained posture by increasing sprawl angle proportionally (P< 0.001, F3,96=24.12; Fig. 1.9). Surprisingly, the distance from the foot to the body midline, as

viewed from the top (Tarsus Midline Distance), did not change significantly across ceiling heights (11.89±0.96 mm; P=0.64, F3,96=3.61; Fig. 1.10). This foot placement is similar to that most effective for maximizing ground thrust as predicted from cockroach musculo-skeletal models [51]. Cockroaches used an alternating tripod gait at all ceiling heights except the smallest where the gait became irregular with the middle legs often applying force in synchrony to thrust the body forward. Consequently, at the smallest ceiling height, animals were unable to follow straight-lined paths (decreased Tortuosity Index; P=0.002, F3,96=5.49; Fig. 1.10). Foot slippage also increased at the smallest ceiling height (decreased Stride Success Ratio; P=0.005, F3,96=3.31; Fig. 1.10). The ability of cockroaches to maintain performance with minimal changes in kinematic parameters at the three greatest ceiling heights is similar to outcomes in experiments with ferrets running in tunnels with back height reduced by 40% and hip height by 25% [52]. However, at the smallest ceiling heights, results for confined space crawling suggest that cockroaches were attempting to generate sufficient thrust through ground engagement, but because of body contact with the ground and ceiling were operating in a 'friction limited' regime.

To determine if cockroaches undergo confined space, frictional legged crawling in a unique regime where drag is exerted on the body, friction dominates thrust, but the media does not flow, we varied the ground and ceiling friction of the apparatus (Fig. 1.11). We directly measured the coefficients of friction using anesthetized animals interacting with different surfaces to produce three levels of friction for both the ceiling (5-fold change) and ground (2-fold change; Methods and Table S2). We hypothesized that increased ceiling friction and dorsal drag would decrease velocity by decreasing stride length and increasing slipping (reduce stride success ratio). At the smallest crevice height (4 mm), an increase in ceiling friction significantly decreased mean velocity (P< 0.001, F2,72=37.87; Fig. 1.12). The decrease in velocity can be explained by a decrease in stride length (P<0.001, F2,72=122.58) and an increase in foot slippage (decrease in Stride Success Ratio; P<0.001, F2,72=48.16). Stride period remained unaffected by ceiling friction (P=0.1, F2,72=7.27). For an increase in ground friction, we hypothesized that the trend in these locomotor variables would depend on the differential effect of ventral body drag versus an increased thrust from greater leg purchase. At the smallest crevice height (4 mm), an increase in ground friction significantly increased mean velocity at medium friction levels (P<0.001, F2,69 =73.4) compared to both the low and high conditions (Fig. 1.13). Stride length (P<0.001, F2,69 =246.7) and Stride Success Ratio (foot slippage; P<0.001, F2,69=89.10) showed a similarly significant trend with a performance peak at the medium friction condition. Stride period remained unaffected by changes in ground friction (P=0.07, F2,69=12.36). Results from an increase in ground friction imply a trade-off between increasing leg thrust and increasing body drag.

Confined space crawling in cockroaches appears to have features of both the body friction of undulatory swimming in frictional fluids by sandfish lizards [6][42] and the thrust produced by flipper-driven surface locomotion by sea turtle hatchlings [9] except here the surrounding media does not flow (Fig. 1.11). Frictional legged crawling deserves further attention.

1.6 Model of Frictional Legged Crawling

To begin to understand the mechanics of cockroaches crawling in confined spaces, let us consider the following simplified model comprising of a compressible body with a single leg (leg length, l) hinged at its center (pin joint) and confined between two flat plates a distance $2h$ apart (Fig. 1.14). The body is assumed to make contact with both the top and bottom confine surfaces at all times and this interaction is considered frictional. A foot is located at the end of the leg and makes contact only with the ground surface. We simplify the complex interaction (adhesion, interlocking, friction) of the foot structures with the ground surface and assume that friction is the primary mode of interaction. Further, all surface interactions (including foot-ground) are assumed to be Coulomb friction based i.e. tangential forces are uniformly proportional to normal forces (proportionality constant is coefficient of friction), and independent of speed. Let us further consider that coefficients of static and kinetic friction are identical.

Force balance at the foot

$$N_f = F_L sin(\theta) \tag{1.1}$$
$$f_f = F_L cos(\theta) \tag{1.2}$$
$$f_{fmax} = \mu_f F_L sin(\theta) \tag{1.3}$$

The friction force at the foot (f_f) balances the horizontal component of the leg force (F_L) to prevent the foot from slipping. We refer to this condition as the stick regime because the foot sticks to the ground surface (no relative movement). Here, the leg extension is equal to the body displacement and determined using kinematics. As the leg angle (θ) decreases, the horizontal (or forward) component increases until it reaches max friction from the surface (f_{fmax}). We refer to this critical angle as the slip angle (θ_{slip}) and for all leg angles smaller than slip angle, the foot slips (and hence referred to as the slip regime) and hence the body displacement is lesser than the leg displacement and needs to be computed using kinetics (or inertial methods using force balance).

$$\theta_{slip} = cot^{-1}(\mu_f) \tag{1.4}$$

At the end of slip phase, we assume that the leg is instantaneously returned to touchdown position (perpendicular to the surface). To compute body displacements, we need to first determine the limits of leg extension Đ where the thrust (T) from the legs overcomes the frictional drag (D) on the body. The same can be obtained via force balance on the body.

$$T = min\{F_L cos(\theta), \mu_f F_L sin(\theta)\} \tag{1.5}$$
$$T \geq D = f_c + f_g = \mu_c N_c + \mu_g N_g \tag{1.6}$$
$$N_c + mg = N_g + F_L sin(\theta) \tag{1.7}$$

From our experimental measurements (Table 1.2) and previous literature [2], we find that the animal body weight is at least an order of magnitude smaller than the other forces

involved and hence is assumed to be insignificant. To determine the leg excursion when stick mode is possible, we estimate the maximum leg angle (θ_{max}) until which thrust overcomes drag.

$$T = F_{max}cos(\theta_{max})$$
$$D = (\mu_c + \mu_g)N_g + \mu_c F_{max}sin(\theta_{max}) \tag{1.8}$$
$$C_h = \frac{N_g}{F_{max}}$$

$$\theta_{max} = cot^{-1}(\mu_c) - sin^{-1}\frac{((C_h(\mu_c + \mu_g))}{(\sqrt{(1 + \mu_c^2)})} \tag{1.9}$$

Therefore, the body displacement under stick mode per leg cycle (x_{stick}) is determined as

$$x_{stick} = \frac{(h(cot(\theta_{slip}) - cot(\theta_{max})))}{2} \tag{1.10}$$

Using a similar approach, we can calculate the extent of slip mode by estimating the minimum leg angle (θ_{min}) when thrust overcomes drag, provided it is greater than the kinematic limit ($cot^{-1}(h/2L)$).

$$T = \mu_f F_{max}sin(\theta_{min})$$
$$D = (\mu_c + \mu_g)N_g + \mu_c F_{max}sin(\theta_{min}) \tag{1.11}$$

$$\theta_{min} = sin^{-1}(\frac{C_h(\mu_c + \mu_g)}{\mu_f - \mu_c}) \geq cot^{-1}(\frac{h}{2L}) \tag{1.12}$$

To determine body displacement under slip mode, we need to know the velocity at the end of stick mode and use Newton's second law thereafter. Therefore we need an actuator model for the leg. Let us consider a simple, reciprocating leg actuator with a linearly decreasing force-velocity relationship [53] limited in both force (F_{max}) and velocity (v_{max}) (Eqn. 1.13) driven by a controller that attempts to output maximum propulsive force as possible during slip phase. Further, we assume that the leg forces are sufficient to overcome drag (at least at some leg orientation) but insufficient to compress the body (thus unable to reduce normal forces due to confinement).

$$\frac{F_L}{F_{max}} + \frac{v_L}{v_{max}} = 1 \tag{1.13}$$

Balancing forces on the body in the horizontal direction during stick mode,

$$F_L cos(\theta) = (\mu_c + \mu_g)N_g + \mu_c F_L sin(\theta)$$
$$\frac{F_L}{F_{max}} = \frac{C_h(\mu_c + \mu_g)}{cos(\theta) - \mu_c sin(\theta)}$$
$$\frac{v_L}{v_{max}} = 1 - \frac{C_h(\mu_c + \mu_g)}{cos(\theta) - \mu_c sin(\theta)} \tag{1.14}$$

Further, the body velocity (v_b) and leg velocity (v_L) can be related using the geometric constraint below.

$$x^2 + h^2 = l^2$$

Differentiating,

$$x\dot{x} = l\dot{l} \implies \dot{x} = \frac{l}{x}\dot{l}$$

$$v_b = v_L sec(\theta) \tag{1.15}$$

Combining Eqn. 1.14 and Eqn. 1.15, we obtain the velocity of the body under stick (v_{stick}) as

$$\frac{v_{stick}}{v_{max}} = (1 - \frac{C_h(\mu_c + \mu_g)}{cos(\theta) - \mu_c sin(\theta)})sec(\theta) \tag{1.16}$$

The mean velocity ($\widetilde{v}_{stick}$) during stick mode is obtained by the following equation and is computed numerically.

$$\widetilde{v}_{stick} = v_{max} \frac{\int_{\theta_{slip}}^{\theta_{max}} (1 - \frac{C_h(\mu_c + \mu_g)}{cos(\theta) - \mu_c sin(\theta)})sec(\theta)d\theta}{\int_{\theta_{slip}}^{\theta_{max}} d\theta} \tag{1.17}$$

Additionally, the stick duration (t_{stick}) is

$$t_{stick} = \frac{x_{stick}}{\widetilde{v}_{stick}} \tag{1.18}$$

The velocity at end of stick mode (or beginning of slip mode, v_0) is obtained as

$$v_0 = v_{max}(1 - \frac{C_h(\mu_c + \mu_g)}{cos(\theta_{slip}) - \mu_c sin(\theta_{slip})})sec(\theta_{slip}) \tag{1.19}$$

Assuming that the leg slides back at the fastest speed it can once the foot starts slipping, we can estimate the net slip duration (τ_{slip}).

$$\tau_{slip} = \frac{h(cot(\theta_{min}) - cot(\theta_{slip}))}{2v_{max} \frac{\int_{\theta_{min}}^{\theta_{slip}} sec(\theta)d\theta}{\int_{\theta_{min}}^{\theta_{slip}} d\theta}} \tag{1.20}$$

We can compute the instantaneous and mean acceleration (a_{slip} and $\widetilde{a}_{slip}$ respectively) on the body during the slip mode as

$$ma_{slip} = (\mu_f - \mu_c)F_L sin(\theta) - (\mu_c + \mu_g)N_g$$

$$\widetilde{a}_slip = \frac{\int_{\theta_{min}}^{\theta_{slip}} ((\mu_f - \mu_c)F_L sin(\theta) - (\mu_c + \mu_g)N_g d\theta)}{\int_{\theta_{min}}^{\theta_{slip}} d\theta} \tag{1.21}$$

Therefore, the instantaneous and mean body velocities (v_{slip} and $\widetilde{v}_{slip}$ respectively) are computed as below.

$$v_{slip} = v_0 - \widetilde{a}_{slip}t, t \leq \tau_{slip}$$
$$t_{slip} = \frac{v_0}{\widetilde{a}_{slip}}, t_{slip} \leq \tau_{slip}$$
$$\widetilde{v}_{slip} = \frac{v_0 - \widetilde{a}_{slip}t_{slip}}{2} \tag{1.22}$$

The step length i.e. body displacement during this period is computed as below.

$$x_{slip} = \widetilde{v}_{slip}t_{slip} \tag{1.23}$$

Therefore, the total step length (x_{step}) is

$$x_{step} = x_{stick} + x_{slip} \tag{1.24}$$

Therefore, the mean step velocity (v_{step}) is

$$\widetilde{v}_{step} = \frac{x_{step}}{t_{stick} + t_{slip}} \tag{1.25}$$

Finally, assuming a stride to be two steps like in a hexapedal gait observed in cockroaches, we estimated the performance metrics, stride length (x_{stride}) and mean forward velocity ($\widetilde{v}_{forward}$), as

$$\widetilde{v}_{forward} = \widetilde{v}_{step} \tag{1.26}$$
$$x_{stride} = 2x_{step} \tag{1.27}$$

The computed body displacement in the slip regime was considerably smaller relative to that in the stick regime and did not affect the overall trends. Using the above formulation, we quantified (Fig. 1.15) the effect of friction (ceiling, ground) and gap size on performance (stride length, forward velocity).

In accordance with our experimental data (Fig. 1.12), the model predicts that increasing ceiling friction monotonically increases the overall resistance due to friction-based drag, and, therefore, reduces forward velocity by decreasing stride length (Fig. 1.15). The model suggests that smaller crevice heights are likely to decrease performance at a given ceiling friction. Further, the model predicts that maximal forward velocity and stride length occurs at intermediate ground friction conditions, since the magnitude of thrust depends on the differential friction between the foot and body (Fig. 1.19). As in ceiling friction predictions, the model suggests that smaller crevice heights are likely to decrease performance at a given value of ground friction.

While predictions of our initial model follow trends observed in experimental measurements, the model reveals at least three areas of future study for frictional legged crawling.

First, an improved understanding of foot contact mechanics is needed to provide insight into the complexities of thrust generation beyond simple coulomb friction type attachments that include interlocking [15][54][55], adhesion [56][57][58] and resistive forces in granular media [1][59]. Secondly, a leg actuation model that more effectively captures dependence of force production on such factors such as leg morphology, lever and transmission systems and muscle mechanics [51][60]. Finally, a more developed quantification of body and leg kinetic friction as they relate to contact geometry and exoskeletal material properties could improve estimates and reveal principles underlying the interesting complexity of the stick-slip interactions as a novel locomotor challenge for both animals (and robots). Incorporating these biologically relevant measurements into our initial model will move us closer to generating predictions concerning the habitats and environments animals might exploit using frictional legged crawling.

1.7   Dynamic Compressive Forces

As a first step towards quantifying the exoskeletal material properties that enable cockroaches to traverse crevices and crawl in confined spaces, we performed a series of dynamic compressive cycle tests on living animals (Fig. 1.17). We hypothesized that compression of the body and legs would demonstrate non-linear, viscoelastic behavior suggesting crevice crossing might be affected by rate and that the magnitude of peak compression forces would reveal the extent of exoskeletal robustness. Compressive force showed a non-linear increase as compression increased (Fig. 1.18; Movie S3). Maximum average stresses ranged from 3.74 ± 0.56 kPa (at 0.5 mm s^{-1}) to 16.21 ± 3.20 kPa (at 4 mm s^{-1}) and were associated with very large strains (up to 0.50). Tangent modulus in the linear strain region (0.475-0.50) ranged from 0.11 ± 0.02 MPa (at 0.5 mm s^{-1}) to 0.50 ± 0.10 MPa (at 4 mm s^{-1}). The cockroach body behaved like a viscoelastic material with a resilience (percentage of energy return) of $60\pm12\%$ (at 0.5 mm s^{-1}) and $44\pm10\%$ (at 4 mm s^{-1}). At the smallest crevice or ceiling height of 3.2 mm, the net normal force (2.25 ± 1.17 N) on cockroaches averaged approximately 300 times body weight (Fig. 1.18). This is significantly higher than forces recorded in soft-bodied annelids that experience about 10 times body weight when compressed to 0.6 body diameter [49]. At the faster rate of compression, net forces (6.08 ± 1.61 N) attained values of 700 times body weight. We observed no damage to any body part. After the tests, cockroaches were able to fly normally and showed no significant changes in unconstrained running velocity (76.67 ± 7.34 cm s^{-1}) compared to controls (P= 0.49, F1,35=6.21). The relatively lower strain and higher buckling stiffness (3.36 GPa) measured in fresh sclerotised locust tibia [61] suggest the cockroach's compressibility derives from their soft arthrodial membranes rather than compression or bending of stiff exoskeletal plates [43] or tubes [40].

1.8   Soft Robot with Legs

Our discoveries from cockroaches inspired the design of a soft, legged hexapod robot named CRAM (Compressible Robot with Articulated Mechanisms) that we built using the Smart Composite Microstructure (SCM) manufacturing [44][45][46] approach involving laser-cutting, laminating and the folding of exoskeletal-like plates (Fig. 1.19; Methods and Fig. 1.4). Like the animal, the robot successfully locomotes in vertically confined spaces by compressing its body in half and benefits from possessing a low friction shell (Movie S4). This prototype can increase sprawl angle by using compliant exoskeletal flexures to conform to the confined environment. Further, it can withstand compressive forces twenty times body mass by benefitting from over-lapping abdominal plates and potentially dissipate impacts and collisions demonstrating capabilities of robots constructed using soft materials [62][63][64]. The advantages of dedicated propulsive appendages in compliant robots are clearly demonstrated by nearly an order of magnitude faster forward sustained speeds (both absolute and relative to body length) compared to current state-of-the-art soft robotic crawlers [63][65][66]. Future directions include addition of feet-like attachment mechanisms onto an upgraded leg design to improve peak forward velocity, control of leg actuation to improve energy efficiency [67] and the demonstration of new capabilities like turning [66], climbing [4], and jumping [64].

As Rus et al. [68] pointed out, "many of the exciting applications for soft robotics (such as search-and-rescue operations or environmental monitoring), require an autonomous, mobile system", a major limitation for current soft robots that rely on power and/or control signals delivered through pneumatic [28] and/or electric tethers [65][66] making them very heavy (for example, 1.2 kg [63]). By relying on SCM manufacturing techniques, that have proved highly successful in the design of a fast running hexapedal family of robots [69][70], we have been able to make our palm-sized, confined space crawling robot completely autonomous in power and control, while weighing just 46 g including onboard electronics and battery. A promising future direction for soft arthropod inspired legged robots is to combine the advantages of soft-bodied robots [26][68] with appendages shown to be effective in tubular environments such as gastrointestinal tracts [4]. Our bio-inspired soft robot prototype presented here is a first step towards the creation of a swarm of search-and-rescue robots that can perform crevice traversal and confined space frictional legged crawling in an effort to rapidly locate survivors trapped in the rubble left by tornados, earthquakes or terrorist bombings.

Table 1.1: Morphometric measurements of individual cockroaches. a1-a4 represents the four animals used in the morphology study.
UL - Unloaded (Intact animal anesthetized); L - Loaded with a 100 g point mass on a string across the cross-section at the given length from the head;
Cross-section heights were measured at 10, 25, 37, 50 and 75 % of the body length in the rostrocaudal direction.

Cockroach	Mass (mg)	Length (mm)	10% (mm)		25% (mm)		37% (mm)		50% (mm)		75% (mm)	
			UL	L	UL	L	UL	L	UL	L	UL	L
a1	0.99	35.0	7.2	2.5	10.7	3.7	10.0	3.9	9.3	3.5	7.9	3.1
			(0.1)	(0.0)	(0.2)	(0.1)	(0.1)	(0.1)	(0.2)	(0.1)	(0.1)	(0.1)
a2	0.87	32.3	6.9	3.4	8.7	4.7	8.7	4.0	8.5	3.3	5.1	2.8
			(0.1)	(0.1)	(0.1)	(0.1)	(0.2)	(0.2)	(0.2)	(0.2)	(0.1)	(0.0)
a3	0.74	28.3	5.7	3.3	7.1	3.3	6.8	3.1	6.7	4.5	4.6	3.2
			(0.1)	(0.0)	(0.2)	(0.1)	(0.1)	(0.1)	(0.2)	(0.1)	(0.1)	(0.1)
a4	0.86	31.8	6.4	3.1	8.5	3.6	7.9	3.4	6.4	2.8	4.2	2.9
			(0.1)	(0.1)	(0.1)	(0.1)	(0.2)	(0.1)	(0.1)	(0.1)	(0.1)	(0.0)
Mean	0.87	31.9	6.6	3.1	8.8	3.8	8.4	3.6	7.7	3.5	5.5	3.0
s.d.	0.10	2.75	0.7	0.4	1.5	0.6	1.3	0.4	1.4	0.7	1.7	0.2

Table 1.2: Friction coefficients for dorsal and ventral surfaces relative to the body and feet.
N = 50 trials, n = 2 animals; no effect of individual.
All values mean ± (1 s.d.).

Surface	Material	Normal Force (N)	Peak Drag (N)	Sliding Drag (N)	Coefficient of Friction Body (Static)	Body (Kinetic)	Leg (Kinetic)
Ceiling							
Low	Acrylic (graphite powder)	0.28 (0.01)	0.03 (0.00)	0.02 (0.00)	0.09 (0.00)	0.09 (0.01)	1.73 (0.08)
Med	Acrylic	0.29 (0.02)	0.06 (0.02)	0.04 (0.00)	0.21 (0.01)	0.14 (0.01)	1.73 (0.05)
High	Sandpaper (40-grit)	0.28 (0.02)	0.19 (0.02)	0.13 (0.01)	0.69 (0.04)	0.46 (0.04)	1.73 (0.09)
Ground							
Low	Sandpaper (100-grit)	0.26 (0.04)	0.12 (0.01)	0.10 (0.00)	0.47 (0.03)	0.37 (0.03)	0.84 (0.04)
Med	Sandpaper (40-grit)	0.28 (0.02)	0.19 (0.01)	0.13 (0.01)	0.69 (0.04)	0.46 (0.02)	1.73 (0.05)
High	Sandpaper (20-grit)	0.27 (0.02)	0.22 (0.01)	0.20 (0.01)	0.83 (0.05)	0.76 (0.06)	2.04 (0.11)
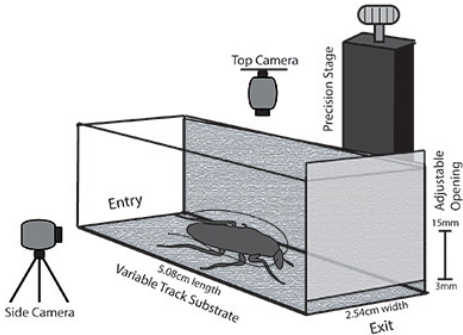
Figure 1.1: Crevice traversal setup featuring a clear acrylic tube with adjustable opening
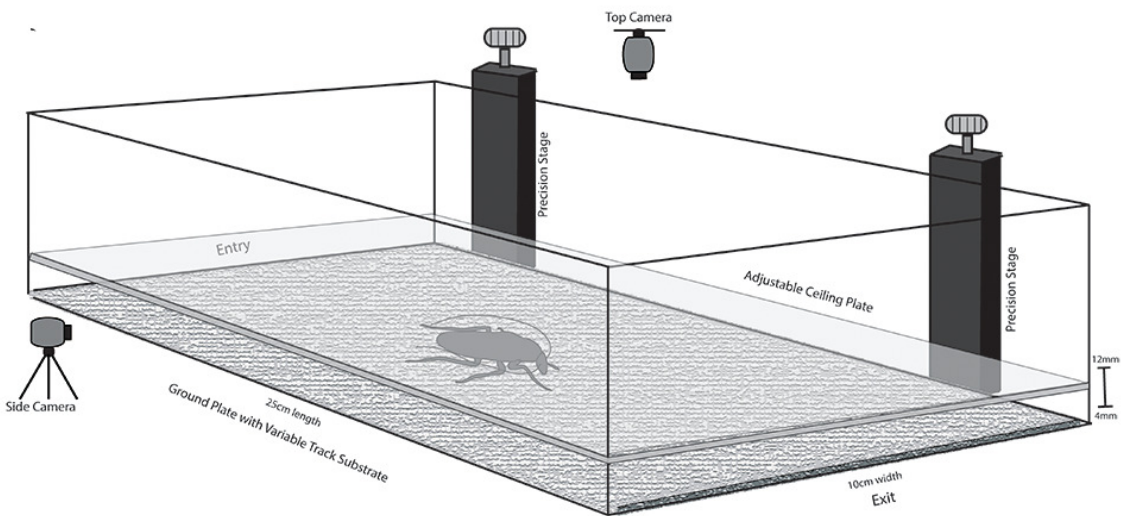
Figure 1.2: Confined space crawling setup featuring acrylic track with an adjustable ceiling plate and fixed ground plate for determining the effect of gap size. To measure the effect of friction, the ceiling and ground plates were fixed 4mm apart and surfaces were varied with different grades of sandpaper.
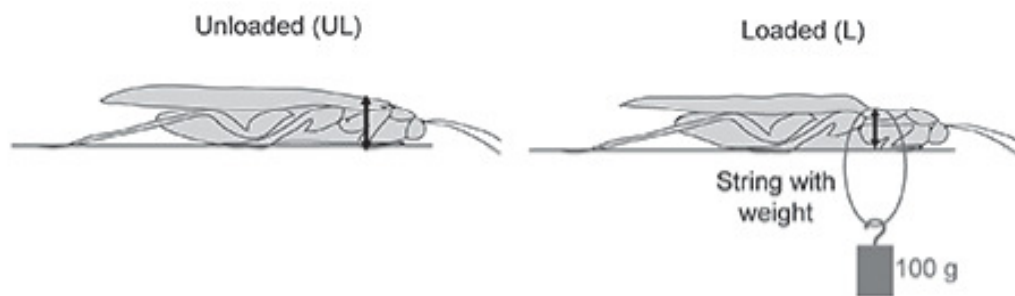
Figure 1.3: Exoskeletal compression process with an anesthetized cockroach and 100g weight in unloaded (left) and loaded (right) configurations.
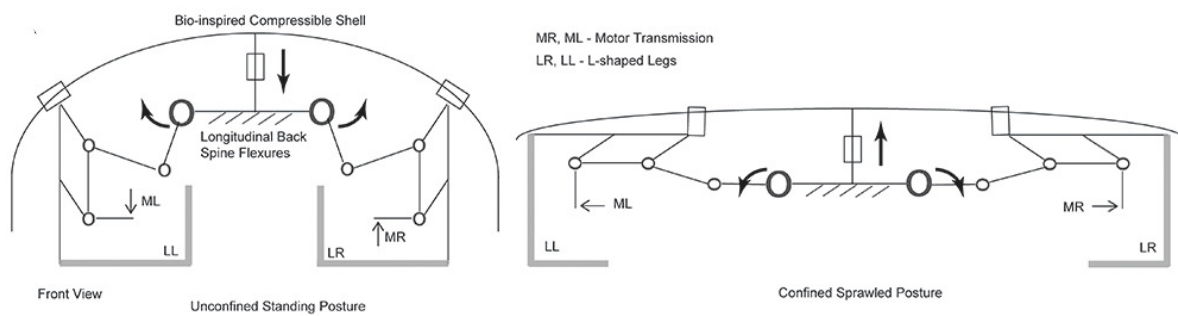
Figure 1.4: Schematic of the robot with a bio-inspired compressible shell to visualize the degrees of freedom in unconfined standing (left) and confined sprawled (right) postures.
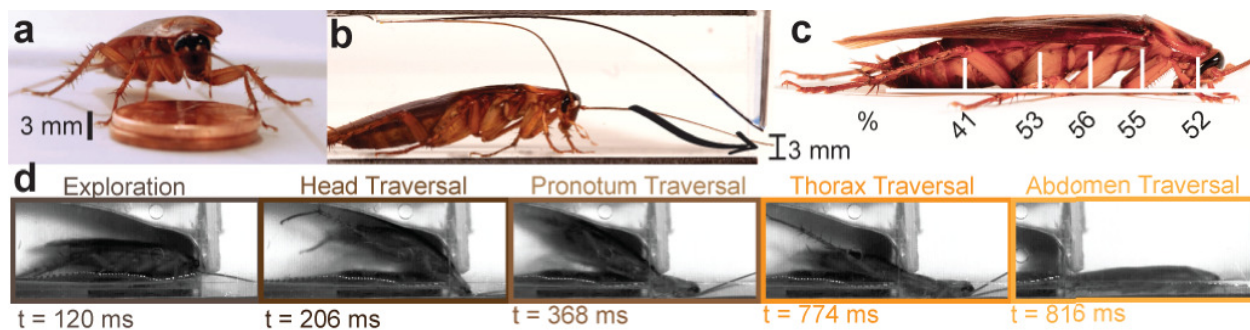
Figure 1.5: Performance of cockroaches traversing crevices. (A) Comparison of free-standing height of American cockroach, Periplaneta americana, relative to the near minimum crevice height traversed equal to 3 mm, two stacked pennies. (B) Crevice traversal apparatus with cockroach about to enter (Fig. S1A). (C) Body compression (white vertical bars) resulting from a 100 g load across segment. Percent body compression shown below segment (Fig. S1C & Table S1). (D) Crevice traversal stages extracted from high-speed video frames with corresponding time stamp for 3 mm height (Movie S1)
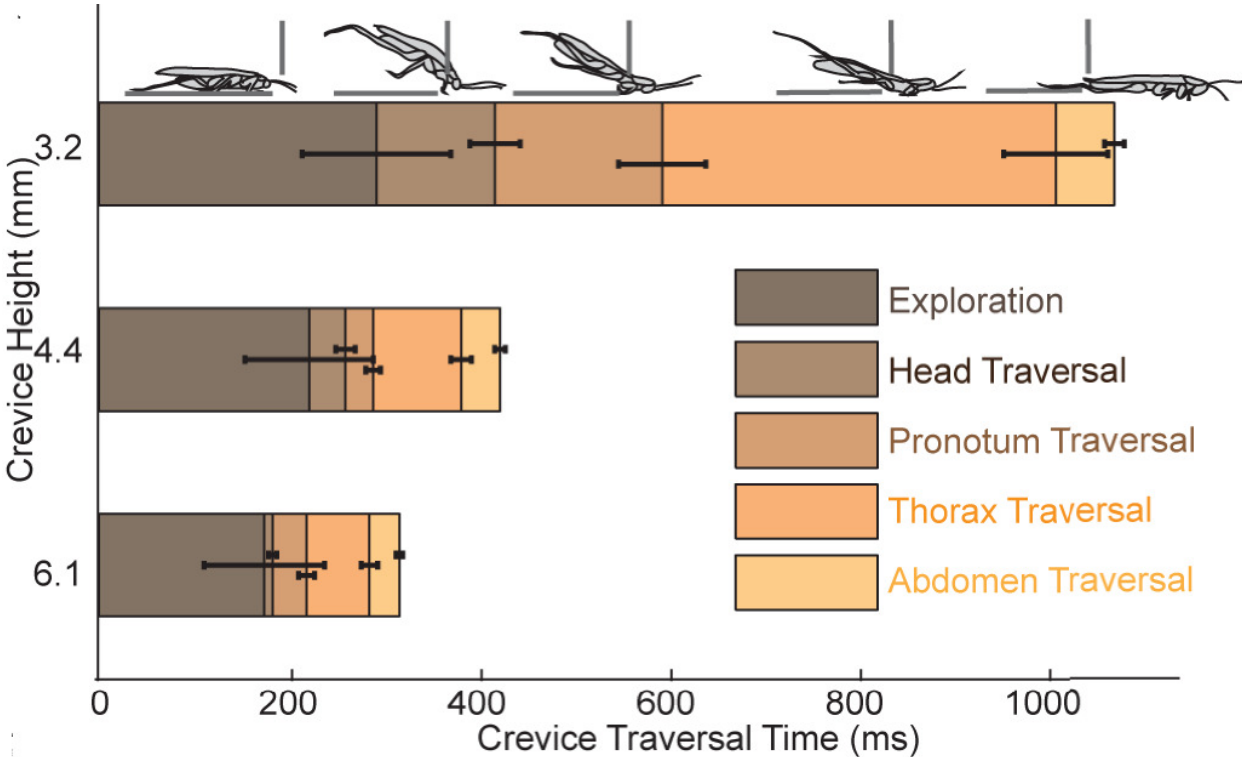
Figure 1.6: Crevice traversal time at three crevice heights. Each behavioral stage duration is stacked onto the next from left to right to also show total time. Points and error bars represent mean $\pm$ 1 s.d.
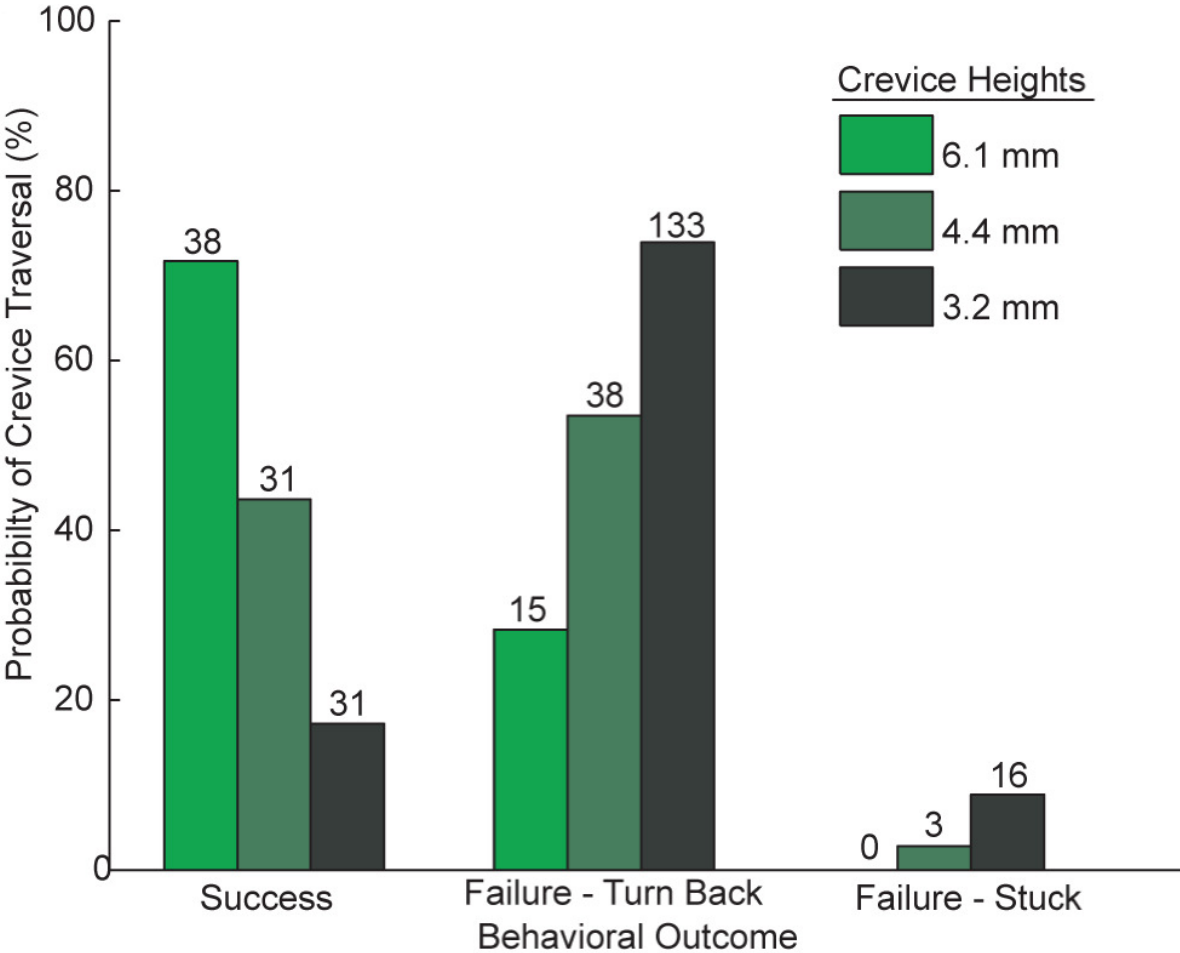
Figure 1.7: Probability of crevice traversal for three crevice heights (represented by three colors). Cockroaches successfully traversed the greatest heights more frequently and failed to traverse the lowest crevice heights by turning back or getting stuck within the crevice. Number of trials shown above bar.

Figure 1.8: Crevice crawling apparatus with cockroach about to enter (Fig. S1). Ceiling heights used represent free-standing (12 mm), crouched (9 mm), just beginning to compress body (6 mm), and minimum ceiling height within which animals crawled (4 mm).
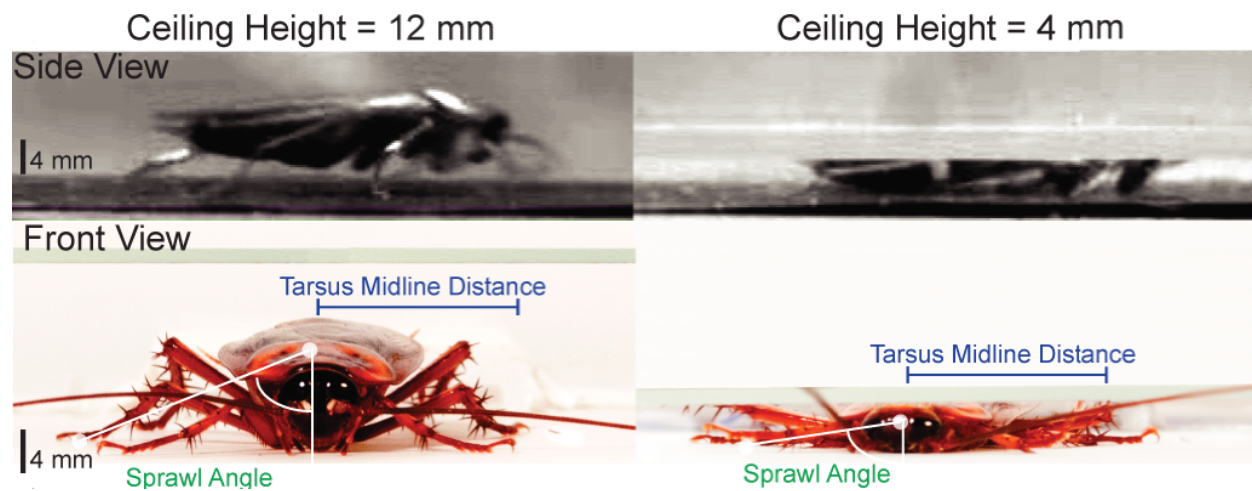
Figure 1.9: Side (from video) and Front view of cockroach crawling within chamber at two ceiling heights. Front view shows the increase in sprawl angle, but not foot to body midline distance (tarsus midline distance) as ceiling height was reduced.
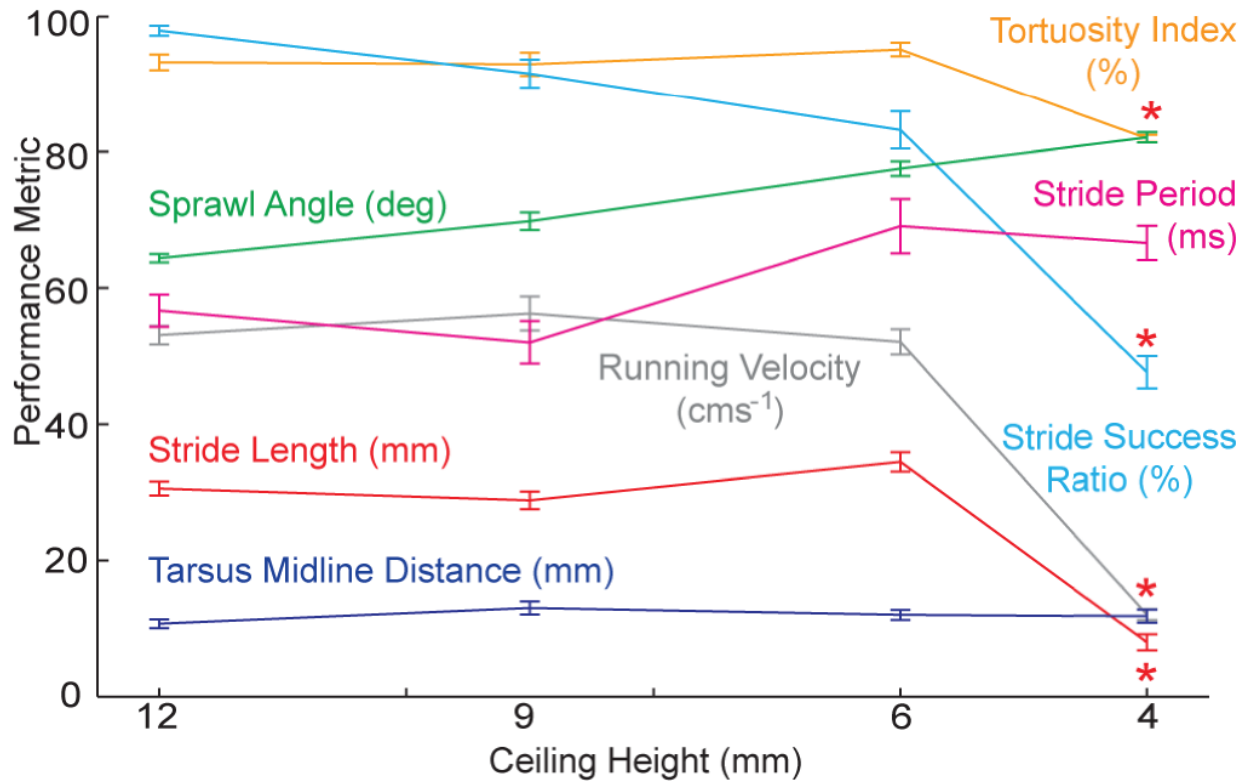
Figure 1.10: Performance metrics, velocity (grey), stride length (red), stride period (magenta), sprawl angle (green), tarsus midline distance (dark blue), stride success ratio (ratio of successful strides with no foot slipping relative to the total number of strides; light blue) and tortuosity index (forward displacement of cockroach relative to the length of the actual path taken; orange) as a function of ceiling height with their respective units are indicated in parentheses after label. Points and error bars show (mean $\pm$ 1 s.d.). Red stars represent a significant difference at 4 mm relative to larger ceiling heights.
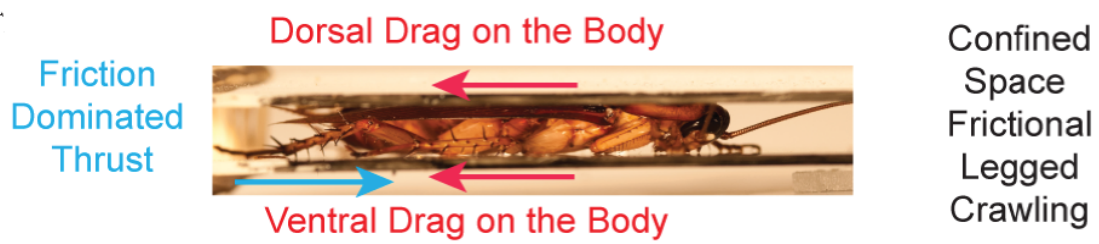
Figure 1.11: Confined space frictional legged crawling characterized by drag on the dorsal and ventral surface of the body and friction dominated thrust by legs in a non-flowing medium.
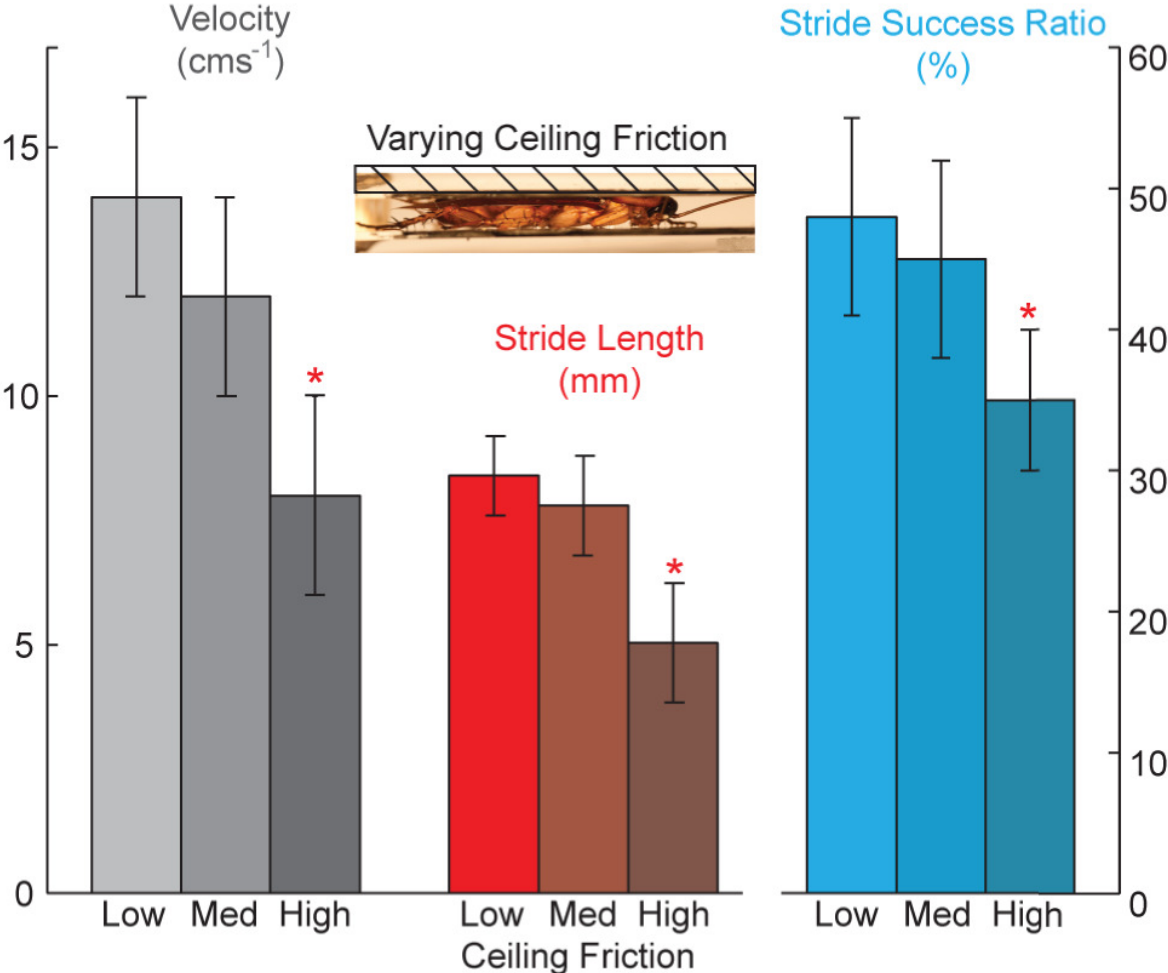
Figure 1.12: Effects of varying ceiling friction for confined space crawling performance. Performance metrics, velocity (greys), stride length (red-brown) and stride success ratio (blues) at 4 mm ceiling height (respective units indicated in parentheses below label) as a function of ceiling kinetic friction varied at three levels (Low, Medium and High) with ground kinetic friction constant. Bars show mean $\pm$ 1 s.d. Red stars represent a significant difference from other kinetic friction levels.
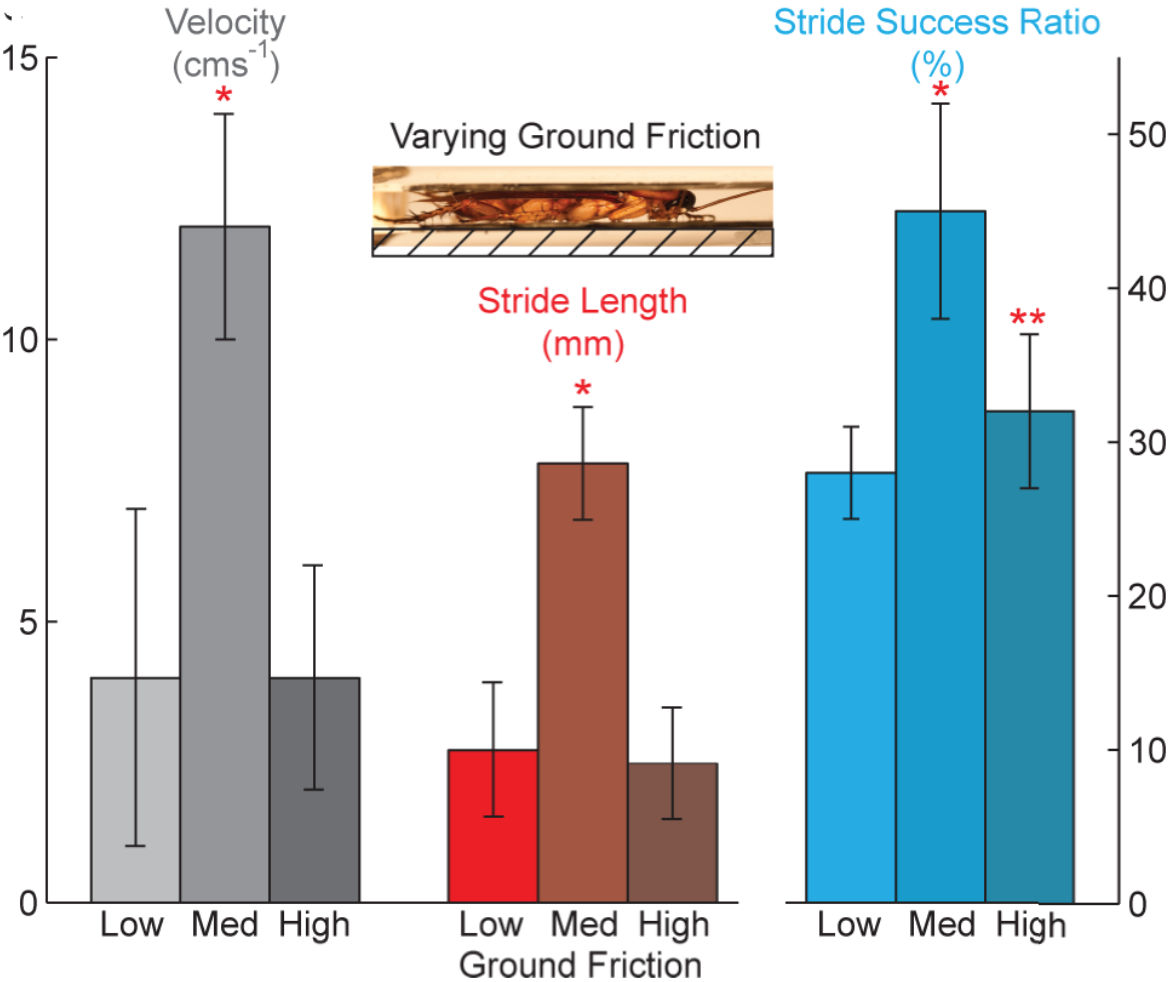
Figure 1.13: Effects of varying ground friction for confined space crawling performance. Performance metrics, velocity (greys), stride length (red-brown) and stride success ratio (blues) at 4 mm ceiling height (respective units indicated in parentheses) as a function of ground kinetic friction varied at three levels (Low, Medium and High) with ceiling kinetic friction constant. Bars show mean $\pm$ 1 s.d. Red stars represent a significant difference from other kinetic friction levels.
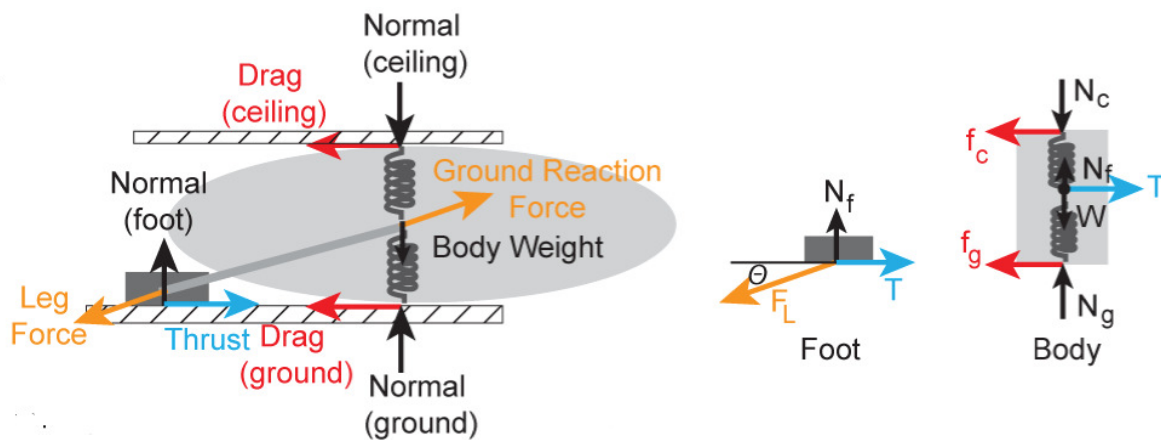
Figure 1.14: Model of frictional legged crawling. (left) Model simplified representation of a cockroach in a confined space depicted as a compressible body (light gray solid oval) with a single leg (gray line) ending in a foot (dark grey box) confined within two parallel plates (hashed boxes). Leg force (F_L) is indicated in orange, thrust (T) in blue, drag - ceiling (f_c) and ground (f_g) in red, body weight (W) and all normal forces - ceiling-body (N_c), ground-body (N_g) and ground-foot (N_f) in black. (right) Force body diagram.
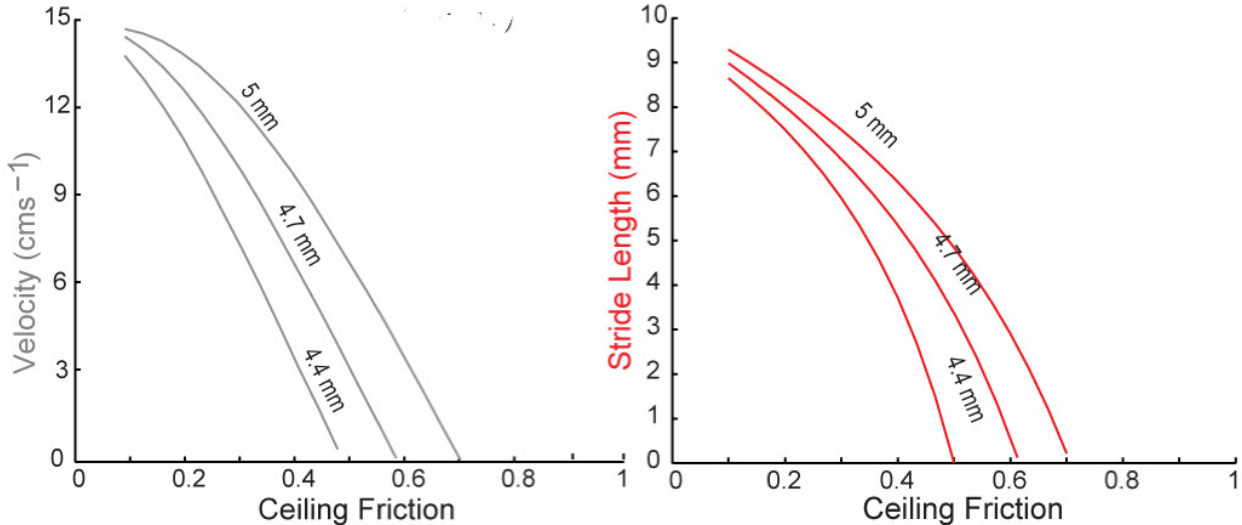
Figure 1.15: Performance metrics, velocity (grey) and stride length (red) at three ceiling heights (4.4 mm, 4.7 mm and 5 mm) as a function of ceiling kinetic friction with ground kinetic friction constant.
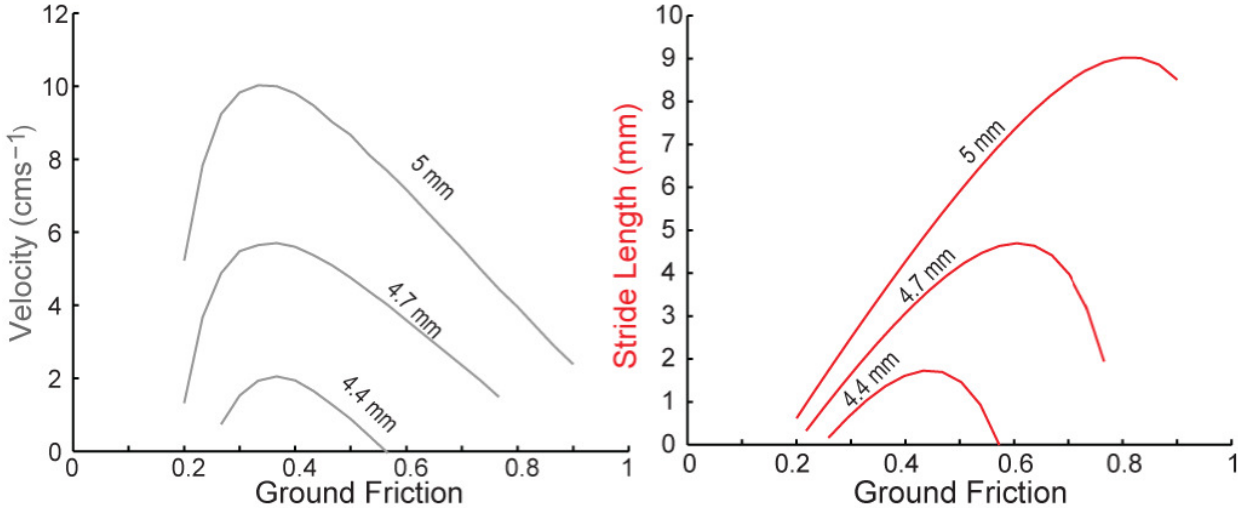
Figure 1.16: Performance metrics, velocity (grey) and stride length (red) at three ceiling heights (4.4 mm, 4.7 mm and 5 mm) as a function of ground kinetic friction with ceiling kinetic friction constant.

Figure 1.17: Materials testing apparatus with custom built chamber positioned atop load cell to the measure force during cyclic compression (Movie S3).
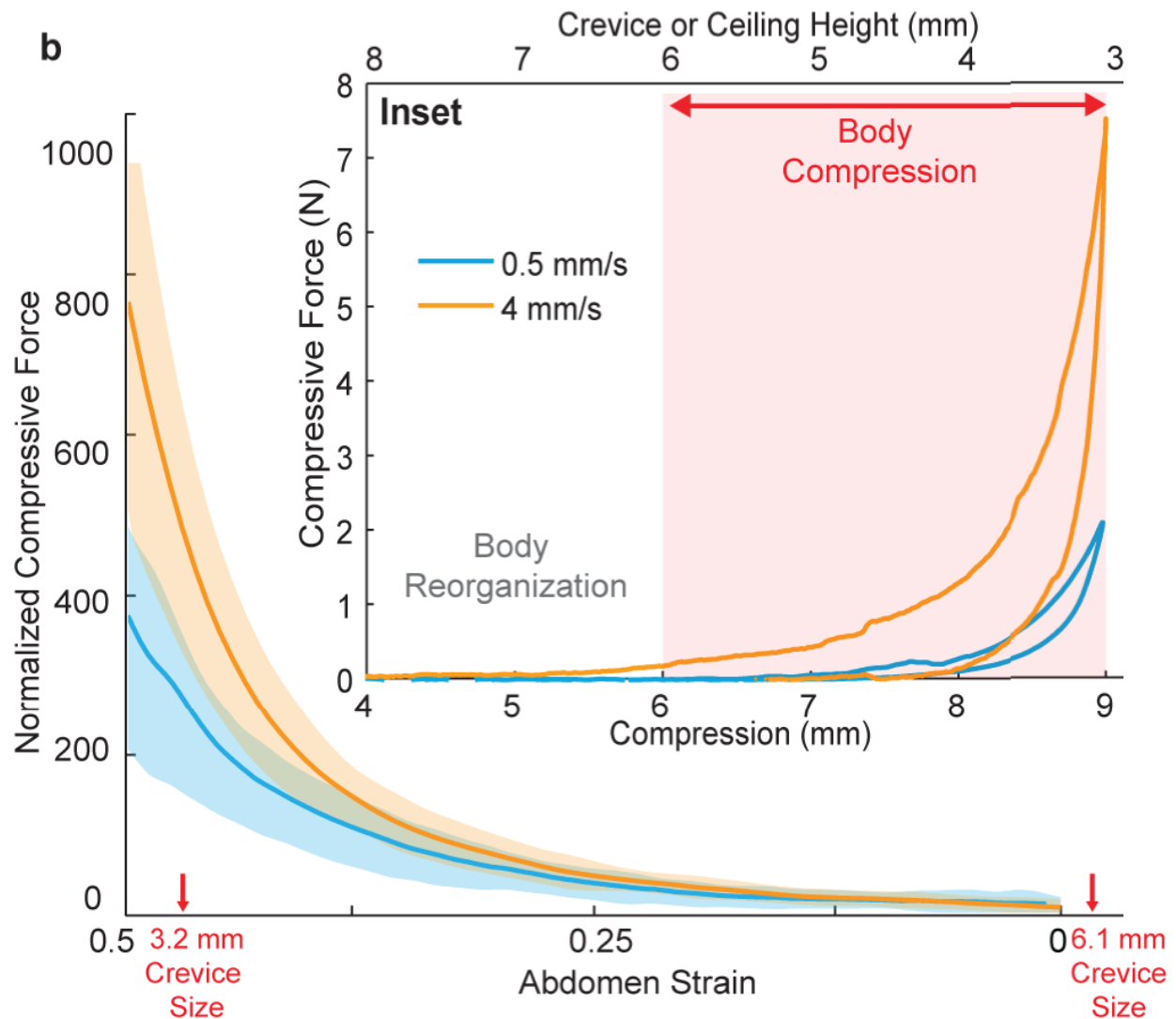
Figure 1.18: Material properties of cockroaches during compression. Normalized body compressive force (measured force / body weight) as a function of crevice size (red) and abdomen strain (change in abdomen compression / maximum abdomen thickness). Abdominal strain decreases from left to right corresponding to an increase in crevice size. Blue lines show a compression rate of 0.5 mm s^{-1}. Tan lines show rate of 4 mm s^{-1}. Shaded bands represent 95% confidence limits. Inset. Compressive force cycles as a function of body compression distance for two rates of compression. The corresponding crevice or ceiling height is shown for comparison. Areas within the loop represent the energy lost per cycle.
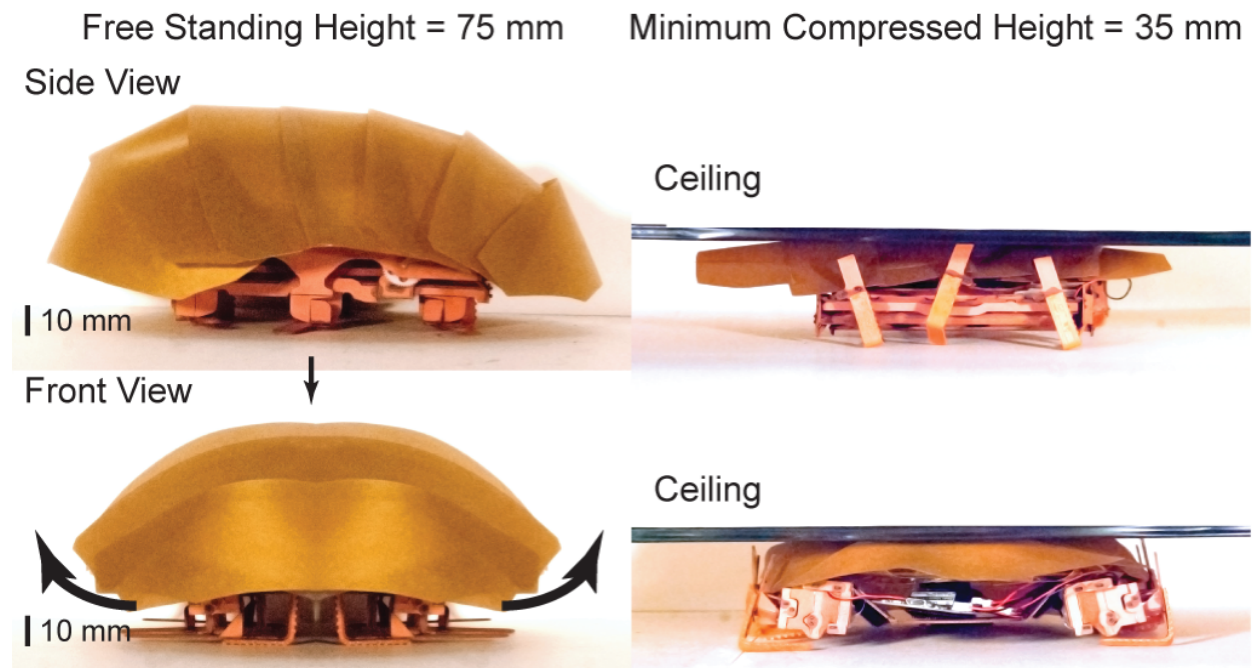
Figure 1.19: CRAM- Compressible Robot with Articulated Mechanisms. Prototype robot with adjustable sprawl and abdominal compression inspired exoskeletal plate-like shell (Movie S4; Fig. 1.4) Top row photos, Side View of free-standing and confined space posture for robot between two surfaces with ceiling labeled. Bottom row photos, Front View of free-standing and confined space posture for robot between two surfaces. Top black arrow small arrow shows direction of compression and bottom black arrows show leg sprawl direction when compressed.
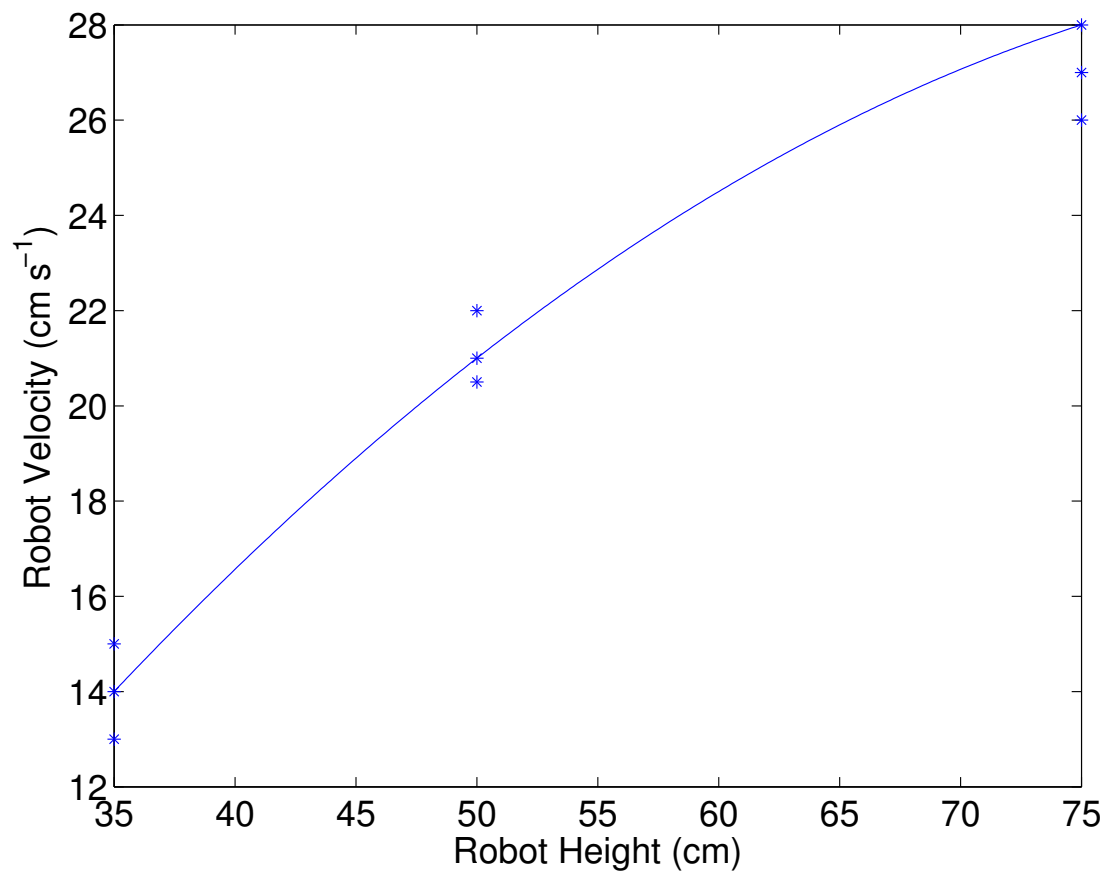
Figure 1.20: Plotted is the robot velocity at three different confined heights.

Chapter 2

Mechanical Mediation via Head-on Collisions

2.1 Summary

Animals in natural environments perform a variety of rapid maneuvers to negotiate complex terrain and escape from predators. It is generally held that these extraordinary capabilities are made possible through extensive neuromechanical feedback involving multimodal sensory systems. Principles inspired from these integrated system have even been adopted as models of control for engineering. A rapid behavior that is not well understood is transition from a horizontal surface to a vertical wall. We found that cockroaches running at over one meter or 50 body lengths per second transition from the floor to a wall within 75 ms by using their head like an automobile bumper as their primary strategy to mechanically mediate the maneuver. We found no significant differences in the strategy across lighting conditions, visual input, wall preview distance and running surface properties. Because of their small size, they have lower kinetic energies yet higher energy dissipation capabilities relative to their larger counterparts. Thus, by relying on a small, 'smart' exoskeleton capable of managing energy, the cockroaches executed effective, high-speed transitions. Inspired by the above behavior, we have demonstrated passive, high-speed, mechanically mediated transitions with our small, palm-sized robot DASH running into a vertical wall at about 80 cm/s. Under extreme conditions or rapid behaviors, when the control systems are less effective due to limited response times or bandwidth constraints, small animals and robots can utilize alternate, yet equally effective, mechanically mediated strategies to ensure successful performance. Therefore, relying on the robustness of its exoskeleton represents a paradigm shift for understanding the control of small animals and the next generation of running, climbing and flying robots.

2.2 Introducing Mechanical Mediation

Recent advances in manufacturing technology have enabled the rapid progress towards faster, more intelligent and more capable terrestrial, aerial and underwater robotic platforms [71]. Yet, even these robots face difficulties in dealing with complex natural terrains, unpredictable environmental conditions or faulty body mechanisms [72]. On the other hand, animals effectively/ masterfully run over complex terrain such as sand [6][59], mesh-like networks [32] and compliant surfaces [73], wedge into confined spaces or through cluttered, three-dimensional terrain [10], jump over [74], fly close to ground surfaces, swim in turbulence [2], and/or despite injury [75] or autotomy [76]. This has led to unprecedented interest and explosive growth in the field of bioinspiration highlighting the importance and need for understanding, from biological organisms, the principles of robustness - maintained performance under perturbations [77].

It is generally held that the secret to an animal's seemingly flawless robust performance stems from the use of extensive neural feedback [78] from numerous multimodal sensory systems [79]. However, during rapid locomotion, the effectiveness of such neural reflexes to perturbations is likely to be reduced due to decreased reaction times available for sensing, feedback and recovery, thereby, increasing the chances of failure and the risks of sustaining damage from collisions as a consequence. Certainly, as observed by Haldane [80], *"you can drop a mouse down a thousand-yard mine shaft; and, on arriving at the bottom, it gets a slight shock and walks away. A rat is killed, a man is broken and a horse splashes,"* suggesting that the cost of collision damage increases with size of the animal. An alternate strategy for control of animal locomotion, especially under high-speed conditions, would be the utilization of preflexes [81] or mechanical feedback [16][3] - near instantaneous non-linear responses from viscoelastic musculoskeletal structures [82] arising from dynamic animal-environment interactions. However, given the diversity in size of animal bodies by over ten orders of magnitude [2] and its constituent materials ranging from soft to stiff, brittle to tough, etc., the dynamic responses from such mechanical structures and consequently, their effectiveness in mitigating the effect of perturbation and stabilizing locomotion must vary.

Here, we explore the capability of cockroaches to rely on the tuned viscoelastic properties of its exoskeleton that permit collisions and stabilize locomotion via mechanical mediation in order to effectively transition from horizontal ground running to vertical wall climbing. To escape predators, cockroaches can run at speeds approaching 1.5 ms^{-1} [31], climb up walls [32], race along ceilings [34] and even ingress into narrow crevices. Aided by their low mass and moment of inertia, cockroaches also exhibit remarkable maneuverability and can rapidly change direction by turning [83][84][85] or disappear instantly by swinging under ledges [35]. The mechanical system of the cockroach has been demonstrated to passively stabilize the center of mass dynamics [86] and/or specific body structures [82], reject rapid perturbation and aid recovery [87][88], and even run on rough terrain with obstacles upto three times their hip height [3]. Besides categorizing instances of collisions during behavior as 'mis-steps' or 'failure' in cockroaches [89][90][78] or other animals [91], no study thus far has examined the potential of body robustness for mechanically mediated locomotion control.

We selected the American cockroach, *Periplaneta americana*, because of its ability to seamlessly transition between running and climbing. Since it tends to use high-speed escape maneuvers [35], there is high probability of collisions with obstacles and opportunities for utilizing mechanically mediated strategies. To elucidate rapid horizontal to vertical transitions, we ran the cockroaches, into and up a high-contrast vertical wall, after eliciting an escape response and hypothesized that cockroaches would rely on mechanically mediation. Using high-speed video, we identified two principal transition strategies and quantified performance using frequency and transition time for each strategy. We hypothesized that the experimental conditions would not have an effect on strategy and verified the same by independently varying lighting conditions, visual input, wall preview distance and running substrate properties. We also calculated coefficient of restitution [92] for trials involving head-on collision.

Following Haldane's predictions [80], we hypothesized that body robustness decreased with increase in size. As a first step towards quantifying the same, we developed a simple model relating bulk mechanical properties such as stiffness, damping and damping ratio to performance metrics such as kinetic energy, coefficient of restitution and percentage energy dissipation as a function of body size. Further, using elastic energy and toughness [61] as measures critical for preventing body injury and thus robustness, we predict the Haldane limit - maximum body size for dissipating energy upon collision without damage.

Inspired by the mechanically mediated cockroach transition strategy, we modified Dynamic Actuated Sprawled Hexapod (DASH, [69]), our palm sized robot manufactured using Smart Composite Microstructures (SCM) manufacturing technology [44][46] to perform rapid horizontal to vertical transitions by relying only on viscoelastic responses from its tuned body structures and demonstrate the generality of this behavior. This reliance on body robustness represents a paradigm shift for understanding the control of small animals and the next generation of running, climbing and flying robots.

2.3   Methods and Materials

Animals

We used 18 male cockroaches *Periplaneta americana* (Carolina Biological Supply, Burlington, NC, USA) with an average mass of 0.71±0.13 g (mean ± s.d.). Prior to experimentation, cockroaches were kept in communal plastic containers at room temperature (22 ^{0}C) on a 12h:12h light dark cycle and provided water and food (fruit and dog chow) ad libitum.

Track and climbing surfaces

To demonstrate horizontal to vertical transitions, we constructed a horizontal acrylic track - 100 cm long and 10 cm wide (Fig. 2.1). The sidewalls of the track were coated with petroleum jelly to prevent the cockroach from climbing, while the running surface was lined

with paper to ensure adequate friction. A vertical wall (made of hard posterboard (Royal Brites, US)), 10 cm high was placed across the track to produce a transition. The available running track length for the cockroach, henceforth referenced as preview distance, was 55 cm in the standard condition. The vertical wall had a black and white checkerboard design to provide high contrast for easy visual detection.

Kinematics

We recorded videos of cockroaches running on the level surface, transitioning to a vertical posture, and climbing the wall using synchronized high-speed video cameras (AOS X-PRI, AOS Technologies, Switzerland) recording at 500 frames per second (fps) at a resolution of 1280 by 1024 pixels. One camera was positioned directly above the track, capturing the top view, and the other recorded the side view. Additionally, the track was evenly lit with minimal shadows using diffusers and two large high-power flood lamps (Lowel, Brooklyn, NY, USA) located on either ends of the track. Images were buffered through the camera memory until post-triggering, after which a video clip (4 s) from each camera was reviewed and cropped to the relevant time segment (usually 500-800 ms). All video capture, downloading, and conversion were done with a software program (AOS Imaging Studio v2.5.6; AOS Technologies, Switzerland). We determined the kinematics of the transition from the above videos using a motion tracking software package (Pro Analyst v6, Itronx Imaging Technologies, Westlake Village, CA).

Animal experimental protocol

All experiments were performed at 28 ± 2 ^{0}C (mean $\pm$ s.d.). Before starting any experiment, a total of four kinematic markers (small dots of white liquid paper) were placed on the pronotum and the abdomen (one each on dorsal surface and the side at both positions) to aid in the motion tracking. The top (or dorsal) markers were used to calculate running velocity and yaw, whereas the side markers were used to estimate body pitch. To encourage the animals to run and climb up the wall, we evoked an escape response by light stimulation of their cerci or by gently blowing. We accepted trials when the animal ran rapidly and transitioned successfully onto the vertical wall. We rejected trials where: 1) the cockroaches stopped or climbed the side-wall within 25 cm of the vertical wall or during the transition, 2) their body (excluding their legs) collided with the side-wall, or 3) exhibited turns of more than 150 during the run or while transitioning.

Cockroaches with intact antenna, compound eyes and ocelli, running on a paper surface with wall preview distance of about 55 cm, under ambient lighting conditions represented our standard (or normal) condition. To ensure that these particular conditions were not biasing the behavior of the cockroaches, we conducted experiments varying lighting conditions, visual input, wall preview distance and type of running surface. Each individual served as its own control by running each individual at all manipulations within each condition allowing us to use paired statistics.

'Ambient' lighting conditions refer to default lighting conditions which included ordinary room lighting in addition to flood lamps. Since cockroaches prefer dark conditions in nature, we tested the animals under low-light conditions to remove any possible bias induced as a result of the brighter environment. The 'low-light' condition was the minimum lighting that enabled high-speed video capture at 500 fps and was about four times darker than the ambient condition.

Further, to allow the cockroach sufficient time to detect the wall and prepare for transition, we systematically varied the wall preview distance. We chose 80 cm as the upper limit of the wall preview distance because the cockroaches either slowed down or stopped during the runs of longer lengths. Similarly, 30 cm was chosen as lower limit to allow for a steady run satisfying our operational definitions. A mean value of 55 cm was used as the standard.

To test of the role of visual sensors involved in the transition behavior, we blinded cockroaches by covering their compound eyes and the ocelli with white nailpaint, taking care to avoid the head/scape joint as described by Cowan et. al [93]. Finally, we switched the running substrate from the default paper to felt, a softer material, and 40-grit sandpaper, a hard and rough surface, to test for any role of the substrate in influencing the behavior.

Robot experimental protocol

We simulated a head-on impact transition using DASH (Dynamic Autonomous Sprawled Hexapod Robot) [69] by running the robot into the vertical wall at maximum speed ($\approx$80 cm s^{-1}). A cone shaped extension, slightly inclined nose upwards, was added to the front of DASH to facilitate the robot orienting upward upon wall collision. We lined the running surface with cork to provide effective traction and used a preview distance of 55 cm. We video recorded the robot as we did with the animal.

Coefficient of restitution calculations

To perform controlled head-on impacts, we suspended freshly dead cockroaches like a pendulum at their center of mass using light music wire (125 μm; 30 cm in length). The cockroach pendulum was then released from suitable initial angles such that the speeds before collision were about 1 m s^{-1} (similar to those observed during head-first impact behavior). A 1 lb brass paperweight was used as the wall into which the animals collided. The entire process was filmed at 1000 Hz providing us the time resolution to measure the velocities before and after impact.

Data analyses and statistics

All the data collected were analyzed using custom software on MatLab (Mathworks Inc.). We performed all statistical analysis using Minitab (Minitab Inc.). Statistics were performed on animals with at least 5 trials per experimental condition.

2.4 Strategies for Transition

Under the naked eye, cockroaches appeared to perform a smooth, 'elegant' transition onto the vertical wall. However, high-speed videography revealed two prominent transition strategies - head-first impact and body-angled impact. For the former strategy cockroaches approached the wall at full speed, crashed head-on and even bounced back, before transitioning up the wall (Video S1). We refer to this 'erroneous', yet successful, behavior as the head-first impact strategy (Fig. 2.2). For the latter strategy cockroaches ran towards the wall with their body pitched head upwards and used their legs to decelerate and climb up the wall (Video S2). We refer to this as the body-angled impact strategy (Fig. 2.3). Under the standard condition (n= 18 animals, 107 trials), we observed that the head-first strategy represented a significant portion of our trials (86/107, greater than 80%). In the remaining cases, the animals employed the body-angled impact strategy to transition. In extremely rare instances, cockroaches either jumped (4/296) or flew (1/296) towards the target. We found no effect of individuals on transition strategy for animals running under standard conditions (n = 13 animals, Pearson χ^2 test, P = 0.289). To ensure that standard conditions were not biasing the behavior of the cockroaches, we varied the following experimental conditions - light, visual input, wall preview distance and running surface (Table **??**). We found no significant differences (Pearson χ^2 test, P = 0.631) in the strategy across lighting conditions (low-light or ambient), visual input (blinding or intact vision), wall preview distance (30, 55 or 80 cm) and running surface properties (sandpaper, paper or felt). Further, the animals used in the standard and above experimental groups showed no significant differences in strategy (Pearson χ^2 test, P = 0.224). This allowed us to combine the datasets and reveal no effect of individuals (n=18) on transition strategy (Pearson χ^2 test, P = 0.839). The absence of an effect of the conditions suggests that head-first impact is not an anomalous behavior introduced due to the experimental conditions. The above results lead us to propose that the primary strategy for transition - the mechanically mediated head-first impact might be driven feedforward.

2.5 Performance Comparison across Transition Strategies

In order to compare the transition performance for the two strategies under the standard condition, we measured the transition time, the time from the first wall contact -excluding the antennae- to both hind-legs on the wall. Contrary to our expectations, the two strategies show no significant difference in the mean transition time (75±28 ms; ANOVA, P = 0.635). This result indicates that head-first impacts do not pose a disadvantage to the animal in terms of transition times. It must also be noted that irrespective of the strategy used, the transition times are extremely short (about 1-2 strides) which makes such maneuvers look like smooth transitions to the naked eye. As shown in Fig. 2.4, irrespective of the transition strategy, the animals maintain steady horizontal velocities while approaching the wall. But during

transition, the kinetic energy is rapidly dissipated and the horizontal velocity decreases to below zero within about 20-30 ms. Negative horizontal velocities suggest that the animals bounce back after impacting the wall. Further, it is interesting to note that head-first transitions (65-148 cm s^{-1}) occurred at significantly greater (ANOVA, P $<$0.001) mean running speeds (averaged over at least 25 cm before first wall contact) compared to the body-angled transitions (51-92 cm s^{-1}). Therefore using the head-first impact strategy to transition is potentially advantageous to the cockroach as it offers a greater chance of escaping from chasing predators. Further, a typical transition is characterized by rapid changes in pitch angle following wall contact for both strategies (Fig. 2.4). Prior to transition, we found no evidence of any characteristic changes in body pitch angle enabling body posture adjustment to facilitate a particular transition strategy. The lack of clear changes in horizontal velocity and body pitch angle as the animal approaches the wall suggests limited neural influences during transition behavior. To further characterize the head-first transition, we used the coefficient of restitution (COR) as our metric. COR is defined as the ratio of the velocity of separation to the velocity of approach (15) and is often used as a measure of kinetic energy loss (= 1-COR^2) upon impact to describe the severity of collisions. For our case, we used the instantaneous running speed of the animal, one frame before and after head-contact as the approach and separation velocities respectively (Fig. 2.4). The mean COR for head-first impact transitions was 0.22, indicating that about 95% of the kinetic energy was dissipated by the exoskeleton surrounding the cockroach. The independently measured COR using a cockroach pendulum was 0.26±0.1 (2 animals, 14 trials), which is in close agreement with the experimental measurements.

2.6 Scaling of Mechanical Properties

Not all animals can use the head-first strategy to transition without severe injuries, as the responses from visco-elastic body elements are size-dependent (Fig. 2.5). Assuming dynamic similarity for the scaling of velocity as a function of mass [94], we expect velocity (v) to scale as $M^{0.16}$ or $l^{0.5}$, where M is the mass and l the leg length. This prediction is in close agreement with studies on the scaling of maximum running speed of animals, estimated at $M^{0.17\pm0.04}$ [95]. Therefore, for an animal running at its top speed and colliding with a wall, the kinetic energy upon impact will scale according to

$$KE \propto Mv^2 \propto l^3(l^{\frac{1}{2}})^2 \propto l^4 \qquad (2.1)$$
$$\frac{KE}{M} \propto M^{\frac{1}{3}}$$

Thus, kinetic energy rapidly increases with the length of the animal according to the power law (l^4).

Further, the ability to dissipate energy (COR) is also size-dependent. This result directly follows from the dependence of damping ratio on mass, stiffness and damping (see supplement), which scale with size. Assuming the animal's body to be composed of linear

viscoelastic elements consistent with the Kelvin-Voigt model [96], we can model the head-first impacts as responses of a simple mass-spring-damper system whose dynamics are governed by a following second order ordinary differential equation (Eqn. 2.2).

$$m\frac{dx^2}{d^2t} + C\frac{dx}{dt} + Kx = 0 \tag{2.2}$$

where m, K, C represent the body mass, spring constant (stiffness) and damping respectively. The above equation may be re-parameterized as follows (Eqn. 2.4) in terms of natural frequency (ω) and damping ratio (ξ).

$$\frac{dx^2}{d^2t} + 2\xi\frac{dx}{dt} + \omega^2 x = 0 \tag{2.3}$$

$$\xi = \frac{C}{2\sqrt{Km}}; \omega = \sqrt{\frac{K}{m}} \tag{2.4}$$

Damping ratio (Eqn. 2.4) is a dimensionless number indicative of how oscillations in a system decay after a disturbance. Several studies on impact pounding [92][97][98][99] have correlated damping ratio with the COR as an inverse relationship and it is therefore is a measure of system's ability to dissipate energy. Using COR-damping ratio relationship from [92] (equation 5 in [92]), we estimate the damping ratio for a typical head-first transition (COR = 0.18) as $\xi = 0.479$. We acknowledge that most of the above models have been derived for well-behaved engineering materials and additional modeling might be required before adapting them to non-linear biological materials. However, the inverse relationship between damping ratio and COR by definition, still holds and careful determination of the above relationship will aid in generating useful engineering design constraints as discussed later.

Further, assuming geometric scaling and homogeneous (isotropic) material composition, a structure (l) scaled 'k' times (kl) can be decomposed into 'k^3' originally sized units (l) and arranged in 'k' layers in series, each composed of 'k^2' such units. Therefore, using parallel and series laws, we obtain that stiffness and damping both increase with body length (l; Fig. 2.5) and thus, the damping ratio (Eqn. 2.4; supplement) decreases with length (l^{-1}) (Fig. 2.6). Therefore, a high damping ratio and consequently low COR value [92] places small animals at a definite advantage for impact mitigation because of their higher energy dissipation capabilities and lower kinetic energies (l^4) relative to their larger counterparts.

The similar result is obtained by comparing the maximum kinetic energies [95][100] of animals (KE_{max}; Fig. 2.9) with the maximum energy absorption (EA_{max}; Fig.Fig. 2.8, 2.8) possible in biology materials (27), which is obtained by as a product of the material toughness [37][36][101] and cross-section area of the animal. The cross-section area was estimated by assuming an animal to be a homogeneous cube with uniform density of 1000 kgm^{-3} [102]. The resulting plot (Fig. 2.10) reveals that the KE_{max} and EA_{max} curves intersect each other indicating that beyond a critical body mass ($\approx$ 1 kg), the animal's entire kinetic energy cannot be fully dissipated without undergoing irreversible plastic deformation, which in the

animal's case means incurring body damage. Thus, this plot serves as indicator of the approximate size scales where mechanics and material properties can potentially influence behaviors especially preflex- driven high-speed ones. We also believe the above result can be particularly useful for engineers by helping them make design choices about mass, material and geometry of their robots and lessen the burden on sensor based regulatory mechanisms to overcome small perturbations or prevent collisions and robot damage.

2.7 Mechanically Mediated Transitions in a Robot

The robust exoskeletons of cockroaches provided inspiration for Dynamic Autonomous Sprawled Hexapod Robot (DASH, [69], Fig. 2.11A). The robot without any kind of sensing collides with a wall at maximum speed ($\approx$80 cm s^{-1}) and performs a mechanically mediated transition (Fig. 2.11A, Video S3, COR$\approx$0.4), remaining undamaged. The use of Smart Composite Manufacturing (SCM) process (35) enabled DASH not only be small (10 cm body length) and light (16 g), but also physically very robust, enabling it to passively overcome obstacles and even sustain 8-story falls (over 28 m) without damage. Thus, we have successfully demonstrated a passive, head-first impact transition using DASH as a physical model to justify the hypothesis that the cockroach head-first transition is mechanically mediated maneuver driven feedforward.

2.8 Scaling of Robustness

Effective performance is often thought to be elegant, free of errors or mis-steps. Animals have been long admired for their extraordinary ability to rapidly and flawlessly (to the naked eye) navigate the most complex, uncertain environments, even while escaping from predators. One such behavior is the high-speed horizontal to vertical transition by *Periplaneta americana*. This behavior, seemingly a smooth maneuver, is completed within 75 ms and thus impossible to observe with the naked eye. However, the primary mechanism behind the success of this high-speed maneuver involves a head-on impact at maximum speed into a vertical wall. Similar strategies involving mechanical mediation utilizing the head have been observed previously in false death-head cockroaches, *Blaberus discoidalis*, during obstacle climbing and categorized as a head-butt [90][103] or brute-force climbs [47] described as "the cockroaches pushed their head and body into an obstacle until that force resulted in its body pushing up and over the obstacle." Similarly, studies on *Periplaneta americana* have revealed that these cockroaches, although capable of negotiating obstacle using a single front limb movement without that limb ever touching the front of the obstacle [104][47], have been observed to impact head-first into obstacles. Quoting the authors [104], "It is tempting to suggest that these collisions represent failures to fully initiate a climb response despite the presence of the obstacle." However, this study reveals that collisions during head-first transitions do not significantly affect the transition time making the strategy just as effective

as any other at the animal's disposal. In addition, a head-first impact transition may be potentially advantageous as it enables the animal approach to an obstacle or a vertical wall at higher speeds (also observed in [104]). Therefore, we contend that such collisions in fact represent the animal's ability to utilize alternate yet effective strategies to overcome the task at hand, making them robust in executing such behaviors.

Overcoming 'Failure' under High-speed Conditions

The role of distributed neural feedback in enabling locomotion has been studied extensively. In particular, cockroaches have been studied for their ability to follow walls utilizing mechanosensory cues from their long antennae [105][106][107][108], avoid collisions during running by utilizing a combination of visual and antennal mechanosensory inputs [105] and even begin to escape from approaching predators utilizing wind-receptive cerci in 60 ms [109]. These behaviors have been adopted as models for engineering control systems [93] and inspired the development of crash avoidance systems for road vehicles [110]. However, to our amazement, cockroaches predominantly crashed into a wall head-first enroute to making a successful transition. Changing the magnitude of sensory stimuli in our control experiments had an insignificant effect on the strategy of transition. Specifically, the weak contribution of visual information in determining the transition strategy is in agreement with earlier studies [104]. Similarly, ablating the antenna completely, we observed both head-first and body-angled impact strategies ruling out a necessity for antennal mediation during horizontal to vertical transitions. Also, the typical time between the antenna contact to head impact is about 20 ms, which is of the same order as the neural conduction delays in antennae of Periplaneta [93] and faster than known antennae-touch escape responses ($\approx$35-40 ms) [108]. There we suspect that antennal influences are minimal here, and since complete ablation seemed to hinder the animal's running abilities, we did not include it as one of our experimental conditions. Therefore, under computational and bandwidth limitations of the nervous system, cockroaches did not implement careful sensor-based control but instead relied on mechanical properties of their exoskeleton. This highlights the importance of mechanical feedback as a vital characteristic of robust control systems enabling them to recover from large system-level perturbations and achieve effective performance particularly under extreme conditions.

Advantages of Being Small

Quoting Haldane [80], "You can drop a mouse down a thousand-yard mine shaft; and, on arriving at the bottom, it gets a slight shock and walks away. A rat is killed, a man is broken and a horse splashes." This has been attributed to relatively greater resistance to air in smaller animals owing to larger ratio of surface area to volume [80]. Alternately, it can be argued that the terminal velocity [102] increases with body length ($l^{0.5}$) and therefore, the speed of impact is higher for larger animal making them more susceptible to damage. Similarly, the maximum running speeds [100][95] of animals increases with animal size ($l^{0.5}$)

resulting in higher kinetic energy (l^4) in large-sized animals leaving them vulnerable to head-on collisions at the highest running speed. Went [111] further argued that while infants trip and fall routinely stay usually uninjured but adult humans are far more likely to end up with fractured bones because the momentum at ground contact upon tripping increases dramatically (l^5). Using a Kelvin-Voigt model to represent an animal body, we showed that the energy dissipation capability on head-on collision during running was size dependent leaving large animals at a further disadvantage. The maximum specific energy absorption (Fig. 2.7) values calculated based on material toughness decreased with size (l^{-1}) suggesting that except for invertebrates and a few small vertebrates, animals in general, are susceptible to permanent body deformation and bone fractures if involved in high-speed collisions while performing fast maneuvers or escaping from predators. Therefore, mechanical properties favor small sized animals for survival during impacts [80][112][113] enabling cockroaches to perform head-first impact transitions. Furthermore, this even allows small animals to be less precise in controlling their behavior, as the outcome in case of failure is not catastrophic compared to larger counterparts or traditional human-engineered technologies. For example, bees have been routinely observed to collide into walls at high-speed while attempting to enter hives [114]. Thus, the small size adds robustness to animal behavior by enabling access to a variety of alternate, effective strategies to ensure successful performance.

2.9   Mechanical Mediation in Robots

Biological studies have revealed that in dynamic, unpredictable environments, musculoskeletal structures [3] play a vital role in stabilizing locomotion by managing any energetic deviations from steady state produced by perturbations from the environment [115][116] involving energy production, absorption, storage and return and/or transfer [117][118][119][120]. Many of these principles have even been adopted as models for engineering control systems [110][121][122][123][124]. Here, we have demonstrated a mechanically mediated transition at high speed using our hexapod robot DASH. The robot does not carry any sensors onboard and relies on the robust mechanical construction of its body elements to enable it to survive the impact and facilitate the transition. The role of such energy absorbing body elements in control and maneuvers of a robot is not limited to running, but has been successfully demonstrated even during jumping ([125], Fig. 2.11) and flying ([113], Fig. 2.11). The analytical models developed in the impact studies [92][99][97][98] indicate an inverse relationship between damping ratio and COR, which means a high damping ratio correlates with low COR i.e. a high energy dissipation capability. This result highlights the importance of tuning the mechanical properties of the exoskeleton as it poses a trade off between energy dissipation and possible energy redirection during mechanically mediated maneuvers. In particular, such tuning would be critical in order to ensure successful performance during passive transition behaviors, especially in the case of robots inspired by the cockroach head-first transition.

Fortunately, advancements in manufacturing technologies can now enable the production of robots in varying size scales with fine control over mechanical properties of individual

body elements. Techniques such as Shape Deposition Manufacturing (SDM) [126] and Smart Composite Microstructures (SCM) [44][46] allow for precise machining and rapid prototyping of robots with dimensions in the centimeter scale [69][45]. Moreover, the above techniques offer the possibility of integration with the electronics, sensors and actuators during manufacturing, facilitating robots to robustly operate in real world environments, or allow them to be manufactured consistently and in high volume. In particular, flexure based millirobots, due to their inherent lightweight and low-loss joints, can easily be extremely dynamic, agile and have very high power densities making it possible to realize the amazing capabilities we see in nature's small animals. Therefore, they not only serve as ideal platforms for testing biological predictions, but also, can generate novel insights and testable hypotheses about biological systems.

2.10 Robustness - A Paradigm Shift

Robust systems can be identified by characteristics such as multi-functionality, stability, damage resistance, fault tolerance, self-repair, heterarchical organizational structure, learning, adaptation, anticipation, awareness, creativity, etc. Even in complex and new environments, the above properties enable systems to operate effectively overcoming 'mistakes'. By relying on the mechanics of the body to mediate the maneuver rather than only careful sensor-based control makes animals and robots robust even under extreme conditions (Fig. 2.10). We see this as a paradigm shift in defining performance and contend that a successful performance must include a greater emphasis on robustness - not necessarily what we perceive as the most elegant solution of motion without errors or miss-steps. Combining mechanical responses with neuromechanical feedback [3][2] involving multimodal sensory systems [108] leads to effective performance in biology. Incorporating the same in the design of robots can improve their overall robustness more significantly than regulatory mechanisms [127] superimposed after the fact on the mechanisms of functionality like in traditional engineering design approaches. Utilizing this approach also overcomes the shortcomings resulting from limited response times (delays) during high-speed tasks in typical sensor based control systems - engineering or biological. Furthermore, in a sensor based control system, the cost of recovery in such situations is huge and often results in a failure at the intended task incurring irreversible damage to the system and environment. With the current trend of moving towards smaller, lighter and more energy efficient robotic platforms, nature tells us that we would benefit from more robust designs.

Table 2.1: The following table summarizes the data for the transition experiments performed under different conditions and compares the frequency, transition times and running speeds for the head-first (HF) and body-angled (BA) transitions. Column 3 representing the frequency of transitions strategies expressed as a percentage indicates that under the different conditions, HF is the dominant strategy used by the cockroaches to climb onto the vertical wall. Further, the transition times are similar for the two strategies while the running speeds before transition is higher when the animals choose to perform the HF transition

Control	Condition	# Trials [# Animals]		Transition Times (ms)		Running Speed (cm/s)	
		HF	BA	HF	BA	HF	BA
None	Standard*	47 [7]	10 [6]	73±29	75±24	97±14	79±10
Light	Ambient	16 [4]	1 [1]	84±40	68	94±16	75
	Low	13 [4]	6 [4]	68±23	92±29	99±16	81±1
Visual	Normal	15 [4]	4 [3]	94±24	69±21	94±12	84±12
Input	Blind	17 [4]	4 [3]	76±13	97±11	101±12	96±2
Wall	55 cm	9 [4]	6 [3]	75±18	69±26	100±11	91±10
Preview	80 cm	7 [3]	1 [1]	98±34	72	105±10	78
Distance	30 cm	12 [4]	7 [4]	94±17	65±13	90±10	88±7
Running Surface	Paper	11 [4]	5 [3]	102±24	91±34	99±15	88±15
	Sandpaper	12 [4]	4 [2]	99±31	81±14	80±12	102±36
	Felt	12 [4]	6 [4]	105±27	113±31	90±23	85±16
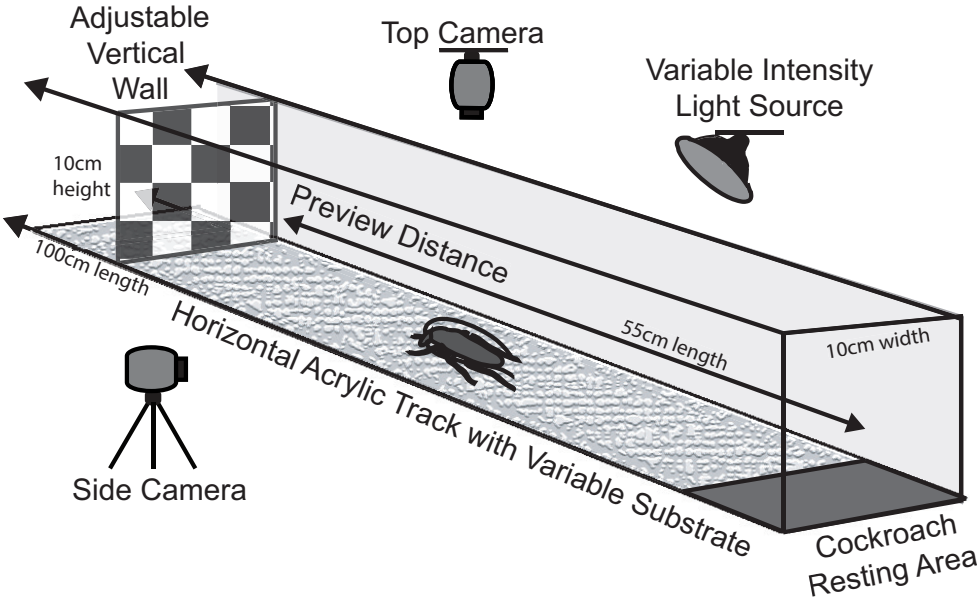
Figure 2.1: Horizontal floor to vertical wall transition setup.
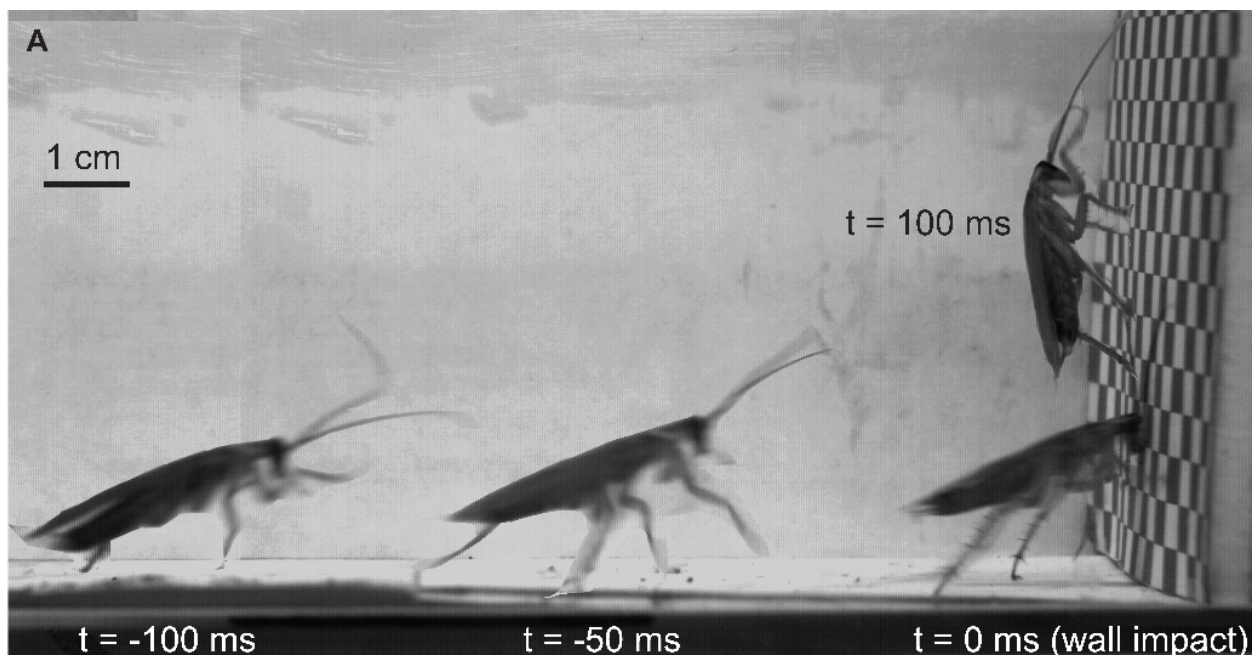
Figure 2.2: Time course of the major high-speed transition strategies ($\approx$75 ms) used by the cockroach, Head-first impact, occuring ($\approx$81%) and often at higher wall-approach speeds ($\approx$1ms^{-1}).
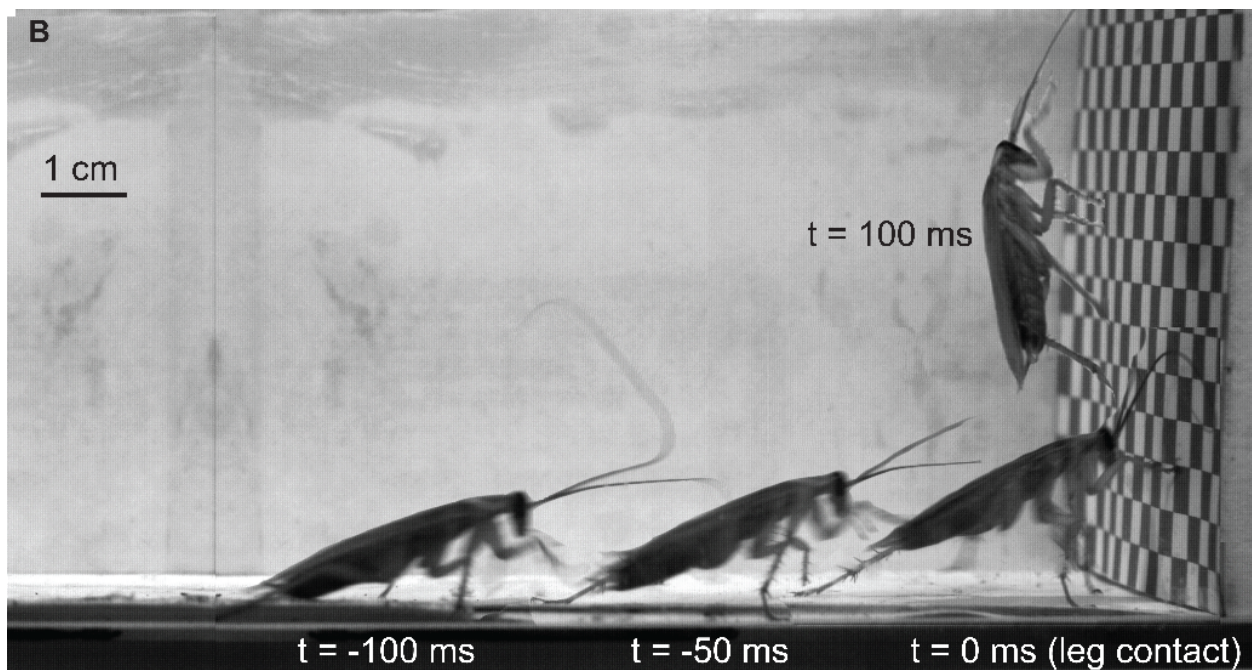
Figure 2.3: Time course of the body-angled impact transition strategies ($\approx$75 ms) used by the cockroach.
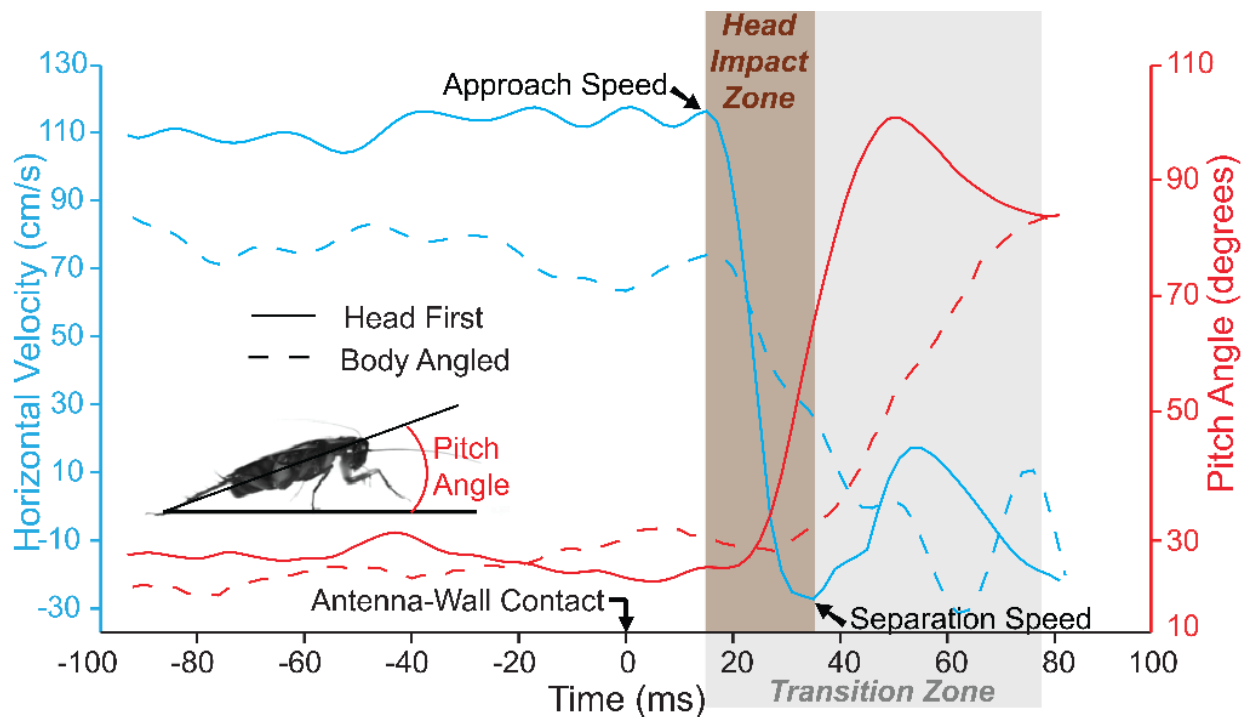
Figure 2.4: Plot of the horizontal running velocity and pitch angle during a typical Head-first (solid line) and Body-angled (dotted line) transition under the standard condition (intact vision, ambient light, 55 cm wall preview distance and paper as running surface). The transition zone is shown shaded in gray with the head impact zone further highlighted. Approach and separation speeds, which are the horizontal running velocities of the animal before and after head collision respectively, are also indicated.
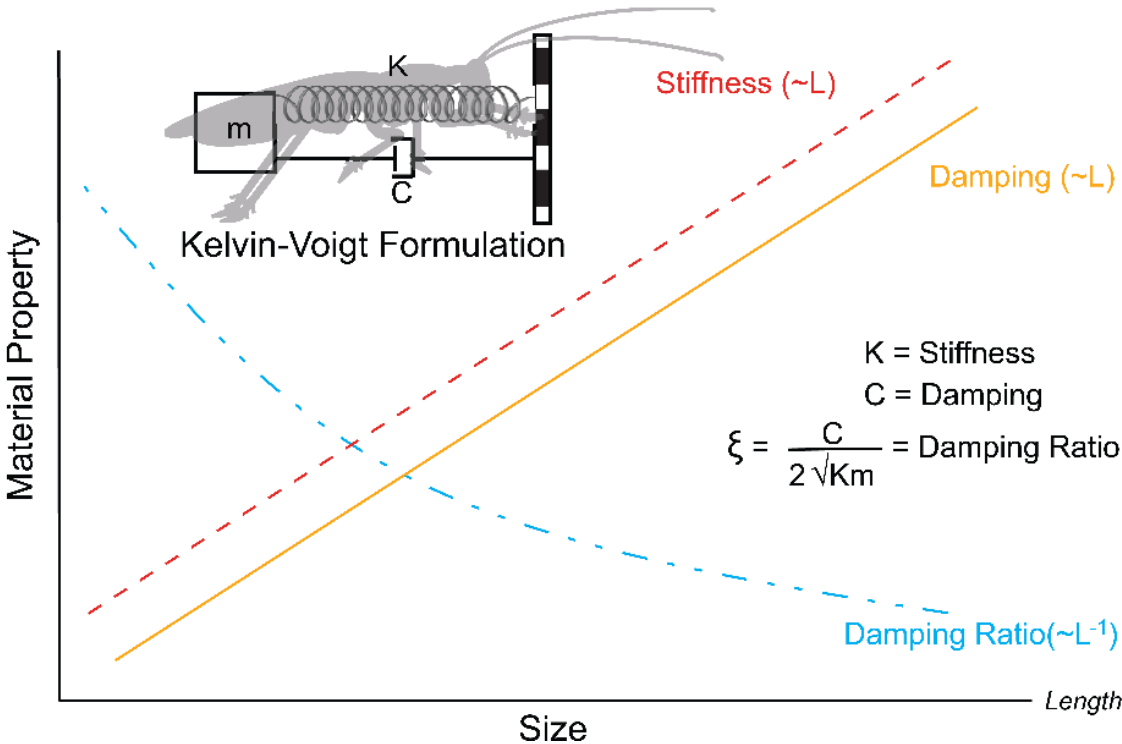
Figure 2.5: Scaling of material properties - stiffness and damping and its consequence on damping ratio as predicted by an analytical model based on Kelvin-Voigt formulation. Stiffness and damping increase linearly with length, while damping ratio decreases with length.
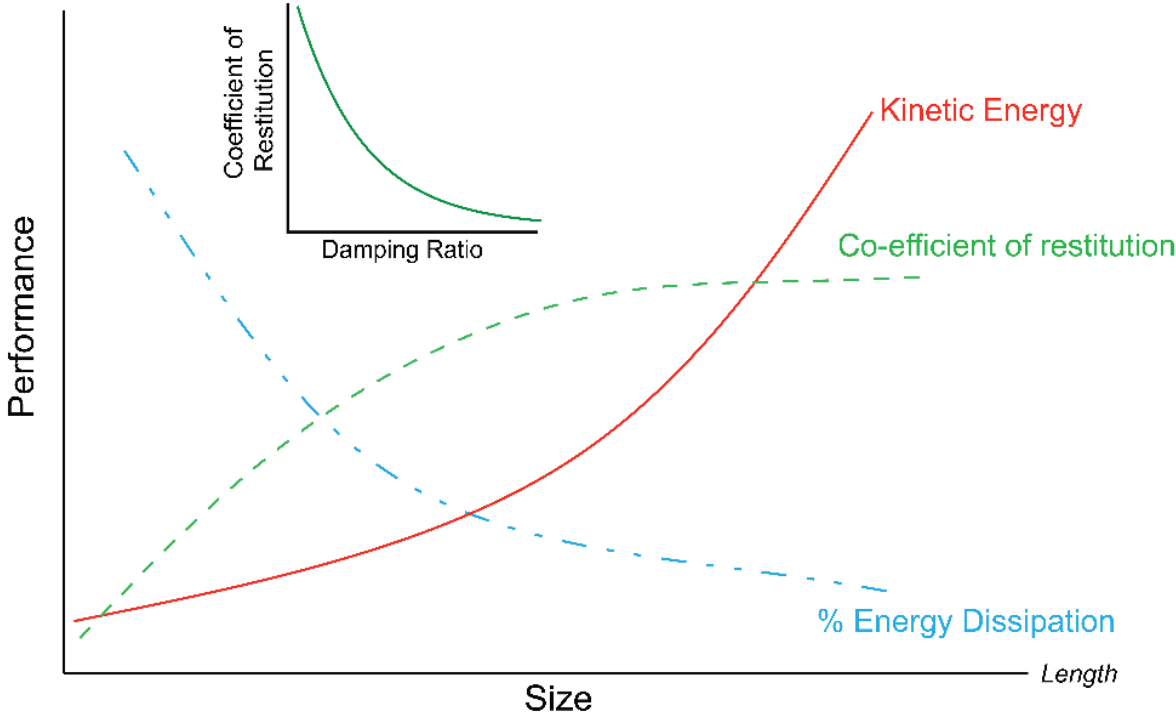
Figure 2.6: Scaling of performance parameters - kinetic energy, coefficient of restitution and percentage energy absorption as predicted by an analytical model based on Kelvin-Voigt formulation. Kinetic energy increases with size, as does coefficient of restitution indicating that percentage energy absorption decreases with size placing larger animals at greater danger of injury or damage upon collisions as compared to their smaller counterparts.
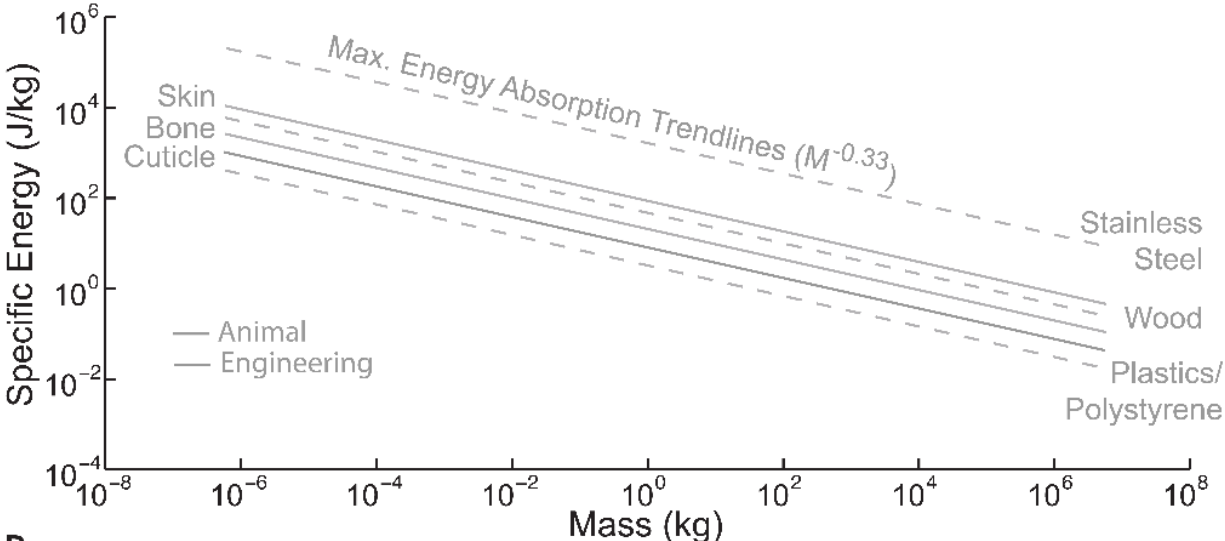
Figure 2.7: Scaling of specific energy absorption determined using toughness. Since toughness is constant for a material and independent of size, we see a linear decrease in specific energy with size. Shown are plots for materials used for construction of animals (bone, skin and cuticle) and human technologies (wood, concrete, plastics).
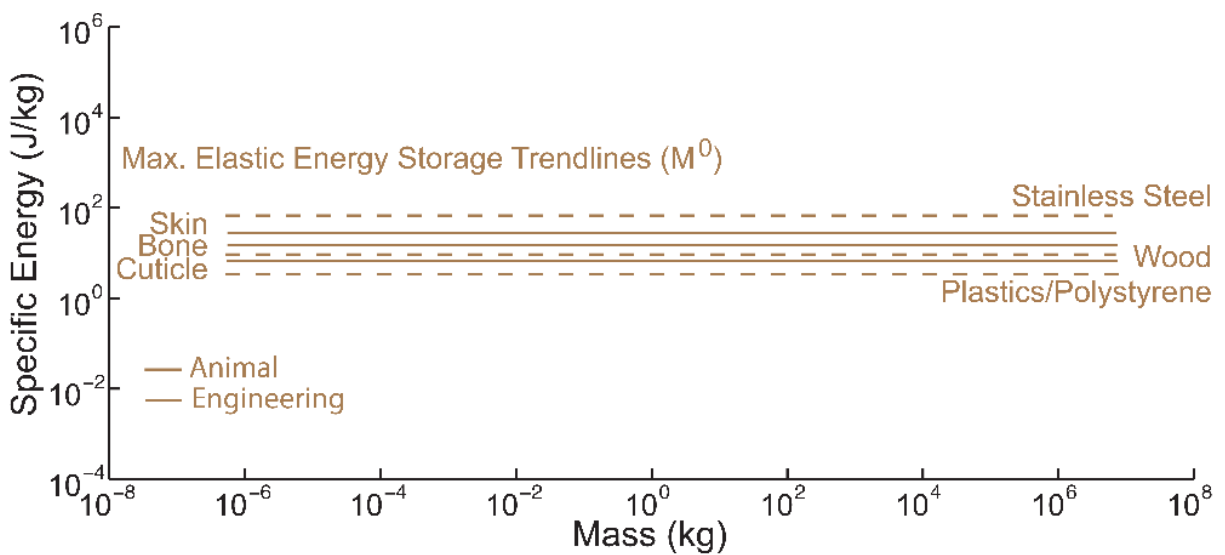
Figure 2.8: Scaling of specific elastic energy storage determined using young's modulus and yield strength. Since both these properties are constants for a material, we find that the elastic energy capacity is independent of body size. Shown are plots for materials used for construction of animals (bone, skin and cuticle) and human technologies (wood, concrete, plastics).
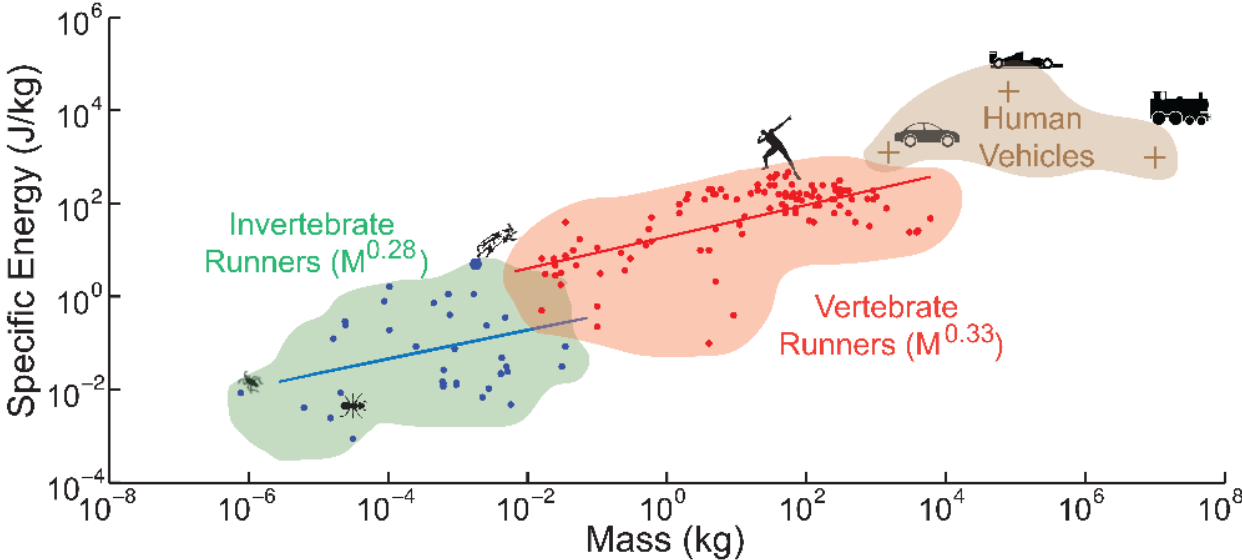
Figure 2.9: Log-log plot of the scaling of specific kinetic energy in terrestrial animals. Kinetic energy increases with mass exponentially and closely follows the trend predicted by inverted pendulum running ($m^{\frac{1}{3}}$). The green cloud shows invertebrate runners including cockroaches while the red cloud depicts vertebrate runners including humans. A tan cloud is added for comparison with human vehicles (car, jet plane, train).
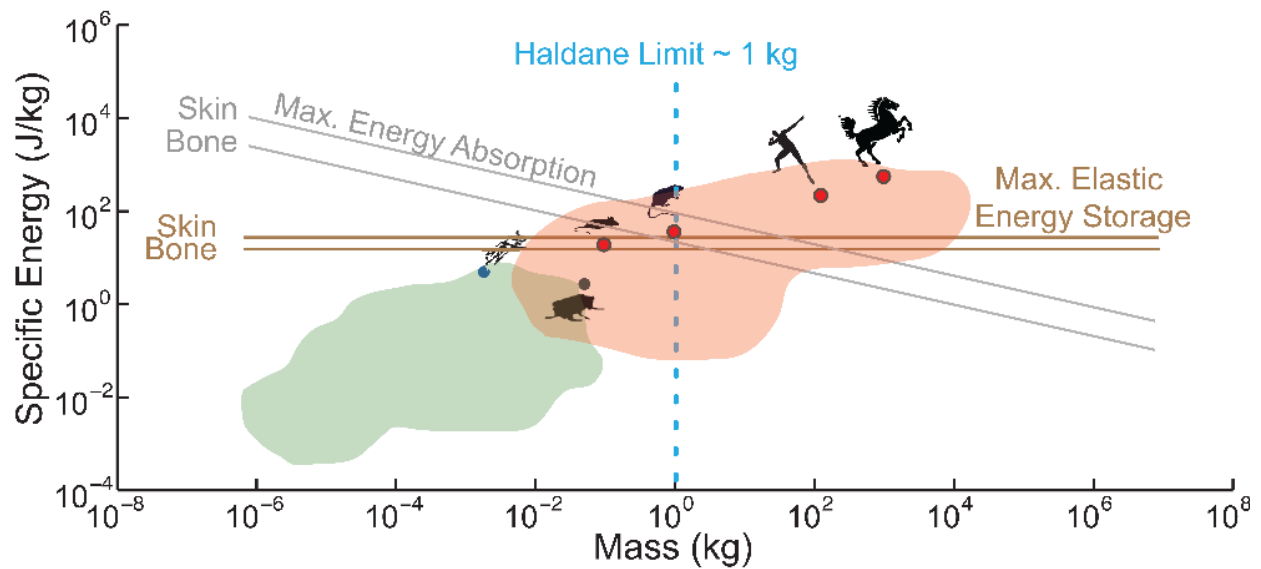
Figure 2.10: By combining figures 2.7, 2.8 and 2.9, we find that the curves intersect around 1kg (blue line). For sizes smaller than this, animals might be able absorb all the kinetic energy though the body materials. However, for sizes to the right of the blue line, animals will be unlikely to completely dissipate their kinetic energy though material properties alone and would need to utilize mechanisms to either reduce speed if colliding into environment or avoid collisions completely. This predictions of the above model match well will Haldane's observations about size dependence on energy dissipation and magnitude of injury upon collision
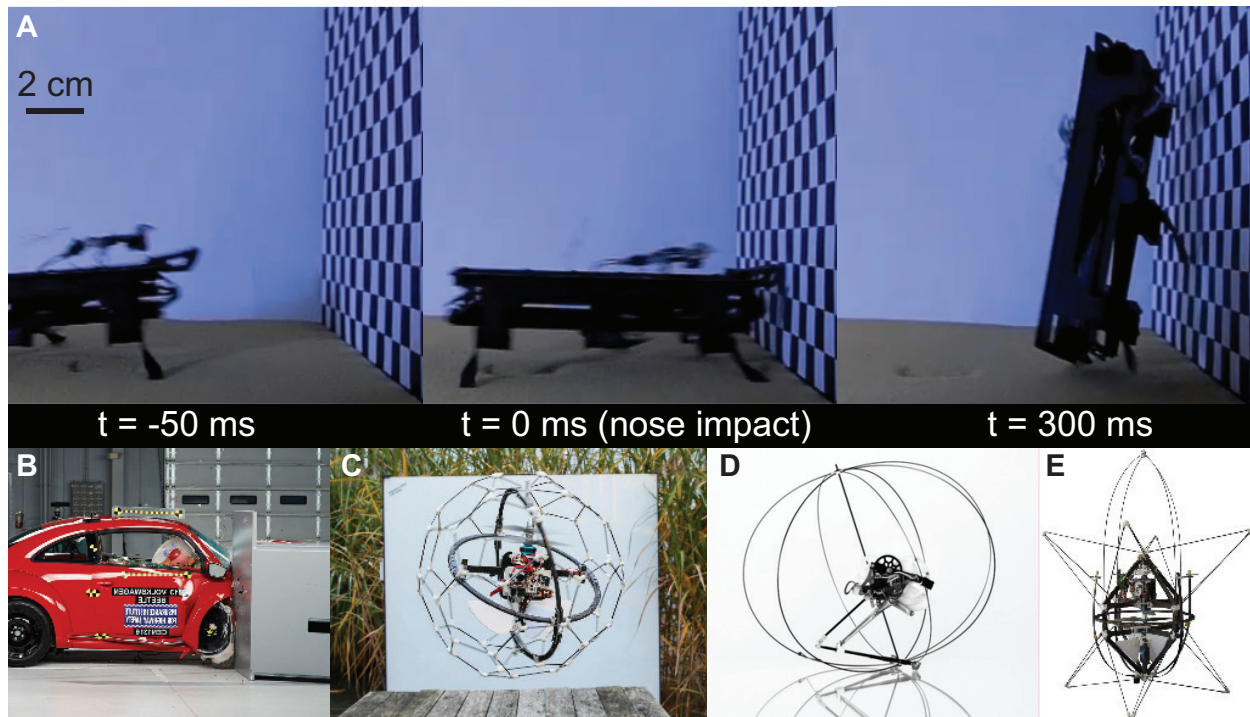
Figure 2.11: Robustness in human technologies - robots, cars.
(A) Dynamic Autonomous Sprawled Hexapod Robot (DASH)(6) performing a rapid head-first impact transition with no sensory input. It robust construction enables it to perform high-speed maneuvers without suffering damage.
(B) Volkswagen Beetle after incurring significant damages during a frontal impact crash test (*Courtesy: Insurance Institute for Highway Safety, www.iihs.org*). A typical coefficient of restitution for a front automobile bumper is $\approx$0.3 or 91% energy absorption.
(C) Gimball robot with passive exoskeletal cage to utilize collisions for maneuvering in cluttered environments.
(D) Miniature (7g) jumping robot (7) with self-recovery capabilities enabled by the robust exoskeletal cage.
(E) Airburr (8), an indoor flying robot designed specifically to withstand collision and self-maneuver utilizing a shock-absorbing exoskeleton.

Chapter 3

Fault Tolerance I: Loss of Feet

3.1 Summary

Cockroaches possess specialized attachment mechanisms such as claws, sticky pads, friction pads etc. on their feet to grip multiple surfaces enabling behaviors like climbing and inverted walking. However, relatively little is known about the effect in case of damage or loss of these structures on animal performance. High-speed video revealed that cockroaches relied on large mechanosensory tibial spines on their legs upon removal of tarsi to run across flat and rough surfaces without any significant changes in velocity, stride length, stride frequency or duty factor relative to their intact state. Further, cockroaches produced identical ground reaction forces before and after complete tarsi ablation providing no evidence for spring-like or damper-like mechanical function for feet like in humans and other vertebrates. Although successful at stabilizing locomotion on rough surfaces without tarsi, when challenged further by applying large lateral impulses, tarsiless cockroaches took longer to arrest body rotations than when intact and unable to recover completely. Further, they were able to climb up near vertical inclination without claws and even the entire tarsi by using tibial spines to interlock with the rough substrate without changing velocity, stride length or stride frequency. However, with spines ablated, cockroaches could only climb small inclines at reduced velocities by taking smaller steps and cycling their legs slower. Climbing on smooth surfaces required all tarsal structures expect claws. In order to compensate for the loss of tarsi, cockroaches made several postural adjustments including arching their body to facilitate spines engagement, pushing their abdomen into the wall to prevent pitching backwards and adopting wide stance to enhance passive stability. Incorporating fault tolerant animal-inspired mechanisms like leg spines into design of feet adds robustness to locomotion, prevent catastrophic failure and prompt the development of next generation of novel legged robots with multi-terrain capabilities.

3.2   Foot structure and Function

Animals locomote on substrates that vary in the probability of surface contact [16], type of footholds [58] and degree of compliance [73] and flow [59]. To meet these challenges, they have evolved a wide variety of pedal structures to attain effective substrate interaction during different locomotory tasks such as running [31][120][3], climbing [128][12], brachiating [95] and swimming [2]. Among insects, the tarsus functions as a foot with a variety of attachment mechanisms used for locomotion in natural habitats such as running over leaf litter [56], climbing up plant stems [129] or escaping predators [108]. The structure and function of such attachment devices have been characterized in various insect groups including beetles [130][131][132][133], locusts [134][135][61], earwigs, cockroaches [136][137], flies [138][139][54], stick insects [140], and hymenopterans [57]. Numerous studies have investigated the attachment ability of insects on different substrates to elucidate the substrate-dependent performance [134][135][61][136][137][138][139][54] [140][57]. Most of the research has focused on the adhesive [57][141][142][143] or hairy attachment pads specialized for rather smooth substrates. Fewer studies have focused rough surface interactions demonstrating that attachment structures like claws [130][144] and tarsal spurs [132][133][16] interlock with surface asperities or penetrate soft substrates to enable locomotion even on complex terrain such as thin rods[133]. Despite the wealth of research on structure and function of numerous attachment mechanisms, a recent study revealed that arthropods and echnioderms in general, and insects in particular, rarely possess 'intact' leg structures including tarsi in their natural habitats [145]. And yet, very little is known about how animals accommodate their reduced condition or compensate for their loss of tarsal structures.

Cockroaches possess highly specialized, complex feet called tarsi with three distinct attachment mechanisms - claws (hooks), arolium (sticky pads) and euplantulae (friction pads), the relative size, form and structure of which vary across different species. When intact, cockroach tarsi can be differentiated into five segments altogether (Fig. 3.6). The first four segments of the tarsus contain frictional pads called the euplantula and serve as the main ground reaction force producing structures during walking and climbing on numerous surfaces with varying levels of friction. The euplantulae have been demonstrated not to act as adhesive organs, but rather as anisotropic frictional mechanisms used to power locomotion by being more effective when pushing against a surface away from the body [55][146]. The fifth segment found at the distal end of the tarsus, also called the pretarsus, is composed of a triangular adhesive pad called the arolium surrounded by two pretarsal claws [128]. The arolium is the primary adhesive organ of the cockroach foot and is utilized for climbing and adhering onto smooth surfaces such as glass or wax [147][146]. The arolium is activated when the leg exerts inward pulling forces towards the body, and thus, cockroaches can also distribute the load between the euplantulae and arolium or switch roles depending on whether their legs are pushing or pulling such as during climbing up or down a vertical wall [131]. The pretarsal claws allow cockroaches to grip and move over rough surfaces by interlocking with surface asperities. During high-speed running on level terrain, the claws along with rest of pretarsus are held up and typically do not make contact with the ground substrate

[137], however, studies have demonstrated their utility during inverted walking (Frantsevich) and vertical wall climbing [128][32]. Assisting the tarsus are numerous mechanosensory structures [148][149] in and around the tarsus that are known to provide feedback about temperature, load [150], and surface texture [151] to direct leg control and modulate behavior. In particular, large mechanosensory hairs at base of the tibia-tarsus joint have been shown to serve an additional mechanical function by aiding mesh running [16] and have been hypothesized to also assist in release of arolium on smooth surfaces [128]. In addition to possessing specialized structures, the cockroach tarsus is highly flexible and complaint. With the tarsal segments arranged as an articulated chain, the tarsus can easily conform to a wide variety of surfaces to provide effective attachment.

Here, we explore the capability of cockroach to locomote effectively with damaged or reduced feet-like surface attachment mechanisms. We chose the false death-headÕs cockroach, *Blaberus discoidalis*, because of its high-speed running [31], maneuverability [35], stability [87] and adeptness at climbing [32][33]. First, we hypothesized that cockroach tarsi significantly enhance locomotion on flat terrain. To establish a baseline performance, we ran intact animals on a flat terrain equipped with a force platform and measured their steady state kinematics and ground reaction force patterns. We then ablated the tarsi at the tibia-tarsus joint from all six legs, repeated the experiment and compared their running velocity, stride length, frequency and duty factor as indicators of performance before and after ablation. After observing that cockroaches could run even with complete tarsi ablation, we suspected that tarsi might play a mechanical function to increase locomotor effectiveness and hypothesized that tarsi are employed to (1) modulate leg forces and manage energy storage and return by acting like springs, (2) dissipate leg-substrate impact energy acting like dampers, (3) mitigate the effect of rough terrain acting like stabilizers, and (4) reject large lateral perturbations to aid recovery again acting like stabilizers. We tested the spring and damper like behavior of tarsi by comparing the ground reaction patterns in intact and tarsi-less animals as they ran over force platforms on flat terrain. To test stabilizer-like tarsal action, we exposed the animals to two sets of perturbation. First, we compared velocities of cockroaches intact and post ablation, as they ran over rough terrain where the changes in surface heights were over three times their hip heights and experienced perturbations along pitch, yaw and roll axes [3]. Next, we applied large lateral impulses perpendicular to the direction of cockroach motion by running them over a rapidly accelerating cart [88]. We computed the time required to stop body rotation as a result of perturbation and, measured the difference between the final body orientation and the initial direction of locomotion. By comparing these metrics before and after ablation in the same individuals, we identified the importance of tarsi in perturbation rejection and recovery.

Finally, we challenged cockroaches further by having them climb inclined surfaces after each of four successive tarsal ablations. Based on previous literature [128][147], we expected a significant decrease in climbing abilities and hypothesized that tibial spines might be ineffective as attachment devices while climbing on inclines. To test our hypotheses, we encouraged cockroaches to climb up a curved incline track under two friction conditions and, in each case, measured the angle at which they failed by either falling backwards off the

track or slipping downwards along the curved surface [128]. We also utilized high-speed videography to observe detailed kinematics of climbing in cockroaches on a high-friction flat glassbead surface at multiple inclination angles and calculated velocity, stride length, frequency and duty factor at each inclination. Using the above metrics, we compared the climbing performance of intact and tarsiless animals.

Investigation of fault tolerance in the hierarchically structured cockroach foot can inspire the development of novel robots with multi-terrain capabilities and robust performance.

3.3 Methods and Materials

Animals

We used 20 adult male cockroaches, *Blaberus discoidalis*, (Mulberry farms, Fallbrook, CA, USA) with an average mass of 2.17 ± 0.23 g (mean $\pm$ s.d.). Prior to experimentation, cockroaches were kept in communal plastic containers at room temperature (22^0C) on a 12h:12h light dark cycle and provided water and food (fruit and dog chow) ad libitum.

Animal Experimental Design and Protocol

All experiments were performed at 30 ± 2^0C (mean $\pm$ s.d.). Before starting any experiment, each cockroach was marked with retro-reflective paint on the dorsal surface - two on the pronotum, one at the base of the abdomen, one at the tip of tibia-tarsus joint of each hind leg to aid tracking. The dorsal body markers were used to calculate running velocity and body angle changes, whereas the leg markers were used to estimate gait, duty factor, stride length and period. To encourage the animals to perform, we elicited an escape response by light stimulation of their cerci or by gentle blowing. We attained a balanced experimental design by running the same animal across each of the different conditions for a minimum of five (and a maximum of eight) trials. Thus, each individual served as its own control allowing us to use paired statistics.

Kinematics

We recorded videos of cockroaches at 500 frames s^{-1} with a resolution of 1280 by 1024 pixels using synchronized high-speed video cameras. One camera was positioned directly above the track, capturing the top view, and the other recorded the side view. Images were buffered through the camera memory until post-triggering, after which a video clip (4 s) from each camera was reviewed and cropped to the relevant time segment. All video capture, downloading, and conversion were done with a proprietary software program (AOS Studio). We determined the kinematics of the behavior from the videos using custom motion tracking software.

Statistics

We used repeated measures analysis of variance (ANOVA) and Cochran-Mantel-Haenszel tests for continuous and nominal variables respectively with Tukey HSD for post-hoc contrast analyses in JMP software (SAS Inc.). A repeated measures design with a mixed model was used to determine the effect of condition. In our model, the condition (tarsal state) was included as a fixed effect while the animal was included as a random effect. The response was our performance metrics which including running velocity, stride period, and stride length. We used a standard least squares personality with reduced maximum likelihood (REML) as our method to fit our data. We report the P-value, F-ratio in American Psychological Association (APA) format to support/reject our hypothesis as appropriate. For categorical responses (success), we report the χ^2 value.

Flat Terrain

To measure cockroaches' running performance on flat terrain, we constructed a 100 cm long clear acrylic track, 10 cm wide and 10 cm tall, with a custom-built force platform (10 cm by 10 cm, natural frequency $\approx$ 500 Hz; [31]) installed at the center (Fig. 3.1). The bottom surface of the track was lined with balsa wood to act as the running substrate. Our setup was mounted onto a vibration isolation platform (Newport Corp.) and enabled simultaneous recording of high-speed video data for kinematics and three axis force data for center of mass dynamics with a force resolution of ± 0.5 mN in each direction. The force measurements reported in the study were low-pass filtered at 350 Hz.

To determine the mechanical role of tarsi on cockroach running, we measured performance by running the animals down the track before and after complete tarsi ablation (Fig. 3.1 3.6). All cockroaches used in the experiments were visually inspected for damage or accidental loss of any tarsal structures prior to the intact trials. We then ablated the tarsi on all legs at the tibia-tarsus joint leaving the tibial spines intact and cauterized the wounds immediately to prevent heamolymph leakage. We only accepted trials where the animals ran a minimum distance of 25 cm. We rejected trials where (1) the cockroaches slowed down, stopped or tried to climb the wall, (2) their body (including the legs) collided with the side-wall, and/or (3) they exhibited turns of more than 300. We computed running velocity, stride frequency and length, duty factor, peak vertical and horizontal ground reaction forces as the appropriate performance metrics for a total of 63 valid trials across 5 animals.

Rough Terrain

To simulate cockroaches running over rough terrain, we constructed an artificial wooden terrain with a random distribution of surface heights as described in Sponberg and Full [3]. The rough terrain surface was constructed using 1 cm by 1 cm variable height blocks of wood formed into a track 22 cm long by 10 cm wide (Fig. 3.2). The height of each block was randomly assigned to a value selected from a Gaussian distribution with a mean of zero and

a standard deviation of 0.5 cm (i.e. near cockroach 'hip' or coxa-body joint height), so that perturbations in the running surface reached up to three times the cockroach's hip height. We attached 30 cm-long flat balsa wood tracks to the beginning and end of the rough terrain to allow the cockroach to encounter and leave the blocks without stopping. Clear acrylic walls along the trackway restricted the cockroach to running along the track. The terrain was raised by approximately 2 cm with respect to the approach and exit trackways to ensure that the cockroach always encountered a large initial and final step perturbation (2Ð4 cm) during running. The resulting rough terrain produced a mean perturbation of about 30^0 in pitch, 25^0 in yaw and 35^0 in roll per stride [3]. To determine the role of cockroach tarsi in mitigating the effects of perturbations on rough terrain, we compared running velocities before and after complete tarsi ablation similar to the flat terrain experiments. We accepted a total of 70 trials from 4 cockroaches where they ran along the middle of the track without making any side-wall contact.

Large Lateral Perturbation

To expose the cockroaches to perturbations larger than the rough terrain and test their lateral stability [88], we constructed a custom setup (Fig. 3.3) consisting of a cart that we accelerated at a right angle to the direction of the cockroaches' motion using a pre-loaded elastic pulley held fast by a magnetic lock as described by Revzan et al. [88]. When released, the cart translated with an acceleration of 1.9 ± 0.2 g over a duration of 100 ms and continued with a constant velocity until it hit breaking pads at the end of its track. Cart travel distance was nearly 1 m - sufficiently long so that in all analyzed trials the animal finished running the length of the cart before the final braking deceleration. The surface of the cart was lined with retroreflective paper that provided an adequate grip for the cockroach tarsi and made it easy to track its movements.

We induced lateral perturbations by having animals run along a fixed trackway and onto the cart. As soon as the animal was on the cart completely, we released the magnetic lock holding the cart in place, thereby rapidly accelerating the cart. Using the above protocol, we ran the animals with intact tarsi first, followed by complete tarsi ablation as described for flat terrain experiments. We collected a total of 35 trials from 3 animals. For our performance metrics, we defined perturbation rejected time as the time between the release of the magnetic lock to the end of body rotation, and change in body orientation, as the difference in body orientation between the initial direction of travel before perturbation and final direction of travel prior to reaching the end of the cart. Any trials where the animals stopped running on the cart or touched its side-walls were rejected from our dataset.

Continuously Varying Inclined Terrain

To measure cockroaches' climbing performance, we constructed a curved track 10 cm wide and about 100 cm long (Fig. 3.4) using clear acrylic. The curved portion of the track had a uniform radius of 50 cm and was about 77 cm long extending from 0^0 to 90^0 with respect to

the vertical. Beyond the curved section, the track extended further at both ends allowing a horizontal segment of about 13 cm and a vertical segment of 10 cm. The horizontal segment included a resting area and enabled cockroaches to obtain a running start onto the curved portion. The vertical segment had a shelter for cockroaches after they completed climbing the curved portion. Large, clear acrylic walls prevented the animals from leaving the track and enabled filming high-speed video from the side. The surface of the track was easily variable and can either be high friction, comprising of a uniform layer of 700 μm circular glass microbeads glued onto retroreflective paper, or low friction, uncoated acrylic.

We tested cockroaches' climbing performance using two substrates Đ glass-beads and acrylic. For each substrate, we measured a cockroach's ability to climb under four conditions (Fig. 3.6) of tarsal manipulation: (1)*Intact*, where all tarsi were visually inspected to be damage free, (2) *Claw ablation*, where only the two claws on the pretarsus were clipped using surgical knives leaving other attachment mechanisms (arolium, euplantulae) and all tarsal segments intact, (3) *Tarsus ablation*, where the entire tarsus was surgically removed at the tibia-tarsus joint leaving no tarsal attachment mechanisms available for gripping a substrate. The tip of the tibia with the most distal tibial spines made ground contact allowing the possibility of interlocking with a suitable substrate, and (4) *Total ablation*, where in addition to the entire tarsus, the most distal tibial spines are also ablated leaving a rounded peg-like tibia to make ground contact. We attempted to ablate the euplantulae as an intermediate manipulation between claw and tarsus ablation, but found it difficult to manage while preserving the mechanical integrity of the tarsal structure.

To determine climbing performance, we analyzed a total of 196 trials from 4 animals and measured the failure angle defined as the instantaneous slope at the highest point along the track reached by the animal before it slipped or fell backwards. Our operational definition for a valid trial included climbing continuously without slowing or stopping and no body or leg contact with the side-walls of the setup.

Inclined Flat Terrain

To obtain detailed kinematics of cockroach inclined climbing, we constructed a clear acrylic track 50 cm long, 10 cm wide and 10 cm tall. One end of the track was mounted onto a friction-locking adjustable hinge that enabled us to rotate the entire track to any desired inclination between 0^0 and 90^0 with respect to the horizontal and secure it in place (Fig. 3.5). A mirror was rigidly mounted onto the farther walls of the track at an angle of 45^0 with respect to the track ground surface. This allowed us to capture top and side views of the cockroach while climbing using a single high-speed camera. The substrate of the track comprised of a uniform layer of 700 μm circular microglass beads. To encourage the animals to climb along the inclined track, we gently stimulated the cerci and induced an escape response. We collected a total of 266 trials from 4 animals across six different inclinations Đ 0^0, 30^0, 45^0, 60^0, 75^0, 90^0 before and after complete tarsi ablation. Using high-speed videography, we calculated running velocity, stride frequency, stride length and duty factor as the relevant performance metrics for each angle. Valid trials involved continuous climbing

with stopping for at least 15 cm, no body or leg contact with side-walls and no turns more than 30^0.

3.4 Running on Flat Terrain

The false death head cockroach (2.17±0.23 g, 41.15±3.63 mm), *Blaberus discoidalis*, rapidly ran along flat terrain before and after complete tarsi ablation at velocities approaching 60 cm s^{-1} using an alternating tripod gait (Movies). High speed kinematic analyses of marked animals revealed that velocity (57.68±6.03 cm s^{-1}; ANOVA, P=0.65, $F_{1,57}$=0.44) remained statistically similar before and after tarsi manipulation suggesting that the loss of tarsi did not affect this metric of the animals' running performance (Fig. 3.7). Further analyses revealed that cockroaches did not significantly change their stride frequency (16.27±1.45 Hz; ANOVA, P=0.32, $F_{1,57}$=0.95; Fig. **??**) or length (3.54±0.45 cm; ANOVA, P=0.39, $F_{1,57}$=1.01; Fig. 3.9) or duty factor (0.43±0.06; ANOVA, P=0.17, $F_{1,57}$=2.03; Fig. **??**) to compensate for tarsi ablation and thus rejecting our hypothesis that tarsal presence was critical to maintaining performance while running on flat terrain. This provided the first evidence that tibial spines (Fig. 3.6) which made ground substrate contact after complete tarsi ablation could act as 'feet' permitting sufficient traction for flat terrain locomotion.

To test our hypotheses concerning the mechanical role of tarsi on flat terrain, we ran the animals over a force platform (Fig. 3.2) and compared the ground reaction forces. The vertical and horizontal force patterns (Fig. 3.10), before and after tarsi ablation, were remarkably similar and consistent with sagittal plane spring-mass like dynamics [116] associated with high-speed running. We also measured no significant differences in the peak-to-peak vertical (30.31±3.56 mN; ANOVA, P=0.26, $F_{1,57}$=1.34) or horizontal forces (14.21±2.97; ANOVA, P=0.30, $F_{1,57}$=1.18; Fig. 3.11) produced by animals in intact and tarsi-less conditions. The lateral force pattern and peak-peak magnitude (12.40±2.19; ANOVA, P=0.21, $F_{1,57}$=1.88) was unaffected by tarsal ablation. We therefore reject our hypothesis that cockroach tarsi are necessary for spring-like locomotion behavior such as modulation leg forces or managing energy storage and return. Further, we did not find any collision peaks early in stance, unlike during heel striking in humans, after tarsi ablation (Fig. 3.10). This indicates that the cockroach tarsi are not necessary to dissipate leg-ground impacts and unlikely to perform a damper-like role during flat terrain locomotion. Tibial spines and legs can effectively substitute for the tarsi in these conditions.

3.5 Running on Rough Terrain

To test our hypothesis about role of tarsi in perturbation rejection, we challenged cockroaches to run over rough terrain (Fig. 3.2; Movies) and measured their mean velocity of locomotion in intact and tarsi-less conditions. Surprisingly, cockroaches, before and after complete tarsi ablation, show no significant differences in running velocities (35.69±4.17 cm

s^{-1}; ANOVA, P=0.63, F$_{1,66}$=0.55; Fig. 3.12) despite having to overcome obstacles nearly three times their hip height. Video evidence revealed that tibial spines could not only interlock within the interstices of the rough terrain, but also could effectively engage along the surface of wooden blocks to provide effective propulsion. Therefore, the tibial spines, comparable in tip radius size to the tarsal claws [130], are capable of preventing any loss in performance even on rough terrain and provide robustness to the cockroach locomotion system.

3.6 Running during Large Lateral Perturbations

We challenged animals further by applying a large lateral impulse (Fig. 3.3) before and after complete tarsi ablation. As the animals entered the cart, we accelerated it rapidly perpendicular (to the left) to the direction of the initial cockroach motion. This perturbation caused cockroaches to rotate in the counterclockwise direction as observed from top view camera until they slid to a halt (Movies). Intact animals tried to activate their claws, most notably the inside front tarsus, to arrest their body rotation and reject the perturbation within three stride periods (147.15±24.32 ms). Animals recovered their initial body orientation with respect to the direction of travel before the perturbation and often overcompensated to yield the net positive change in body orientation (9.37±19.68^0; Fig. 3.13) by the time they reached the end of the cart (Movie). In contrast, tarsi-less animals took significantly longer (253±26.61 ms; ANOVA, P<0.01, F$_{1,33}$=9.34; Fig. 3.14) to reject the perturbation and showed significantly reduced recovery (-40.15±21.54^0; ANOVA, P<0.01, F$_{1,33}$=11.36; Fig. 3.15) to body orientation before perturbation (Movie). High-speed videography also revealed increased slipping in animals post ablation due to lack of adequate attachment mechanisms. Instead, these animals adopted a wide stance and repositioned their legs, in particular the outer ones, to orient the tibial spines for effective engagement into the substrate to reject the perturbation and aid recovery. These results highlight the importance of tarsal structures and greater effectiveness compared to tibial spines in stabilizing locomotion from large perturbations. Further, based on these observations, we can generate two future hypotheses about the possible mechanisms by which the tarsus performs perturbation rejections and aids recovery. First, the mechanical properties of the tarsus might enable it to behave as a torsional spring to passively help recover body orientation. Second, the tarsus might act like a sensor and provide valuable feedback from its various of mechanosensory structures [150][152] to the cockroach neuromechanical controller [79] that enables the animal to estimate the magnitude of perturbation and take necessary recovery action. Future experiments involving both mechanical characterizations of the tarsus [153][15] and electromyogram recordings from muscles controlling the tarsal structures [137] are clearly needed to test the above hypotheses and reveal the underlying control mechanisms.

3.7   Climbing on Continuously Variable Inclined Terrain

Having demonstrated that tibial spines are robust structures capable of sufficiently substituting for the tarsi and functioning as feet on flat and rough terrain, we examined their effectiveness during climbing. We tested climbing performance on glass-bead (high friction) and acrylic (low friction) substrates at each of the four levels of tarsi manipulation Ð intact, claw ablation, tarsus ablation and total (tarsus+spine) ablation (Fig. 3.6, see Methods for details) by running the animals up a curved track (Fig. 3.5) and measuring their failure angle defined as the instantaneous slope at the highest point along the track reached by the animal before it slipped or fell backwards.

Surprisingly, on the glass-bead surface, intact animals (89.27 ± 2.68^0), claw ablated (85.63 ± 6.14^0) and tarsus ablated (82.63 ± 8.63^0) showed statistically similar (Turkey HSD) high performance, failing only at near vertical angles (Fig. 3.16). However, after total ablation of spines and tarsi, cockroaches failed at significantly (ANOVA, P=0.02, $F_{3,94}$=6.57) lower angles (29.55 ± 7.48^0; Fig. 3.16). This decreased performance indicates that spines are necessary for climbing inclines greater than 30^0 and sufficient even at near vertical inclinations on surfaces that allowed spines to interlock. High-speed videos revealed that claw and tarsi ablated animals failed by pitching backwards and tumbling at steep inclines. No failure was observed in intact animals. This demonstrates a major function of the claw is to provide inward pulling ground reaction forces to prevent pitch-back failure. None of the other tarsal structures or the spines can perform this function adequately resulting in failure at near vertical angles. However, both the euplantulae and spines can sufficiently contribute towards force production to enable the animal to overcome gravity even on steep inclines.

In contrast, on the acrylic surface, intact (58.68 ± 7.71^0) and claw ablated (59.34 ± 4.16^0) animals showed the best climbing performance reaching about 60^0 of inclination (Fig. 3.17). Further, this suggests that presence of tarsal claws is not critical for climbing low friction substrates. But, once the tarsi were removed, the animals performed significantly (ANOVA, P=0.01, $F_{1,89}$=8.86) poorly in both tarsi ablated (22.51 ± 4.43^0) and total ablated (21.97 ± 5.11^0) conditions. This decreased performance highlights the importance of the tarsal structures (euplantulae and arolium) for climbing smooth surfaces and provides opportunities for future experiments to tease out their relative importance. In addition, the mode of failure on the low friction surface was by slipping or sliding backwards unlike the high friction condition indicating insufficient thrust from the feet to overcome gravity and propel the animal forward.

3.8   Climbing on Inclined Flat Terrain

Given cockroaches' climbing performance without tarsi on the curved track setup on the glass-bead substrate, we investigated the role of spines further during climbing on different inclinations using an inclined flat terrain setup (Fig. 3.5) and tested performance before and after tarsi ablation at 0^0, 30^0, 45^0, 60^0, 75^0 and 90^0 inclines. Intact cockroaches climbed

with velocities steadily decreasing with increases in the angle of incline (64.31 ± 9.15 cm s^{-1} at 0^0 to 27.77 ± 4.63 cm s^{-1} at 90^0; Fig. 3.18). The animals decreased both stride length (3.86 ± 0.69 cm at 0^0 to 2.75 ± 0.29 cm at 90^0; Fig 3.19) and stride frequency (16.11 ± 2.27 Hz at 0^0 to 9.89 ± 1.75 Hz at 90^0; Fig. 3.20) while climbing increasing inclinations to produce the observed trends in velocity. No gait changes were observed with elevation changes as cockroaches used an alternating tripod gait at all instances. Similar to their performance in intact conditions, cockroaches exhibited decreasing velocities (59.79 ± 9.34 cm s^{-1} at 0^0 to 4.65 ± 2.72 cm s^{-1} at 90^0), stride lengths (3.94 ± 0.72 cm at 0^0 to 0.71 ± 0.11 cm at 90^0) and stride frequencies (14.86 ± 2.56 Hz at 0^0 to 5.04 ± 3.22 Hz at 90^0) with increases in inclination angles post tarsi ablation. However, beyond inclinations of 450, cockroaches ran significantly slower (ANOVA, P=0.01, $F_{1,260}$=14.32), cycled their legs significantly less frequently (ANOVA, P=0.01, $F_{1,260}$=19.73) and took significantly shorter strides (ANOVA, P=0.01, $F_{1,260}$=15.64) after tarsi ablation than when intact. Additionally, they were unable to maintain an alternating tripod gait at steep elevations (75^0 and above) and exhibited frequent loss of footing resulting in slipping after loss of tarsi and thus reduced overall performance. Despite the above differences in kinematic parameters, cockroaches maintained a nearly constant duty factor (0.49 ± 0.03; ANOVA, P=0.45, $F_{1,260}$=0.64) across all angles of inclination (Fig. 3.21) in both intact and tarsi-less conditions. The findings so far indicate that tibial spines can act as feet by interlocking with ground substrate and effectively replace the tarsal functions at inclination angles up to 60^0.

3.9 Postural Control for Fault Tolerant Performance

As noted previously, the tibial spines are distally pointed and therefore, can only interlock with surfaces when legs are pushing into the surface and away from the body. After tarsus ablation, this condition is 'naturally' imposed on the animal when running on horizontal surfaces enabling the spines to produce ground reaction forces to support body weight and push away the center of mass away the ground substrate. However, on inclined surfaces, due to the morphology and kinematics of the leg, the ideal orientation for force production using tarsi is not maintained on all legs depending on the inclination. Consider the case of vertical climbing (Fig. 3.23). The front legs touch down in front of the animalÕs head and cycle towards the body during stance enabling the proximally pointing claws to produce forces pulling the animal into the surface and preventing excessive pitch back. However, once tarsi are ablated, spines that now contact the ground are distally oriented away from the leg and are more likely to collapse onto the tibia passively rather than engage the substrate. The situation is similar for the middle leg spines, but less pronounced. Only the spines on the hind legs are oriented correctly to produce propulsive forces. Therefore, to apply maximum force parallel to the incline and overcome gravity, cockroaches reoriented their legs such that the tibial spines on all the legs were pointed downward, in the direction of gravity, and climbed upwards effectively (Fig. 3.23).

Another major postural change accompanying the front leg reorientation was adopting

a curved body posture with the abdomen seemingly being pushed into the surface. This behavior was even more evident when the animals lost footing and slipped on the surface especially on a vertical wall. Without this postural adjustment, animals were unable to control backwards body pitching on steep inclinations, as they lack proximally pointed claws, the only structures that can provide inward pulling forces [146] and adequate counter-torques to negate the effect of gravity on the center of mass. In cases, where the cockroaches could not leverage the abdomen maximally, we saw them tumble backwards and fail by 'popping off' the wall surface. This compensatory mechanism can be considered analogous to the 'kickstand reflex' in geckos Jusufi et al., [154] observed when their front feet step on slippery patches while climbing vertical walls. As a reaction to this, the animals swing their tail rapidly into the vertical wall to provide an additional anchor or a 'fifth leg' to help overcome the torque on the body due to gravity and escape failure from pitching too far back.

A third feature of typical climbing without tarsi involved leg reorientation to adopt a splayed posture. Unlike climbing in intact animals where the middle and hind legs were tucked in close to the body and orientated against the direction of travel to provide maximum forward propulsion [32], tarsiless animal tended to touch down with their legs more laterally and thus obtain a larger basin of static stability (Fig. 3.23). This seems to suggest that after loss of tarsal structures, the major compensation for cockroaches climbing vertical walls is likely associated with maintaining stability and preventing failure, and less to do attaining maximal forward speeds.

3.10 Effectiveness of Spines as Feet

By ablating the tarsus completely and leaving the tibial spines intact, we removed all known surface attachments mechanisms and challenged cockroaches to run without feet over a variety of terrain and even overcome large perturbations. We quantified the effectiveness of spines as the ratio of performance of animals after ablation, to their performance before, for a given condition (Fig. 3.22). Contrary to our expectations, tarsi-less cockroaches could easily run on flat or rough terrain without changing their preferred speed, indicating a minimal cost for losing pedal structures or the entire foot itself. Our data suggest that cockroaches are less likely to alter their anti-predator behavior or compromise foraging and feeding as a result of their robustness [145]. For these conditions, the ring of large mechanosensory spines found at the base of the tibia-tarsus joint proved to be a successful compensatory mechanism (effectiveness≈1). These spines are similar in structure and function to the hair sensilla, the most basal of mechanosensors, present all over insect bodies including the antennae, cerci, head, neck and abdomen [155][156][157]. Similar spine structures have been previously implicated in enabling locomotion over terrain with low probabilities of surface contact such as meshes with negligible loss of performance in cockroaches and spiders [16]. Similarily, the large spines on cockroach antennae have been shown to play an important role in manipulating antennae shape for effective wall following by interlocking with surface asperities or corners [155]. This provides evidence that even in the absence of tarsal structures,

cockroaches can use spines as alternate mechanisms that can maintain both function and performance effectively. We contend that the abundance of such mechanisms incorporated into the construction of biological organisms is the reason for their robustness and overall superior performance relative to any human engineered systems.

Spine enabled mesh running and antennal wall following are both behaviors that take advantage of the anisotropic nature of spines. Spines are able to interlock and generate forces when pushing away from the base such as engaging mesh or a wall asperity, but collapsing easily towards the base during leg withdrawal from porous substrates like mesh and sand or, dragging against a wall [16]. Animals running on spines even produced ground reaction patterns indistinguishable to those with tarsi suggesting 'tuning' or matching of mechanical properties between tarsus, ring of spines and the leg. Spine effectiveness was also high ($\approx$1) during climbing on inclines up to 60^0 and rapidly decreased thereafter reaching a minimum on vertical walls ($\approx$0.12; Fig. 3.22). Spines did not assist (effectiveness = 0) climbing at inclines greater than 90^0 or while inverted running. These observations lead us to hypothesize that passive spines are highly effective when the legs push against a surface, but begin to fail when legs generate inwards pulling ground reaction forces [158] for successful behavior. Future experiments involving force measurements on inclined surfaces during climbing will enable us to derive additional metrics to quantify the extent of fault tolerance and consequently robustness in cockroaches.

Therefore, rather than considering just the tarsus as a foot, we must define the cockroach foot as a hierarchical organization consisting of large tibial mechanosensory spines and tarsal structures (euplantulae, claws and arolium) on an articulated chain that includes the whole leg.

3.11 Bio-inspiration and Application to Robotics

In recent years, there has been considerable progress in small, legged robots that can run rapidly and stably over rough terrain [121][122][126][159][44][69][160] utilizing simple leg and foot designs. Without well-tuned leg/foot mechanics, these small legged robots exhibit severely decreased performance in speed, stability, efficiency and even failure in extreme in cases. The fine-tuning of mechanical properties of feet necessary in these physical models prompted our curiosity in investigating the mechanical role of feet in biological organisms. Our studies on the cockroach revealed that the tarsi or 'feet' are not necessary for maintaining spring-mass like ground reaction force patterns and do not affect performance even on rough terrains. By relying on simple, passive, multi-functional structures such as spines on the tibia, cockroaches can achieve effective locomotion as was first hypothesized in studies on cockroaches and spiders running over mesh surfaces utilizing on distributed mechanical feedback [16]. However, under extreme perturbations such as a large lateral impulse, they may be insufficient in completely rejecting perturbations and cause slow recovery. In these cases, specialized structures like claws [161] and adhesive pads [162] serve a critical function and need to be integrated into foot designs for successful locomotion peformance.

Further, climbing and maneuvering on vertical surfaces presents an even more difficult challenge for most robots. While a majority of climbing robots have focused on clinging onto smooth vertical surfaces such as windows and interior walls using suction, magnets or adhesives, very few robots can scale rough surfaces [14] such as brick, concrete, stucco or stone [163][164] and use passively interlocking claw-like mechanisms. However, all of these robots, except the Dyna-Climber, are limited to relatively slow velocities and quasi-static gaits. The key features of biological feet that contribute to impressive animal performance are rapid attachment and detachment mechanisms that take advantage of body dynamics for climbing. Additionally, cockroach tibial spines are directional, require zero or near-zero pull-off force, can generate large forces after only small preloads, and are reusable and resistant to fouling. Inspired by the cockroaches' simple design and effectiveness as passive foot mechanisms, novel dynamic climbing legged robots have been developed [160][165] and rapidly climb steep rough surfaces and even loose cloth [160]. More recent experiments, have demonstrated their enhanced performance during tasks such as load carrying and towing on rough terrain [161]. Integrating passive spines with active attachment mechanisms for rough and smooth surfaces in hierarchical organization will lead to novel robots with multi-terrain robustness.
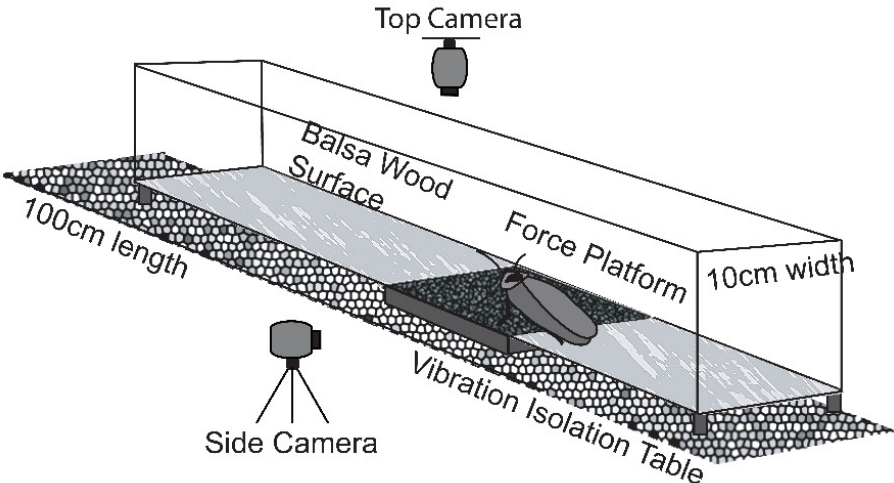
Figure 3.1: Experimental setup for measuring cockroach kinematics using high speed videography and ground reaction forces using a custom built force platform.
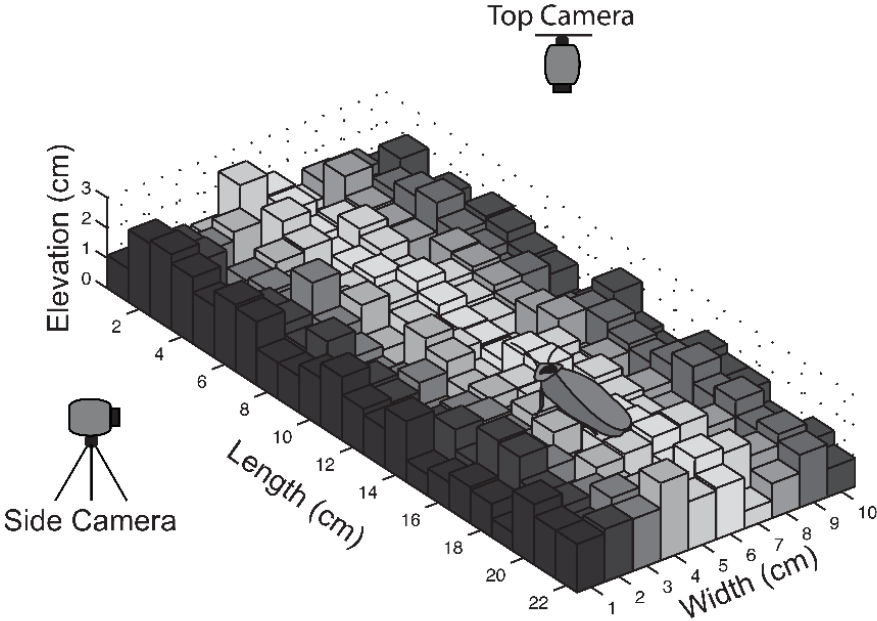
Figure 3.2: Experimental setup for simulating cockroach running on rough terrain. The successive step heights across the track could be as high as 1.5 cm or nearly three times the hip height of the animal. By running over the track, cockroaches experienced perturbations in pitch, yaw and roll directions.
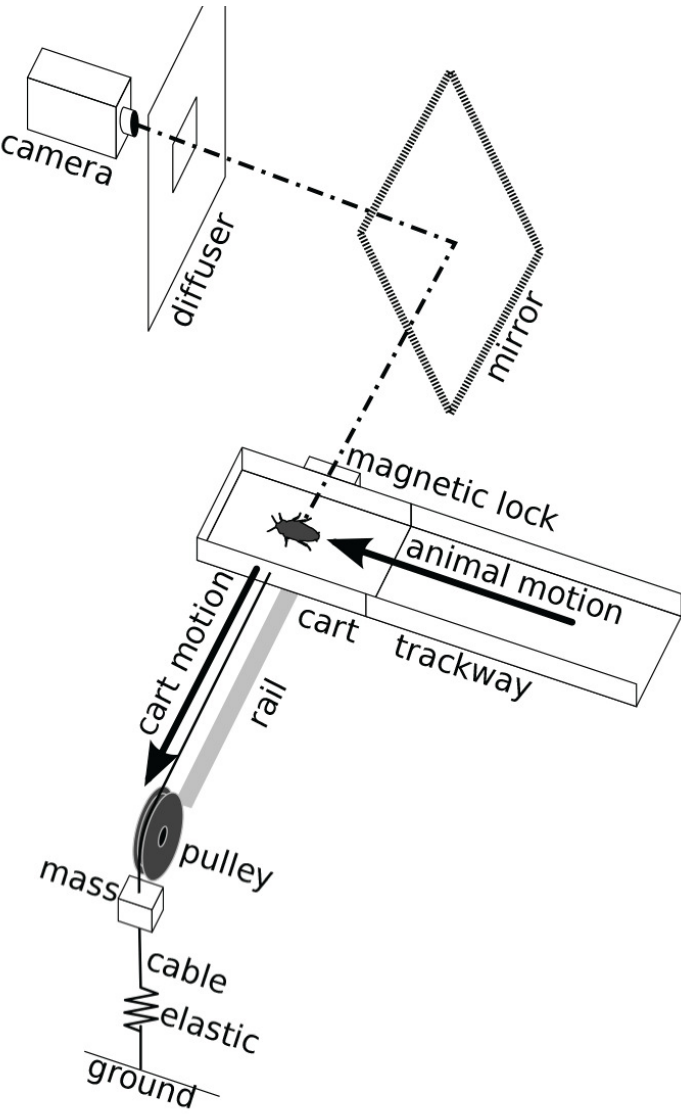
Figure 3.3: Experimental setup for applying a large lateral impulse onto a running cockroach. The animal runs along a trackway onto the cart in the direction indicated. Once the animal enters the cart, the magnetic lock is released accelerating the spring loaded cart sideways at accelerations approaching 2g.
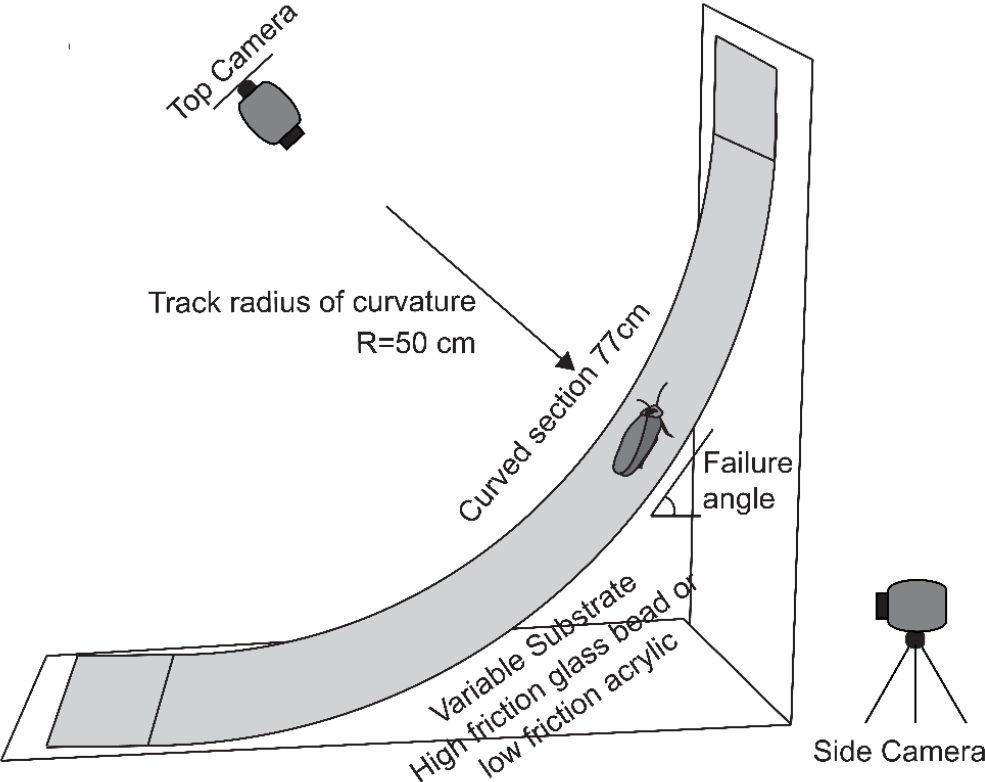
Figure 3.4: Experimental setup to measure failure of cockroaches while climbing with ablated tarsal structures. The surface of the track could be low friction (uncoated acrylic) or high friction (uniform coating of 700 μm glass beads). The radius of the track was 50 cm. The instantaneous slope of the track at the point of cockroach failure (slipping downwards or tumbling backwards) yields the failure angle.
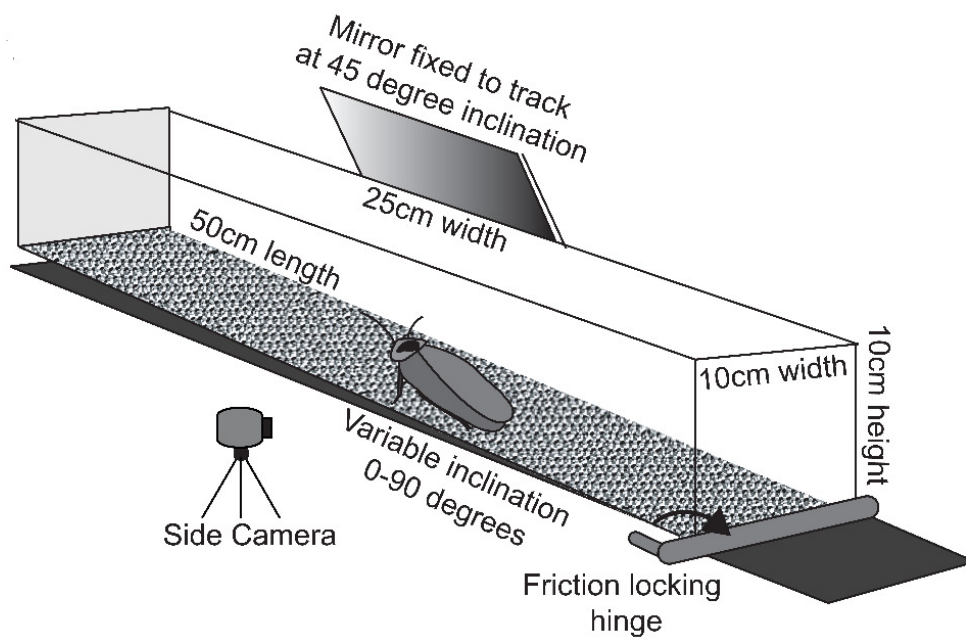
Figure 3.5: Experimental setup to study cockroach kinematics at different inclinations on flat surface covered with 700 μm glass beads. The tracking inclination could be varied between 0 and 90^0 using a friction locking hinge. A mirror mounted at 45^0 to the track enabled the simultaneous capture of side and top views of cockroach climbing using a single camera from side of the track.

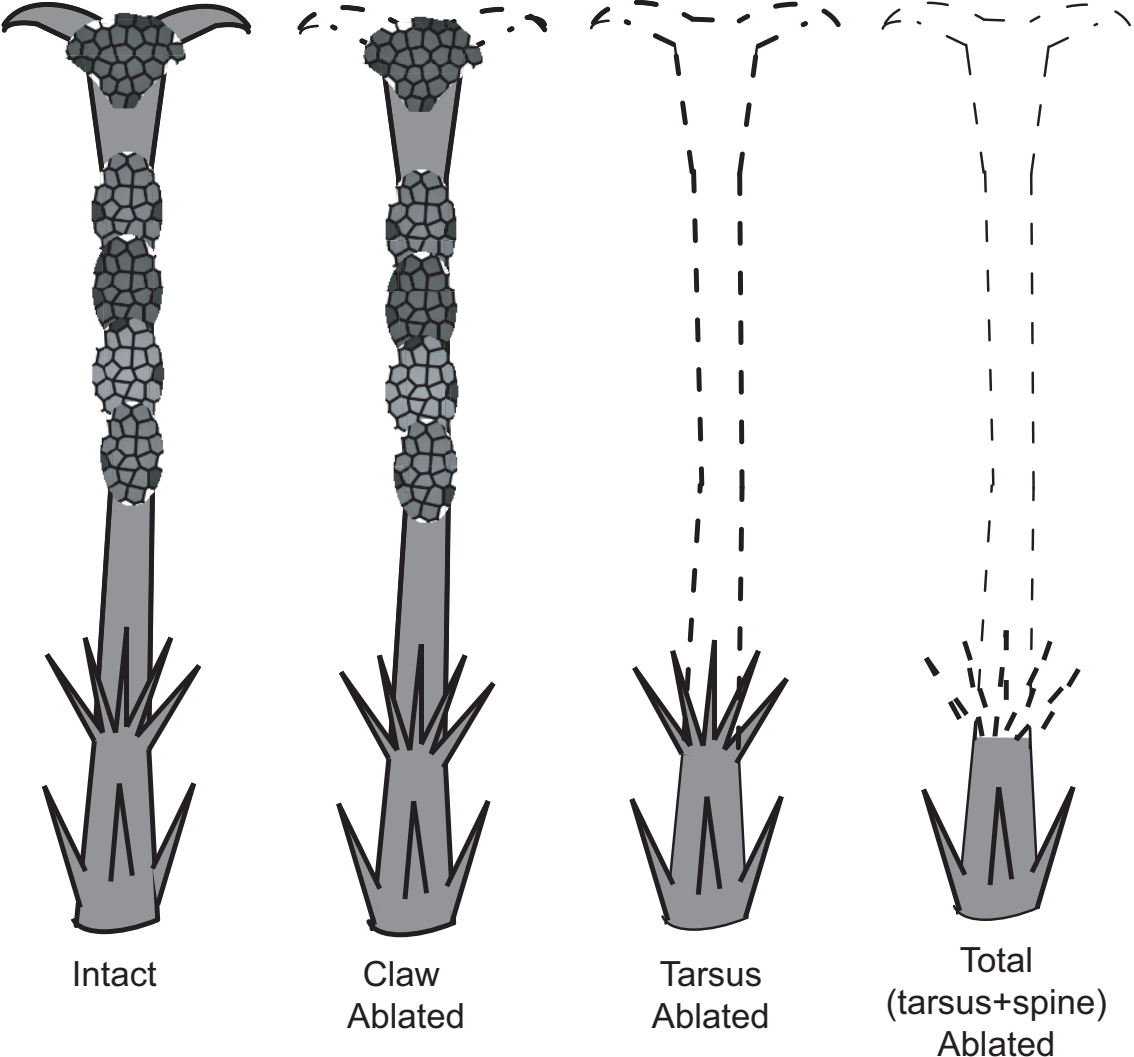Intact | Claw Ablated | Tarsus Ablated | Total (tarsus+spine) Ablated

Figure 3.6: Cartoon illustrating the levels of tarsi manipulation - intact (no structures affected), claw ablated (only the claw is removed leaving arolium and euplantulae intact), tarsus ablation (all tarsal structures are ablated leaving only the tibial spines for foot attachments) and totally ablated (the tarsi and all spines around the tibia-tarsal joint are ablated leaving a rounded peg as foot
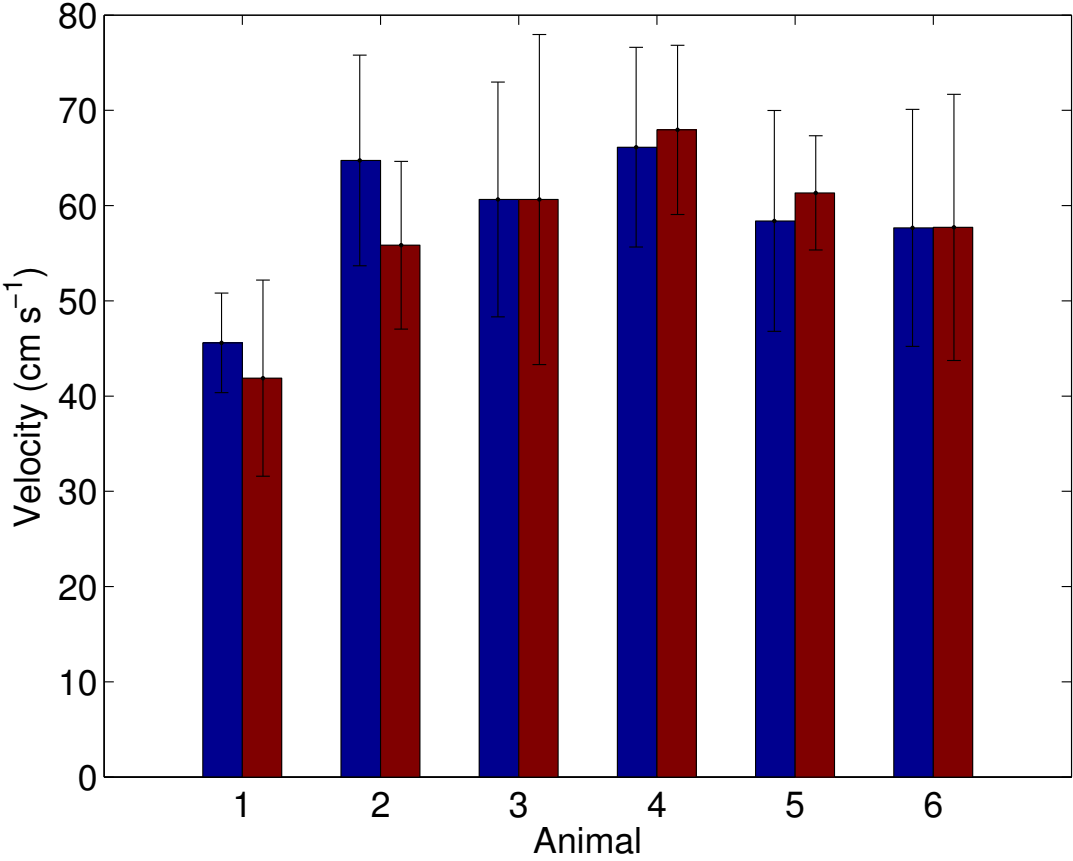
Figure 3.7: Variation of cockroach velocity (cm s^{-1} on flat terrain across animals before and after tarsi ablation. Blue bars represent data for intact animals while red bars represent data for the tarsal ablated condition. Error bars represent mean $\pm$ 1 s.d. Cockroach velocity is not significantly altered by loss of tarsi.
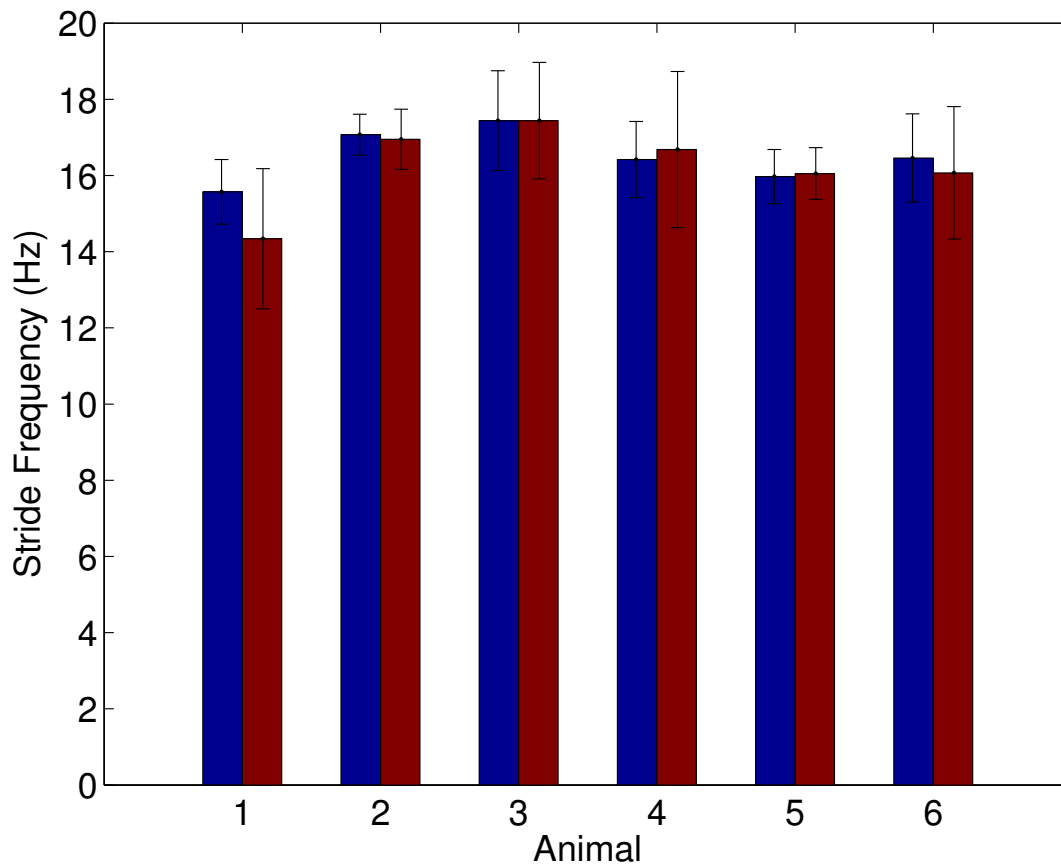
Figure 3.8: Variation of cockroach stride frequency (Hz) on flat terrain across animals before and after tarsi ablation. Blue bars represent data for intact animals while red bars represent data for the tarsal ablated condition. Error bars represent mean ± 1 s.d. Cockroaches do not significantly change their stride frequency after loss of tarsi.
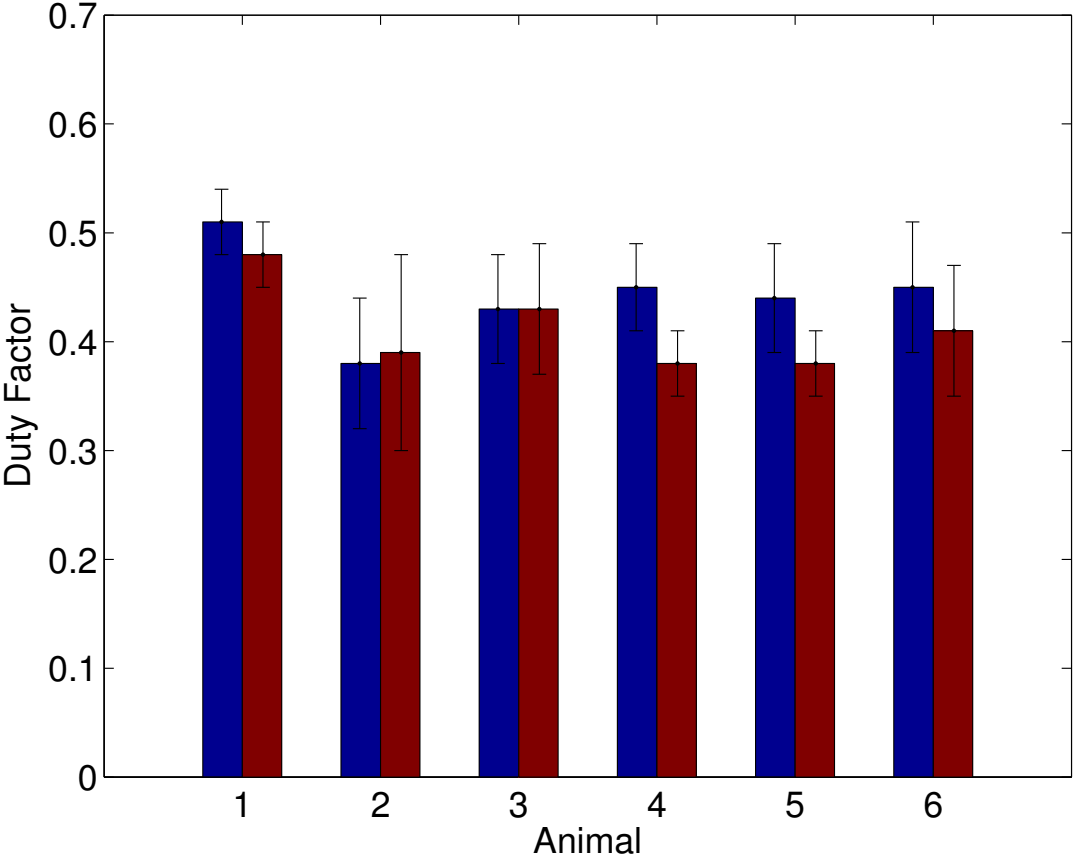
Figure 3.9: Variation of cockroach duty factor on flat terrain across animals before and after tarsi ablation. Blue bars represent data for intact animals while red bars represent data for the tarsal ablated condition. Error bars represent mean ± 1 s.d. Cockroaches do not significantly change their stride frequency after loss of tarsi.
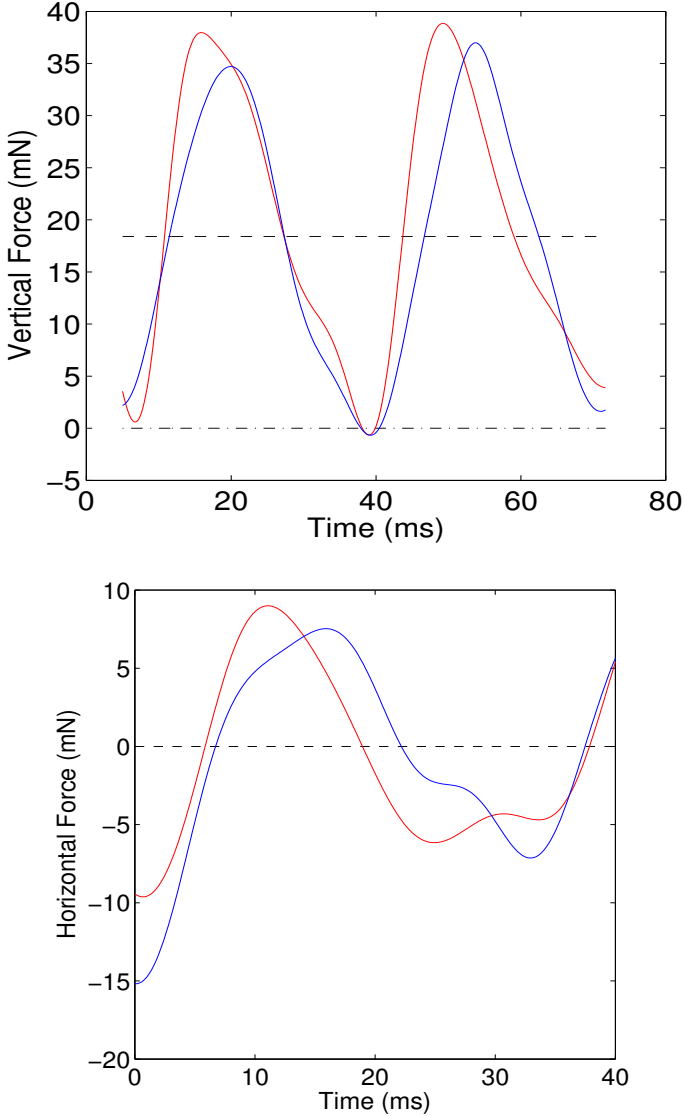
Figure 3.10: Ground reaction force patterns (mN) on flat terrain before and after complete tarsi ablation. Blue traces represent data from intact animals while red traces represent data from the tarsal ablated condition. (top) Vertical force patterns. Both intact and tarsi less animals show spring-like force patterns. (bottom) Horizontal force patterns. No collision peaks are observed after losing tarsi and thus provides insufficient evidence for use of tarsal structures for damping during running.
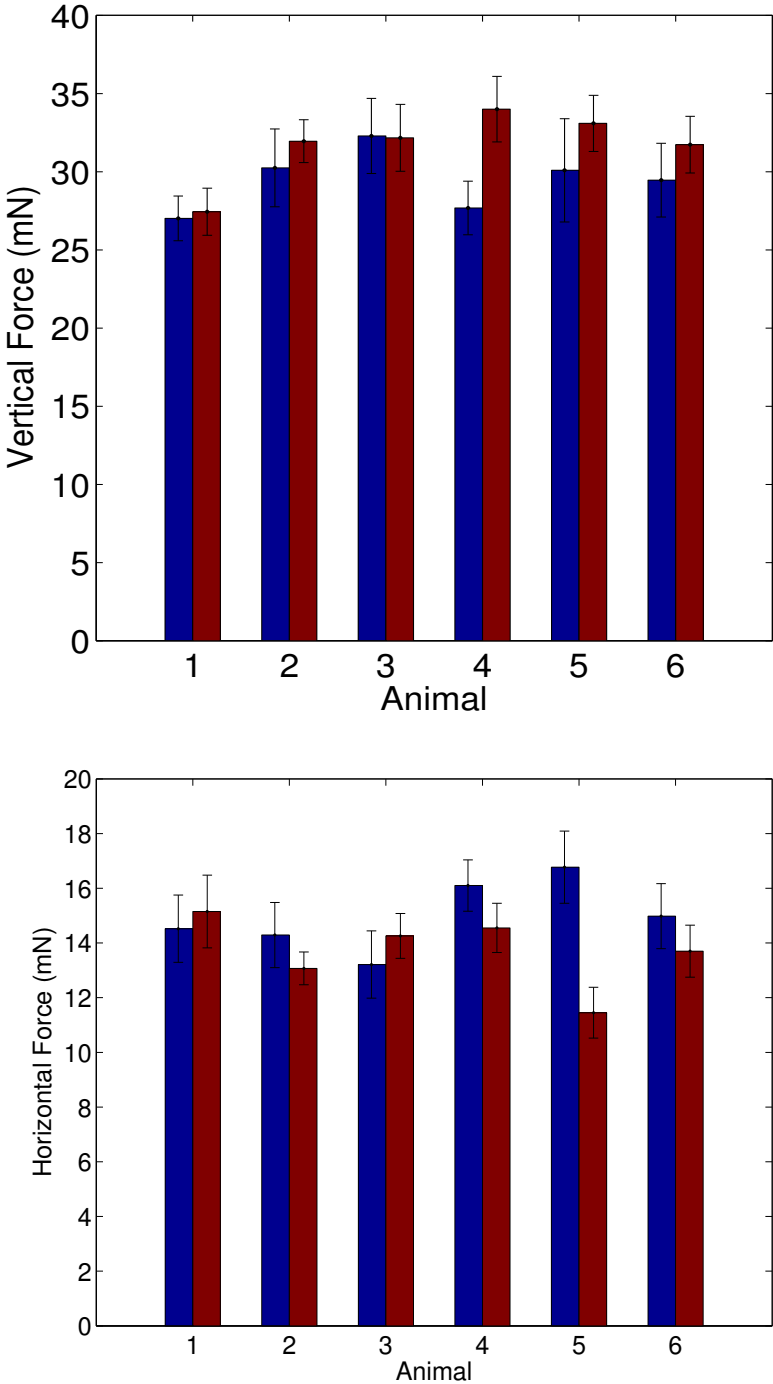
Figure 3.11: Plot of the peak-peak magnitude of ground reaction force (mN) for cockroaches running on flat terrain before and after tarsi ablation. Blue bars represent data from intact animals while red bars represent data from the tarsal ablated condition. Error bars represent mean ± 1 s.d.(top) Vertical force patterns. No significant difference with or without tarsi across animals (bottom) Horizontal force patterns. No significant difference with or without tarsi across animals.
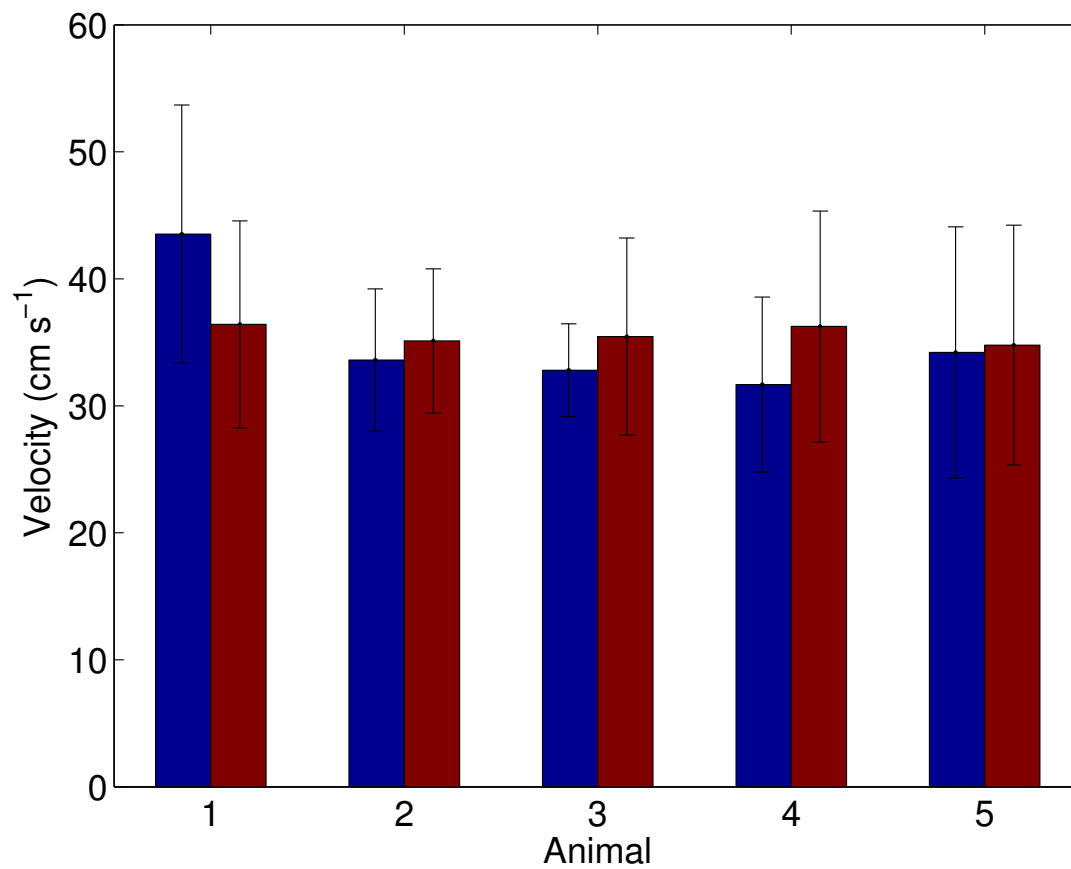
Figure 3.12: Variation of cockroach velocity (cm s^{-1} on rough terrain across animals before and after tarsi ablation. Blue bars represent data for intact animals while red bars represent data for the tarsal ablated condition. Error bars represent mean $\pm$ 1 s.d. Cockroach velocity is not significantly altered by loss of tarsi. By relying on tibial spines, cockroaches mitigate the effect of perturbations on rough terrain and stabilize locomotion.
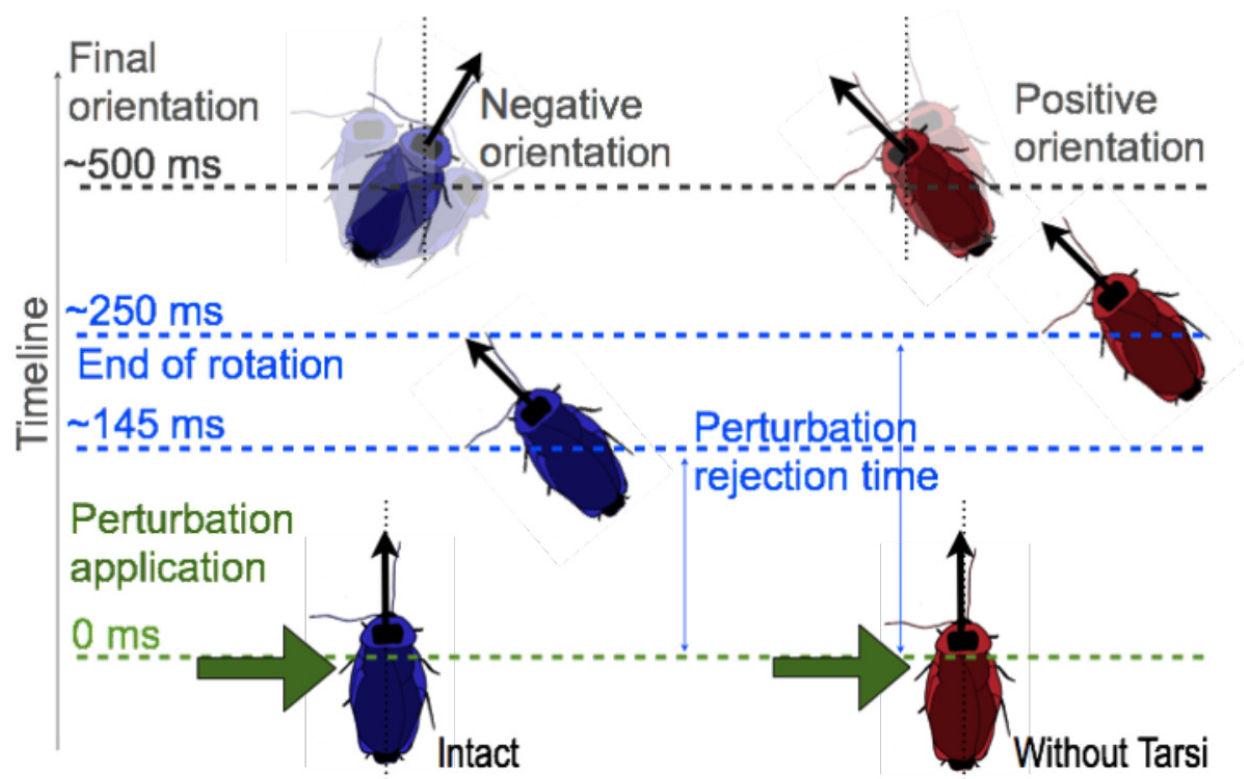
Figure 3.13: The above cartoon illustrates cockroach behavior after experiencing large lateral impulses and highlighting the major differences between intact and tarsiless animals. Blue animals represent intact condition, while red animals represent the tarsi ablated condition. Also indicated are performance metrics, perturbation rejection times - time from perturbation application to the end of body rotation, and change in body orientation - difference between the final and initial orientation of the animal body in the plane of locomotion. After loss of tarsi, cockroaches took longer to reject the effect of perturbation and exhibit lesser recovery than when intact.
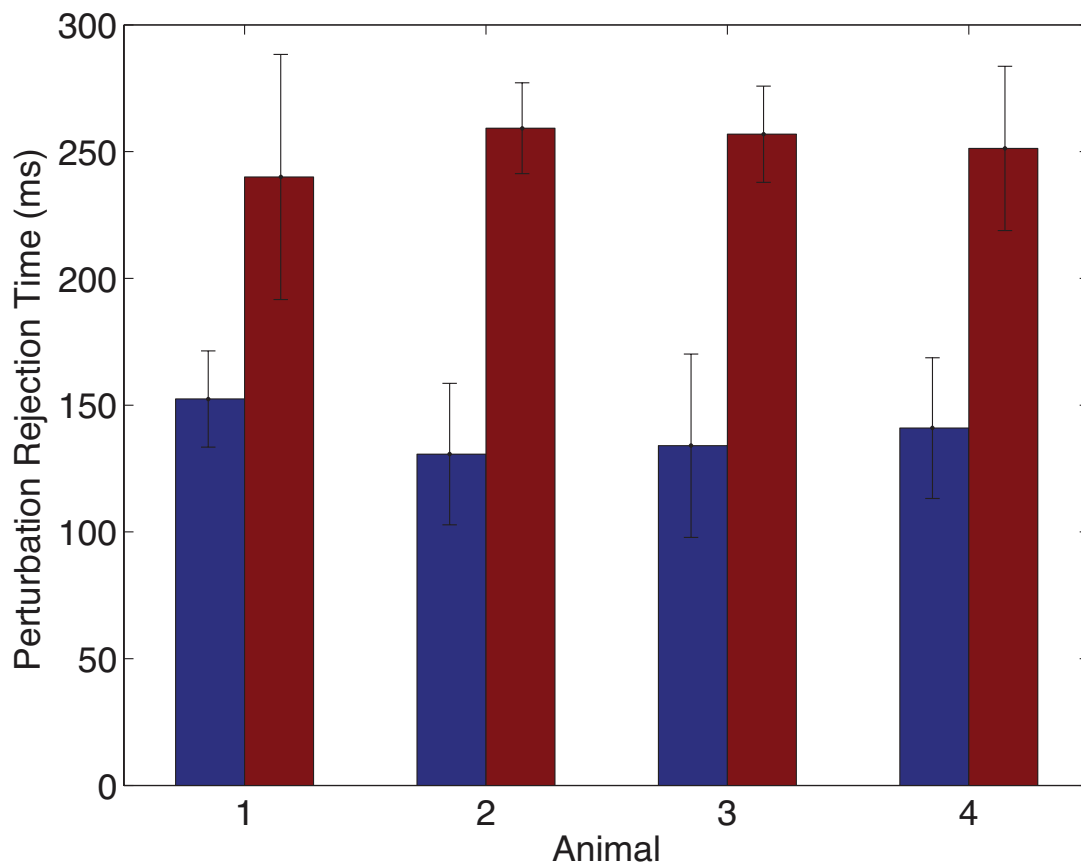
Figure 3.14: Variation of cockroaches' perturbation rejection time (ms) during large lateral impulse experiments across animals before and after tarsi ablation. Blue bars represent data for intact animals while red bars represent data for the tarsal ablated condition. Error bars represent mean ± 1 s.d. After loss of tarsi, cockroaches exhibit lesser recovery than when intact.
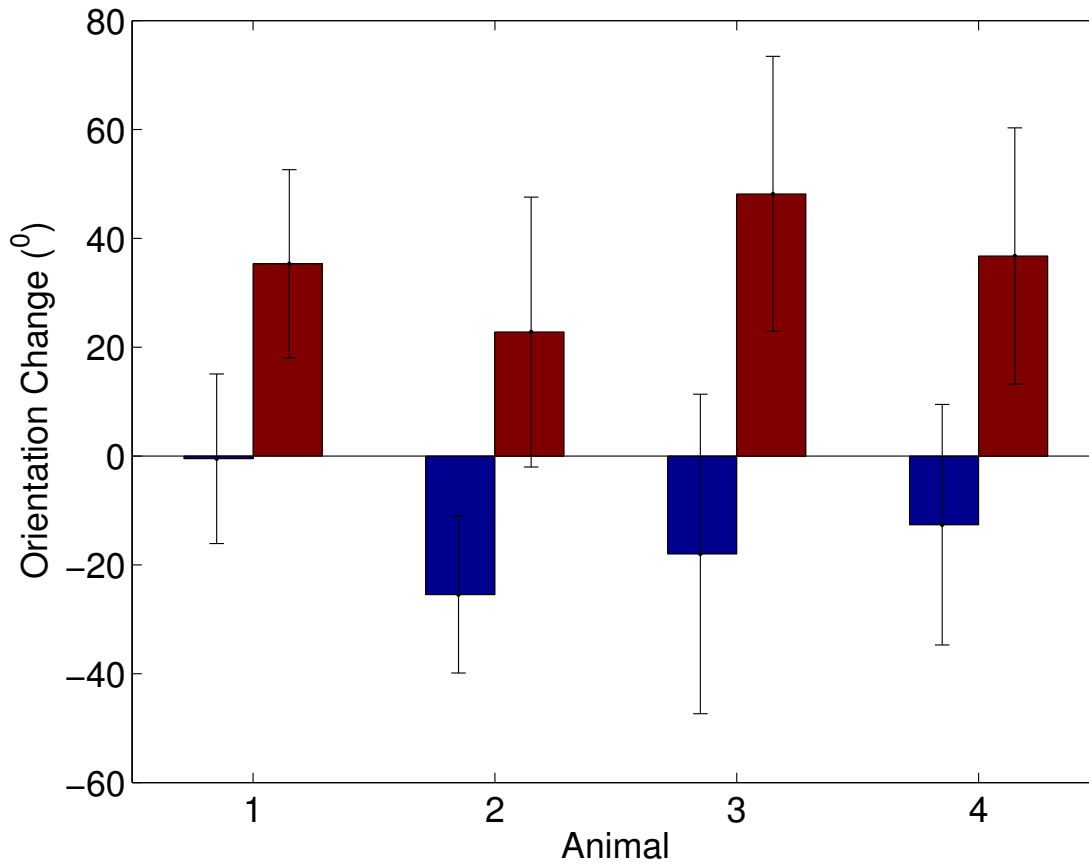
Figure 3.15: Variation of cockroaches' orientation change (^{0}) during large lateral impulse experiments across animals before and after tarsi ablation. Blue bars represent data for intact animals while red bars represent data for the tarsal ablated condition. Error bars represent mean $\pm$ 1 s.d. When intact, cockroach often overcompensated and ended up turning away from the direction of perturbation (cart movement). However, after loss of tarsi, cockroaches took longer to reject the effect of perturbation than when intact.
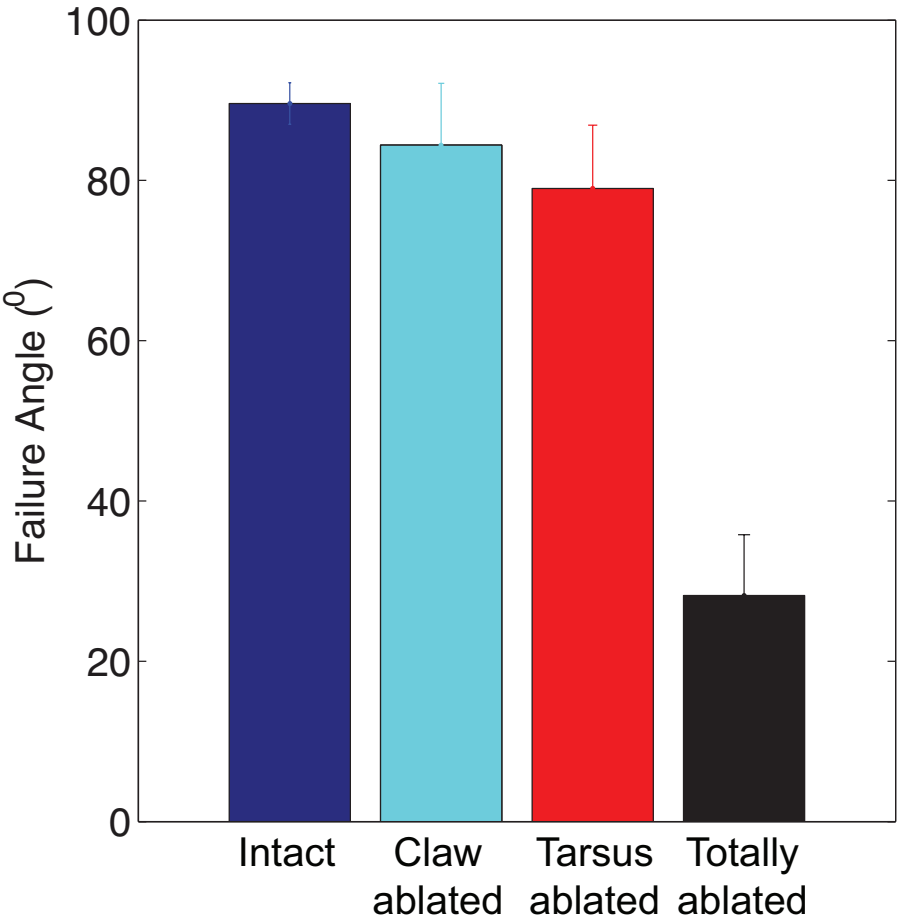
Figure 3.16: Variation of failure angle (^{0}), the slope of the curved track at angle at the height where the cockroaches begin to tumble backwards, on a high-friction curved surface track at four levels of tarsi manipulation - intact (represented as blue column), claw ablated (only the claw is removed leaving arolium and euplantulae intact; represented as cyan column), tarsus ablation (all tarsal structures are ablated leaving only the tibial spines for foot attachments; represented as red column) and totally ablated (the tarsi and all spines around the tibia-tarsal joint are ablated leaving a rounded peg as foot; represented in black). Failure angle does not significantly differ for intact, claw ablated and tarsus ablated conditions, but decreases dramatically after spine ablation. Therefore, spines can effectively compensate for loss of tarsi on high-friction surfaces. Error bars represent mean $\pm$ 1 s.d.
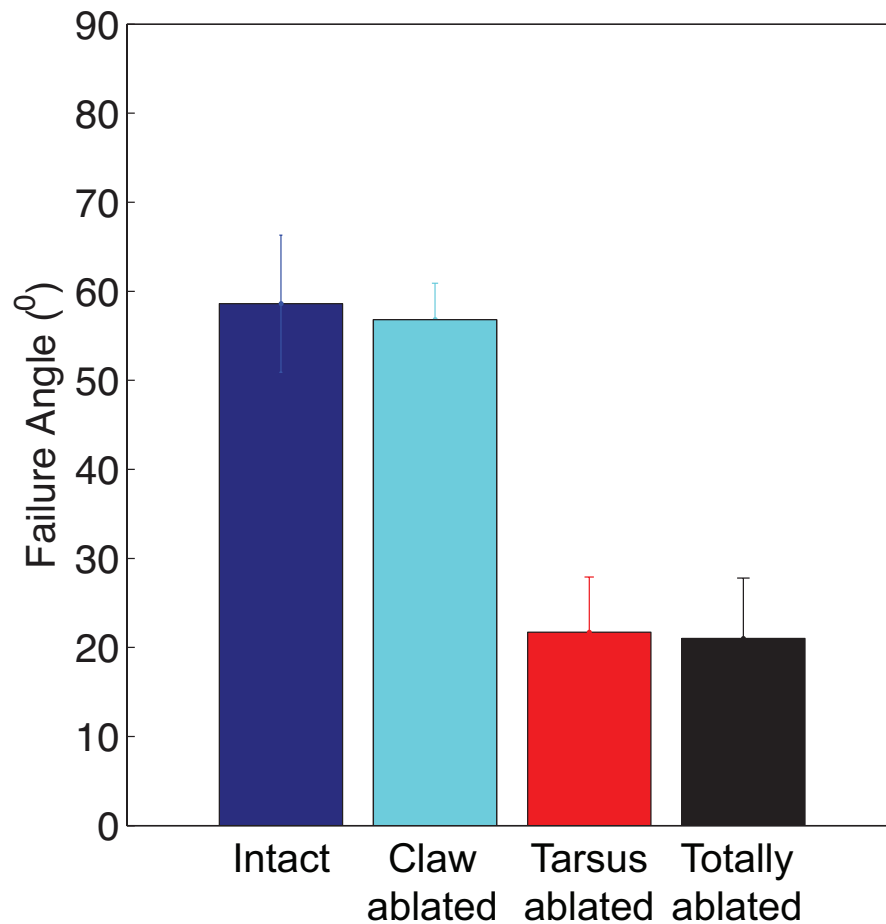
Figure 3.17: Variation of failure angle (^{0}), the slope of the curved track at angle at the height where the cockroaches begin to slip downwards on a low-friction curved surface track at four levels of tarsi manipulation - intact (represented as blue column), claw ablated (only the claw is removed leaving arolium and euplantulae intact; represented as cyan column), tarsus ablation (all tarsal structures are ablated leaving only the tibial spines for foot attachments; represented as red column) and totally ablated (the tarsi and all spines around the tibia-tarsal joint are ablated leaving a rounded peg as foot; represented in black). Failure angle does not significantly change after claw ablation but is significantly lower after the loss of the entire tarsus and/or spines. Therefore, spines are unable to compensate for loss of tarsi on low-friction surfaces. Error bars represent mean $\pm$ 1 s.d.

Figure 3.18: Variation of cockroach velocity (cm s^{-1}) on flat, rough inclined terrain before and after complete tarsal ablation. Blue bars represent data for intact animals while red bars represent data for the tarsal ablated condition. Error bars represent mean $\pm$ 1 s.d. Cockroaches do not change their running velocity upto 45^0 across tarsal conditions. Beyond 60^0, there is a significant decrease in velocity of tarsiless animals relative to their intact condtion.

Figure 3.19: Variation of cockroach stride frequency (Hz) on flat, rough inclined terrain before and after complete tarsal ablation. Blue bars represent data for intact animals while red bars represent data for the tarsal ablated condition. Error bars represent mean $\pm$ 1 s.d. Cockroaches do not change their stride frequency upto 45^0 across tarsal conditions. Beyond 60^0, there is a significant decrease in stride frequency of tarsiless animals relative to their intact condtion.
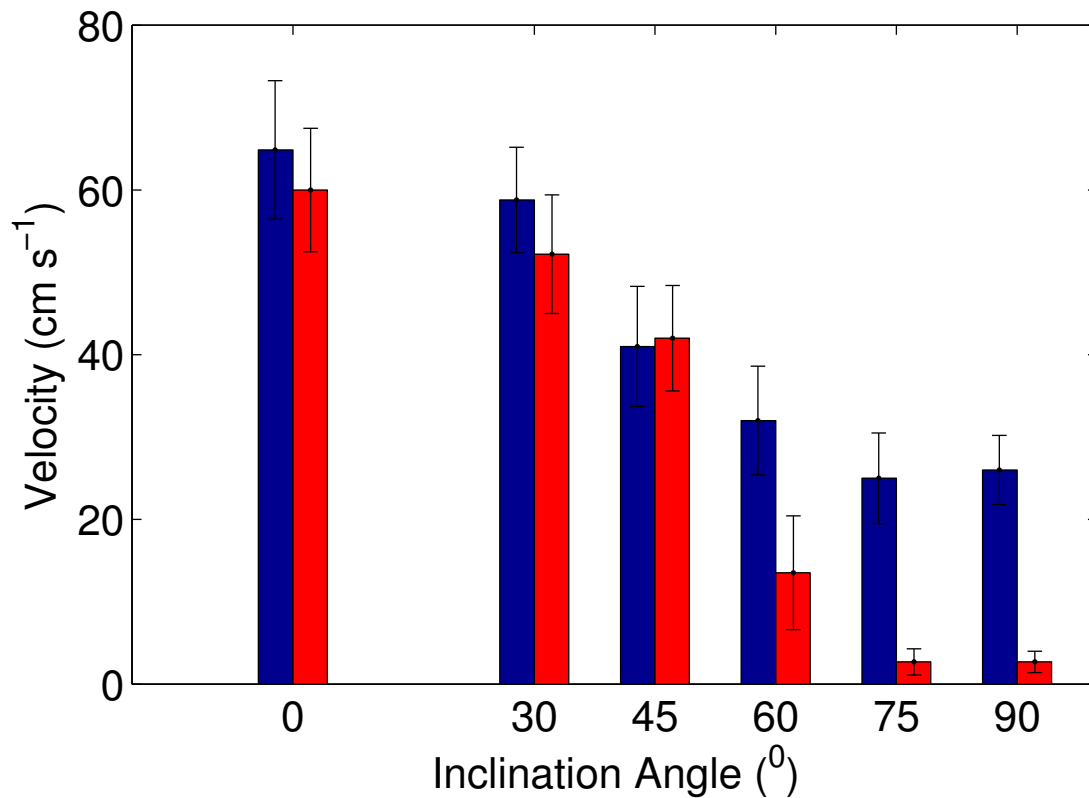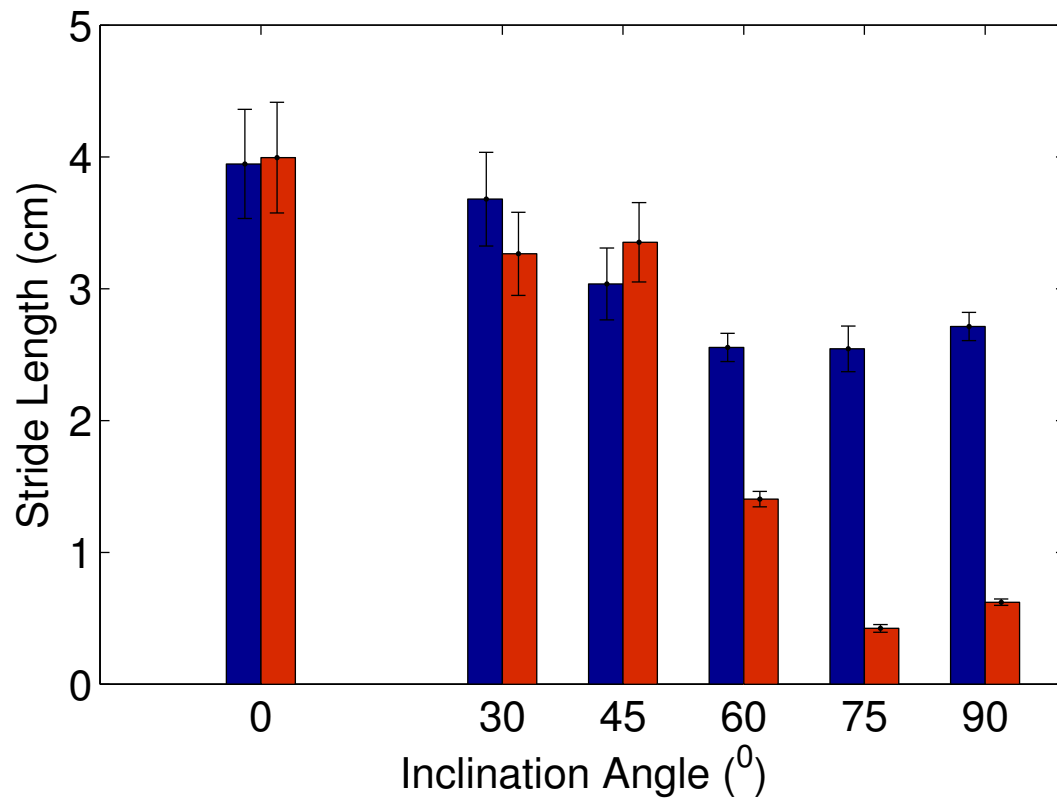
Figure 3.20: Variation of cockroach stride length (cm) on flat, rough inclined terrain before and after complete tarsal ablation. Blue bars represent data for intact animals while red bars represent data for the tarsal ablated condition. Error bars represent mean $\pm$ 1 s.d. Cockroaches do not change their stride length upto 45^0 across tarsal conditions. Beyond 60^0, there is a significant decrease in stride length of tarsiless animals relative to their intact condtion.
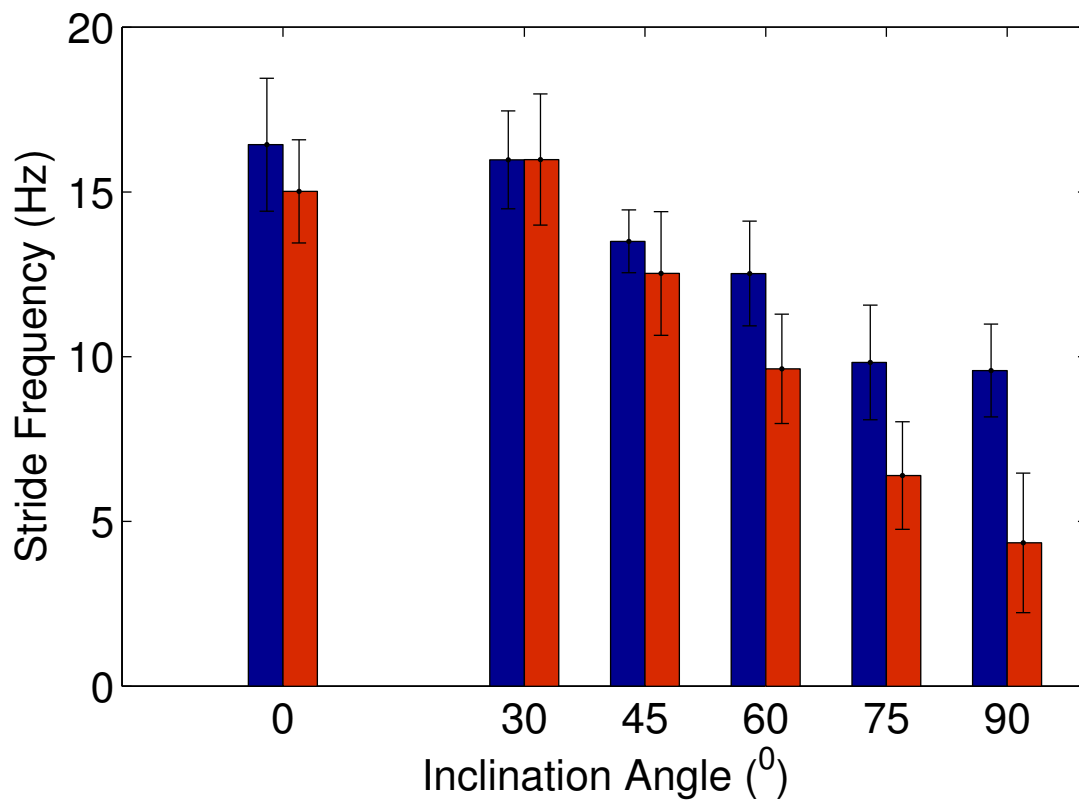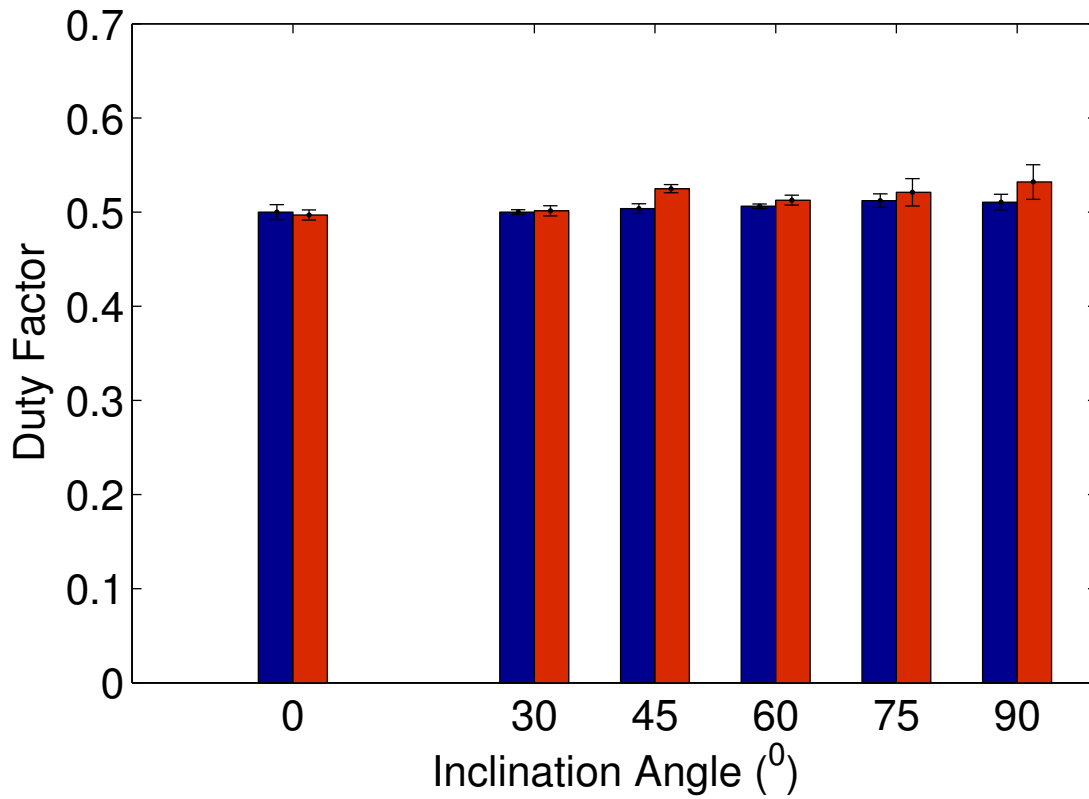
Figure 3.21: Variation of cockroach duty factor on flat, rough inclined terrain before and after complete tarsal ablation. Blue bars represent data for intact animals while red bars represent data for the tarsal ablated condition. Error bars represent mean ± 1 s.d. Cockroaches do not change their duty factor irrespective of tarsal conditions across all inclines.
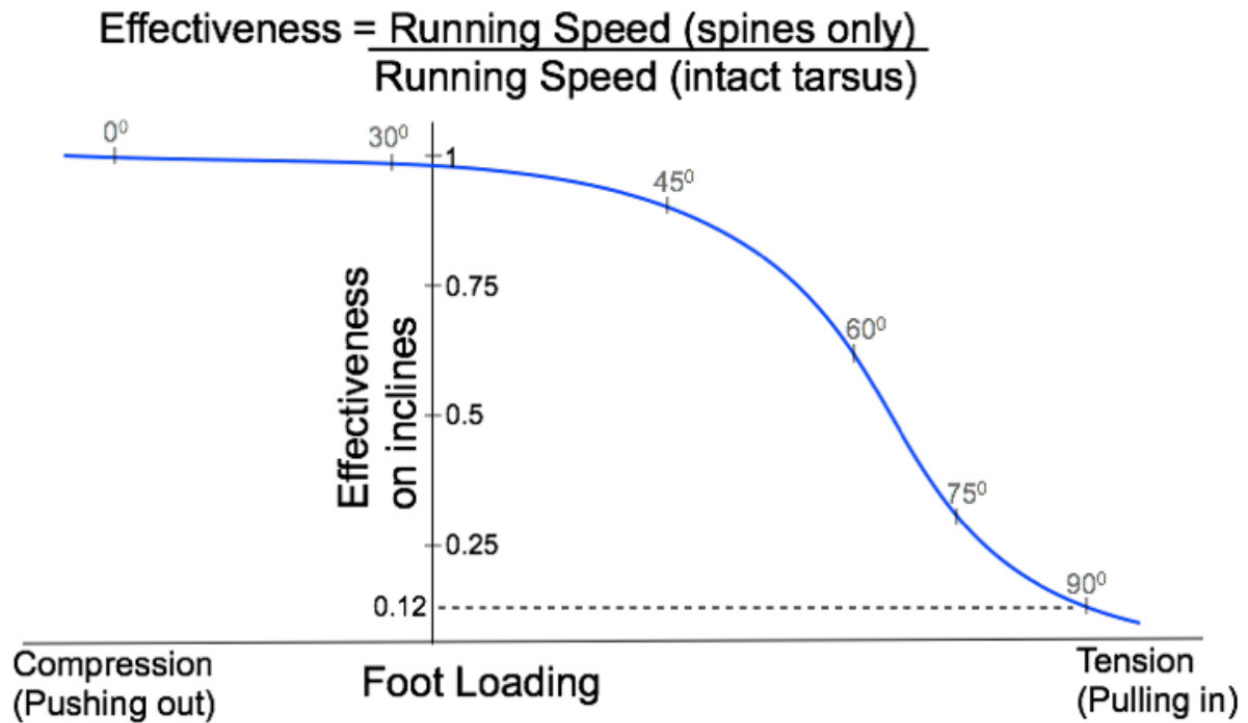
Figure 3.22: Plot showing effectiveness of spines as substituting feet mechanisms against foot loading. Effectiveness is quantified as the ratio of running speed with only spines to the running speed with intact tarsi. At low inclines or on level rough terrain, cockroaches seem to be able to locomote at effectiveness approaching 1. However, when required to pull into the substrate, spines are unable to generate inward forces resulting in lowered effectiveness.
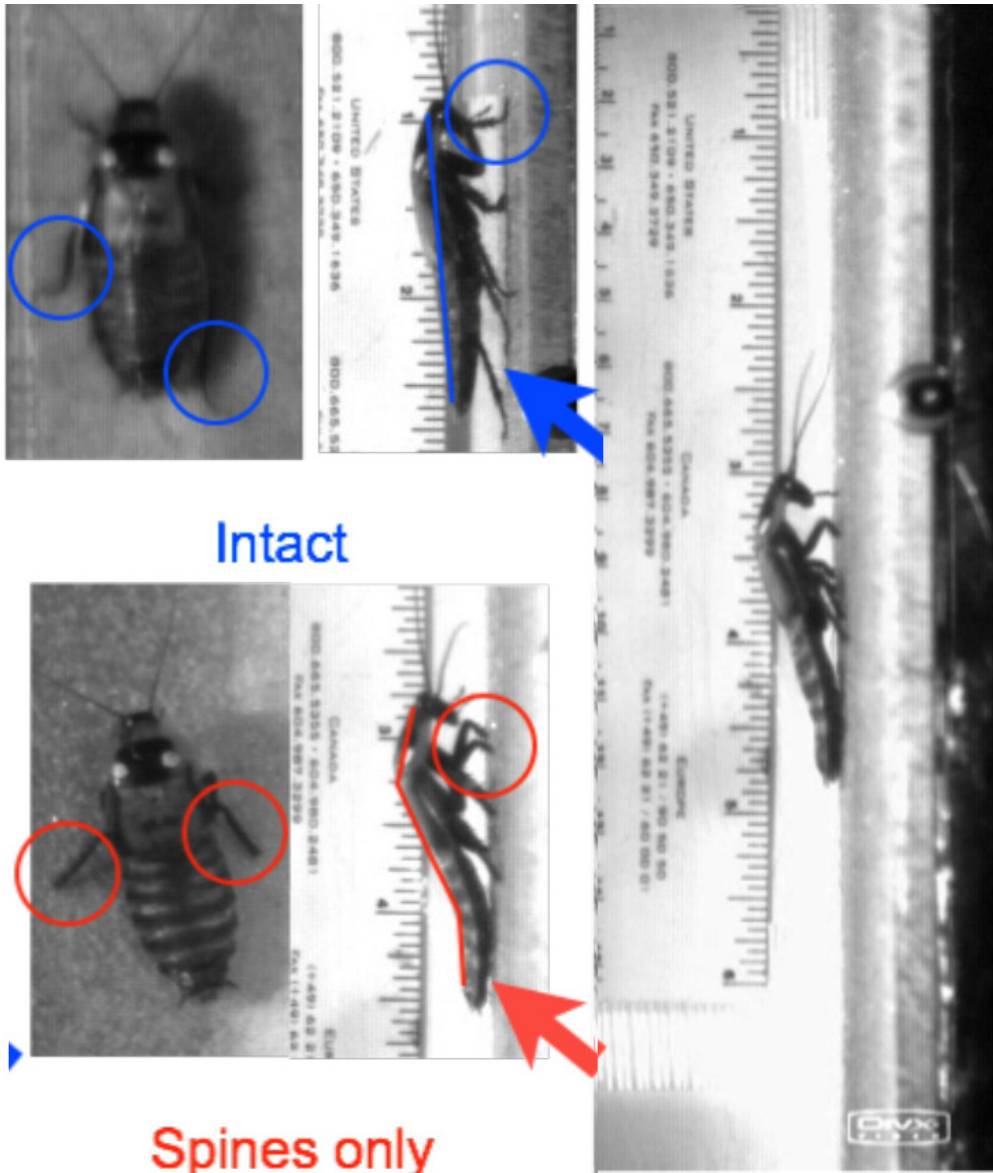
Figure 3.23: While climbing without tarsi, cockroaches adopt (1) splayed foot position to provide greater static stability (2) curved body posture to facilitate leg positioning to enhance spine engagement on the front and middle legs (3) abdomen as a tail to prevent pitchback failure.

Chapter 4

Fault tolerance II: Loss of Legs

4.1   Introduction to Fault Tolerance during Locomotion

Recent technological progress, especially in the field of manufacturing [166], has led to the rapid prototyping of robots [71]. However, despite the promise of societal benefit, such as in search and rescue [122], disaster response [167], and environmental monitoring, the majority of these robots are considered 'fragile' [71] for real-world operation. To be truly useful, robots must be able to locomote, autonomously or with minimal supervision, in natural and human-created environments, that are often complex [10], uncertain [163][16] and dynamic [7]. In contrast, animals masterfully walk on loose sand, run across uneven rubble, climb up slippery plants, jump over irregular rocks, fly through dense canopy and swim in turbulent waters. They perform multiple functions using the same structures [168], anticipate uncertainties to avoid fatal damage [104], tolerate construction flaws [169] and adapt to changing internal [170] and external conditions [20]. We contend that robustness, the ability to maintain performance in the face of disturbances, is perhaps the single greatest single difference between today's human engineered technologies and organisms.

An important criterion for successful locomotion performance for animals and robots in natural environments is the ability to be fail-safe or fault tolerant [171] due to numerous possible uncertainties. Fault tolerance is the property that enables a system to continue operating properly in the event of the failure of (or one or more faults within) some of its components. If its operating quality decreases at all, the decrease is proportional to the severity of the failure, as compared to a naively designed system in which even a small failure can cause total breakdown. Consider the case of high-speed transition presented in Chapter 2. While an animal system 'reacts' to mitigate the effect of disturbances at hand using alternate mechanism including mechanically mediated methods such as collisions (Chapter 2), a majority of robots can only rely on its pre-defined solutions designed to handle a limited number of commonly expected extremities [171] centered around avoiding impacts. And if a collision were to occur, the robot often breaks down. A fault-tolerant design for a robot in this case would enable it to continue its intended operation, possibly at a reduced level, rather

than failing completely. Also, it is important to note that in using traditional engineering design approaches for fault tolerance, the resources required for maintaining performance increase drastically [172]. In many cases, recovery is difficult and if possible, the cost of recovery in such situations is extreme [172][172]. However, animal systems deal with such challenges through out their life span and need to be fault tolerant to avoid extreme failure leading to death.

One of most common sources of disturbance encountered by animals in nature is a loss of an appendage. This could result from birth defects, illness or disease, injury during prey capture, predator evasion or struggles for a mate, regeneration or autotomy [145][76][173][174][175]. In fact, a recent survey [145] revealed that in natural populations, especially with arthropods, appendage loss is regular occurrence with many orders losing one or more appendages in at least 40% of the cases [145]. Furthermore, many arthropods have multiple legs, not all of which are used for locomotor tasks leading some to propose a spare leg hypothesis [176] proposing legs as redundant modules. While studies have focused on decrements to fitness in crabs, and spiders [177], few have examined the effect on the dynamics of locomotion, other than in humans [178][83]. Investigations of locomotion examining leg amputations have detailed inter-leg coordination [179][123], the control of gaits in slow walking such as in stick insects [169], crickets [173] and scorpions, stepping in tarantulas [180] and effect of sensory deprivation [181]. Here, we examine the effect of leg loss on the dynamics of high-speed running in polypedal animals.

Cockroaches are known for their high-speed performance running on level ground [31], locomoting across rough surfaces [3], climbing up walls [32], and performing rapid maneuvers to disappear under ledges [35]. We have shown them to be robust to loss of feet or tarsal structures (Chapter 2), modifications to antennal segments [155] and even in their ability to compress their bodies for ingress and egress in confined spaces (Chapter 1). Several wave gaits have been observed when cockroaches walk at slow speeds [182], but they usually rely on an alternating tripod gait at higher running speeds. The earliest studies on single leg amputation during walking demonstrated marked changes in posture and rhythm of movement [182]. These changes were often immediate, so that the role of a missing leg was taken over by the remaining legs on the side of the lost leg. When two legs, one on each side were amputated, variable gait patterns were observed [183]. Similar results were also obtained by manipulating the thoracic ganglia [41] suggesting the possibility of sensory inflow to the central nervous system as a major contributor to the coordination of leg movement after leg loss. Additionally, amputation has been shown to affect both frequency and timing of motor bursts during leg stepping cycles in the remaining stump of the amputated leg and also its neighbors . However, these effects reduced at faster speeds resulting in movement more similar to that of walking in intact animals [41].

Here, we explore the capability of cockroaches to locomote effectively at high-speed with lost legs by choosing the false death-head's cockroach, *Blaberus discoidalis*, because of the wealth of data existing on the dynamics of locomotion [31]. Unlike previous studies where cockroach leg ablations were performed to understand leg coordination [179] and control, we were specifically interested in a cockroach's ability to perform high-speed, steady-state

locomotion where we hypothesized that all six legs of cockroaches play an important role in the development of whole body ground reaction forces [48]. To test this hypothesis, we ran cockroaches down a horizontal track intact with 6 legs and then with 5 legs (missing one middle leg), 4 legs (missing both middle legs), 3 legs (missing a tripod of legs), and then finally with 2 legs (missing all front and hind legs), progressively ablating legs one at a time. We further hypothesized that cockroaches would need to compensate for the loss of legs by choosing a gait different from an alternating tripod, the preferred gait for high-speed locomotion when intact. Even with gait compensation, we expected that cockroaches running in the ablated configurations would decrease performance and that the magnitude of this decrement would increase with successive leg ablations. We measured steady-state kinematics to compare velocity, stride length, frequency and duty factor as indicators of performance for each cockroach leg ablation configuration. We hypothesized that ablation of legs would necessarily perturb the motion of the center of mass of a cockroach. To determine these dynamics, we computed body rotations (pitch, yaw and roll) about the center of mass and expected the magnitude of oscillations to increase with successive leg loss. We ran cockroaches over a custom force platform and quantified the ground reaction forces in vertical, fore-aft and lateral directions. We hypothesized that leg ablation would affect energy storage and return. We predicted that the sagittal plane dynamics of the cockroach center of mass upon leg loss would differ from its intact state [31] and not follow the predictions of a spring loaded inverted pendulum (SLIP) template [116]. Finally, we hypothesized that leg ablation would also destabilize horizontal plane dynamics, and therefore differ from that predicted by the lateral leg spring (LLS) template [86].

To better understand the fault tolerant performance of cockroaches, we chose two small, high performing physical models, 6-legged robots - RoboXplorer and DASH [69], and subjected them to the leg ablations conditions as we did with the animals. We measured performance by quantifying running velocity and ability to travel in a straight line without change in control. Direct measurements of fault tolerance in cockroaches during locomotion with leg ablation will enable us to begin to quantify robustness as a metric of performance for biological organisms and inspire the development of novel robots capable of robust behavior and approach capabilities similar to organisms for effective real-world operation.

4.2 Methods and Materials

Animals

We used 18 adult male cockroaches, Blaberus discoidalis, (Mulberry farms, Fallbrook, CA, USA) with an average mass of 2.31±0.09 g and body length of 44.15±3.63 mm (mean ± s.d.). Prior to experimentation, cockroaches were kept in communal plastic containers at room temperature (22 ^{0}C) on a 12h:12h light dark cycle and provided water and food (fruit and dog chow) ad libitum.

Animal Experimental Design and Protocol

All experiments were performed at 30 ± 2 ^{0}C (mean $\pm$ s.d.). Before starting any experiment, each cockroach was marked with retro-reflective paint at the tip of tibia-tarsus joint of each leg to aid tracking. Additionally, a light (less than 5% cockroach body mass) 3D printed pyramidal cross (20 mm by 15 mm by 12.5 mm) with five tracking points (Fig. 4.2) was mounted near the center of mass of the animal on the dorsal surface. The dorsal cross markers were used to calculate running velocity and body rotations (pitch, yaw and roll), whereas the leg markers were used to estimate gait, stride frequency, stride length and duty factor. To encourage the animals to perform, we elicited an escape response by light stimulation of their cerci or by gentle blowing. We only accepted trials where the animals ran a minimum distance of 50 cm. We rejected trials where (1) the cockroaches slowed down, stopped or tried to climb the wall (2) their body (including the legs) collided with the side-wall or (3) they exhibited turns of more than 300.

To prepare the animals for ablation, we anesthetized them by placing them in an ice bath for about 15 min. We then ablated each of the legs at the coxa-trochanter joint using a sharp razor and cauterized the wounds immediately to prevent excessive bleeding. For recovery post surgery, we placed the animals at room temperature in a small container. Further, we conducted our experimental trials about 15 min after surgery to limit long term learning effects.

We performed a series of manipulations by successively ablating the legs one at a time to obtain the following five cockroach configurations (Fig. 4.1; (1) Intact, 6-legged - no manipulation was performed. All legs were verified to be undamaged prior to starting the experiment; (2) 5-legged - the middle leg on the left (L2) or right (R2) side was ablated; (3) 4-legged - both middle legs were ablated (L2R2); (4) 3-legged - Right (R1L2R3) or left (L1R2L3) tripod was ablated leaving the other intact; and (5) 2-legged - both front and hind legs on each side were ablated leaving on the middle legs intact (R1R3L1L3). For 5-legged and 3-legged condition, we randomized the trials such that half the cockroaches participated in either left or right ablation, thus eliminating any bias due to 'handedness'. We ran all animals intact (6-legged configuration) and found no statistical difference in their performance. We then divided them into three equal groups. We performed manipulations resulting in 5-legged and 4-legged configurations for the first group, 3-legged configurations for the second group and 2-legged for the final group of animals. Cockroaches ran in each leg configuration for a minimum of seven (and a maximum of ten) trials. Thus, each individual served as its own control allowing us to use paired statistics.

Motion Analysis

We recorded videos of cockroaches at 500 frames s^{-1} with a resolution of 1280 by 1024 pixels using a high-speed video camera positioned directly above the track. Images were buffered through the camera memory until post-triggering, after which a video clip (4 s) from camera was reviewed and cropped to the relevant time segment. All video capture,

downloading, and conversion were done with a proprietary software program (AOS Studio). We determined the kinematics of the behavior from the videos using custom motion tracking software.

Statistics

We used repeated measures analysis of variance (ANOVA) and Cochran-Mantel-Haenszel tests for continuous and nominal variables respectively with Tukey HSD for post-hoc contrast analyses (JMP software, SAS Inc.). We applied a repeated measures design with a mixed model to determine the effect of condition. In our model, the condition (leg number) was included as a fixed effect, while individual animals were included as a random effect. The response was our performance metric (i.e. running velocity, stride frequency, stride length and duty factor). We used a standard least squares approach with reduced maximum likelihood (REML) as our method to fit our data. We report the P-value, F-ratio in American Psychological Association (APA) format to support/reject our hypothesis as appropriate. For categorical responses (success), we report the chi^2 value.

3D Kinematics

To determine the 3D kinematics of cockroach running on flat terrain, we constructed a 100 cm long clear acrylic track, 10 cm wide and 10 tall (Fig. 4.3). The bottom surface of the track was lined with balsa wood functioning as the running substrate. We installed two mirrors (50 cm long and 10 cm tall) on the outside of the track, one on each side, at 450 to the bottom surface. This allowed us to use a single overhead camera to capture simultaneously the top view and two side views of cockroach running for tracking of all legs without any occlusion.

To measure the response to leg loss, we ran the animals in each of the five different configurations and computed gait, running velocity, stride frequency, stride length and duty factor as the performance metrics for a total of 396 valid trials across 18 animals.

Whole Body Ground Reaction Forces

To measure cockroachesÕ whole body ground reaction forces on flat terrain, we constructed a 100 cm long clear acrylic track, 10 cm wide and 10 cm tall, with a custom-built force platform (10 cm by 10 cm, natural frequency ≈ 500 Hz) installed at the center (Fig. **??**). The bottom surface of the track was lined with balsa wood to act as the running substrate. The above setup was mounted onto a vibration isolation platform (Newport Corp.) and enabled simultaneous recording of high-speed video data for kinematics and three axis force data for center of mass dynamics with a force resolution of 0.5 mN in each direction. The force measurements reported in the study are low-pass filtered at 350 Hz as we determined that no high frequency dynamics affected cockroach locomotion beyond the cut-off. We

computed peak vertical, horizontal and lateral forces for a total of 394 valid trials across 18 animals.

Robot

We used two small hexapedal robots, RoboXplorer and DASH, as physical models to measure their robustness to leg loss (Fig. 4.5).

RoboXplorer is 15 cm long hexapod robot with S-shaped legs weighing 213 g. The legs are mechanically coupled to run as an alternating tripod at a fixed cycling frequency of about 10 Hz resulting in a velocity approaching 50 cm s^{-1}. The robot has no sensors.

DASH (Dynamic Actuated Sprawled Hexapod) is 50 g, 10 cm long, palm sized commercial robot, based off a research prototype [69] and constructed using Smart Composite Microstructures (SCM) manufacturing process [46]. The robot has two motors controlling the left and right half of the robot each having three mechanically coupled legs such that front and hind legs are in phase while the middle leg is 1800 out of phase with each of them. Therefore, by operating the motors at identical frequencies and controlling the offset between the two halves while starting, the robot can use a variety of gaits such as alternating tripod gait (left and right halves 1800 out of phase), bouncing gait (left and right halves in phase) or something in between. The robot has no feedback to control the relative phases between the two halves once in operation and therefore, its gait can be variable depending on the environmental perturbations. The robot has an onboard gyroscope that can be used to make the robot run in a straight line or turn as desired. The leg cycling frequency of 20 Hz resulting in straight-line velocity of about 30 cm s^{-1}. The robot dynamics are controlled using commercially available electronics (Dashboard, Dash Robotics Inc.) over Bluetooth 4.0.

Robot Experimental Design and Protocol

For robot experiments, we constructed a custom track 2 m long, 0.3 m wide with clear acrylic. Video from overhead high-speed camera allowed us to determine running velocity, path trajectory and frequency of side-wall collisions. We ran each robot in five leg configurations, just as we did with the cockroach trials.

4.3 Cockroach Kinematics

The false death head cockroach, *Blaberus discoidalis*, when intact, rapidly ran straight down a horizontal track (Fig. 4.3; Movies) approaching velocities of 55 cm s^{-1} using an alternating tripod gait. We found no individual effect on an animal across our various experimental conditions.

Gait

Despite successive leg ablations, cockroaches continued to persist with the alternating tripod gait in each case (Fig. 4.6 4.7 4.8 4.9 4.10). This is unlike earlier studies in cockroaches [184][182][41] or stick insects [179][185] at walking speeds where the legs seem to compensate by adopting alternate gait patterns.

Velocity

High-speed kinematic analyses of marked animals revealed that no significant changes in running velocity (54.02 ± 9.13 cm s^{-1}; ANOVA, P=0.45, F2,165=1.32) for intact, 5-legged and 4-legged configurations suggesting that the loss of legs did not affect the animals' escape running for this metric (Fig. 4.11). These recorded velocities are approaching near maximal performance [31] ever measured for this animal in laboratory environments and it is impressive that even with loss of two legs, cockroaches are able to run as fast. Cockroaches with only a tripod (41.59 ± 8.68 cm s^{-1}; ANOVA, P<0.01, F1,104=7.43) or with only two middle legs (30.48 ± 7.17 cm s^{-1}; ANOVA, P<0.01, F1,108=5.91) remaining ran slower relative to their intact condition. Even with the loss of three legs in tripod and middle leg only configurations, performance was reduced by only 24% and 43%, respectively allowing the cockroaches to escape at velocities of 30 cm s^{-1} or higher to potentially avoid predators. Previous studies on the same species of cockroach have noted that the preferred running speed on level surfaces is close to 30 cm s^{-1}. In our study, it is incredible that the escape velocity even is the most severe leg ablated condition, when left with two middle legs, is comparable to the preferred running speed when intact and thus we expect this fault tolerant performance to allow high fitness for survival in the natural world [145].

Stride frequency, stride length and duty factor

Further analyses revealed that cockroaches did not significantly change their stride frequency (16.13 ± 1.02 Hz; ANOVA, P=0.67, F2,104=0.72; Fig. 4.12) or length (3.35 ± 0.57 cm; ANOVA, P=0.54, F2,165=1.20; Fig. 4.13) or duty factor (0.48 ± 0.07; ANOVA, P=0.77, F2,165=0.93; Fig. 4.14) to compensate for loss of one or both middle legs. These performance metrics are in agreement with previous studies on animals of the same species. The mean duty factor measuring under 0.5 indicates that animals did not typically use double support of the tripods during running. High-speed video evidence confirmed the same with numerous strides involving instances where all animal legs were completely air borne. We further noted that cockroaches, even with just four legs, could easily support their body weight and did not collide with the ground. Cockroaches possessing only a tripod of legs, significantly reduced their stride frequency (14.42 ± 0.76 Hz; ANOVA, P=0.01, F1,104=3.43; Fig. 4.12) and length (2.88 ± 0.31 cm; ANOVA, P<0.01, F1,104=9.46; Fig. 4.13), but did not change their duty factor (0.49 ± 0.05; ANOVA, P=0.77, F1,104=1.16; Fig. 4.14) relative to their intact state. High-speed video revealed that the animals attempted to use their abdomen to land on the

ground at the end of a stride to absorb impact and might be serving a role similar to that of the front legs when intact. Cockroaches with only two middle legs significantly reduced their stride frequency (11.76±0.84 Hz; ANOVA, P<0.01, $F_{1,108}$=11.73; Fig. 4.12), took shorter steps (2.59±0.61 cm; ANOVA, P<0.01, $F_{1,108}$=9.46; Fig. 4.13) and increased their duty factor (0.64±0.06; ANOVA, P=0.77, $F_{1,108}$=1.16; Fig. 4.14) compared to when they were intact. This increase in duty factor suggests that cockroaches used a longer contact time for force development to move forward so as to compensate for the lost legs. Cockroaches with only two middle legs were also noted to drag their abdomen on the ground indicating that with the remaining legs are either unable to support the normal load or result in an unbalanced posture unable to support the heavy abdomen.

Body attitude

We calculated the peak-to-peak body rotations in roll, pitch and yaw as the animals ran along the track. Cockroaches significantly increased their body rotations along the longitudinal axis (roll) upon the loss of middle legs (ANOVA, P=0.01, $F_{2,165}$=4.87; Fig. 4.15). Upon loss of a single middle leg, animals rolled (35.62^0±7.14^0) more towards the side missing the leg relative to intact configuration (18.22^0±6.46^0). However, with loss of both middle legs, animals increased the overall peak-peak magnitude of roll body rotation (54.28^0±8.43^0), but undulated nearly equally on both sides. No significant changes were measured in roll axis rotations in cockroaches possessing only a tripod (15.49^0±5.14^0; ANOVA, P=0.14, $F_{1,104}$=2.07) or two middle legs (17.95^0±7.44^0; ANOVA, P=0.89, $F_{1,108}$=0.66) relative to their intact condition. The animals did not significantly change the pitch rotation magnitude (12.43^0±5.10^0; ANOVA, P=0.19, $F_{3,272}$=1.44; Fig. 4.16) with leg loss except in the tripod only case (25.24^0±8.46^0; ANOVA, P=0.01, $F_{1,104}$=3.78). When left with just a tripod of legs, the animals continued to cycle their legs together like they would in an alternating tripod with six legs, resulting in a hopping motion with the heavy abdomen potentially causing the animal body to pitch upwards higher than when intact. Cockroaches did not significantly change the peak-peak magnitude of yaw oscillations (11.19^0±4.82^0; ANOVA, P=0.27, $F_{4,374}$=1.87; Fig. 4.17) across any manipulation.

4.4 Cockroach Ground Reaction Force Patterns

By running the cockroaches intact and after leg manipulations on the force platform, we measured the ground reaction force patterns generated by the animals in each condition. Upon the loss of one or both middle legs, cockroaches continued to generate force patterns like a bouncing pogo stick similar to their intact condition. Cockroaches missing a single middle leg produced forces in vertical (34.26±6.96 mN; ANOVA, P=0.42, $F_{2,165}$=6.61; Fig. 4.18), horizontal (10.99±5.87 mN; ANOVA, P=0.34, $F_{2,165}$=4.79; Fig. 4.19) and lateral (13.41±5.82 mN; ANOVA, P=0.22, $F_{1,105}$=2.0; Fig. 4.20) directions that were not significantly different from their intact state indicating that the animals could successfully

compensate for the loss of a single leg. However, upon losing both middle legs, the animals produced significantly lower lateral forces (4.19 ± 3.30 mN; ANOVA, $P<0.01$, F2,165=0.51; Fig. 4.20) without changes in vertical or horizontal forces. These results indicate that sagittal plane dynamics remains unaffected by loss of one or both middle legs, and cockroaches can possibly take advantage of SLIP-like dynamics to utilize energy storage and return mechanisms and LLS like dynamics to maintain stability. But, reduced lateral force production after losing both middle legs is likely to decrease the ability to reject horizontal plane perturbations effectively.

When cockroaches were reduced to possessing a single tripod of legs, they still produced forces statistically similar to their intact condition in vertical (37.34 ± 7.30 mN; ANOVA, $P=0.31$, F1,104=5.15) and horizontal direction (9.15 ± 5.03 mN; ANOVA, $P=0.58$, F1,104=7.55), but with significantly lower forces in the lateral direction (6.92 ± 4.37 mN; ANOVA, $P<0.01$, F1,104=0.51; Fig. 4.20). We observed secondary peaks in the vertical direction indicating that cockroaches often landed on their abdomen at the end of their 'hop' before starting the next stride. Finally, when the cockroaches ran with only two middle legs, they produced significantly lower vertical (21.42 ± 9.49 mN; ANOVA, $P<0.01$, F1,104=0.51), horizontal (5.46 ± 3.20 mN; ANOVA, $P<0.01$, F1,104=0.51) and lateral (7.17 ± 3.39 mN; ANOVA, $P<0.01$, F1,104=0.51) forces. Additionally, we observed residual vertical forces as the animals ran across the force place indicating that the animals could not support their entire weight using just two middle legs. Video evidence confirmed that the cockroaches with only middle legs dragged their abdomen during locomotion supporting consistent with the forces recordings. While the ground reaction patterns produced by cockroaches with a single leg tripod or two middle legs share characteristics of SLIP and LLS templates, they may be limited in taking maximum advantage of the energy conserving and self stabilizing dynamics due to interference from body collisions or dragging.

4.5 Physical Model (Robot) Running Performance

Both robots after loss of legs showed decrease in performance and were unable to maintain a straight-line trajectory. RoboXplorer (Fig. 4.21), after loss of one leg ran significantly slower (36.37 ± 3.37 cm s-1; ANOVA, $P<0.01$, F1,18=0.79) than its intact condition (47.61 ± 3.21 cm s-1). Surprisingly, with further ablation of legs, the robot did not reduce the running velocity (35.52 ± 2.91 cm s^{-1}; ANOVA, $P=0.46$, F3,36=5.45). However, with one middle leg missing, the robot was unable to maintain straight-line motion and collided with the side of the track (60% trials). Similarly, with just a tripod of legs, the robot veered towards the side with a single leg support colliding with the track sidewall (70% trials). DASH (Fig. 4.22) showed a monotonic decrease in running velocity with loss of legs (ANOVA, $P=0.03$, F4,45=3.76). After missing one or both middle legs, DASH exhibited similar decrease in velocity. Similarly, DASH with a tripod of legs or just two middle legs ran at statistically indistinguishable velocity. With just one middle leg or with a tripod of legs, DASH was unable to run in a straight line and collided with the side of the track, (70

and 100% trials respectively).

4.6 Conclusion

We have showed that cockroaches are robust to extreme loss of legs and are able to perform high-speed locomotion without all six legs intact. It is surprising that that loss of one or two middle legs does not affect its running velocity enabling it to potentially hunt for prey and evade predators without any performance setback. As remarkable is our observation that cockroaches did not change their gait to maintain speed unlike results from previous studies on slow walking in cockroaches, stick insects and spiders . Cockroaches maintained leg coordination even when reduced to a tripod of legs or left with just two middle legs to reveal novel modes of locomotion (hopping and rowing, respectively). It has been hypothesized that the change is gait is necessitated to maintain stability during walking. However, while running at high speeds, static stability becomes less important. In fact, cockroaches seem to preserve dynamic stability despite loss of legs by generating ground reaction force patterns analogous to SLIP and LLS templates in the sagittal plane and horizontal plane, respectively. We suspect the above mechanism enables cockroaches with missing legs to run over rough terrain by rejecting environmental perturbations and allows them to utilize energy storage and return.

Contrasting the animal performance with that of the robot upon losing legs reveals two major differences. First, even with a single loss of leg, the robot performance decreases significantly unlike the case for animals. Second, passively tuned robots are unable to run in a straight line with asymmetric leg ablations suggesting that subtle changes in control or force generation can required to achieve effective performance. Further direct measurements of fault tolerance in animals will enable us to begin to quantify robustness as a metric of performance and inspire the development of novel, multi-legged robots with capabilities approaching that of organisms for effective real-world operation.
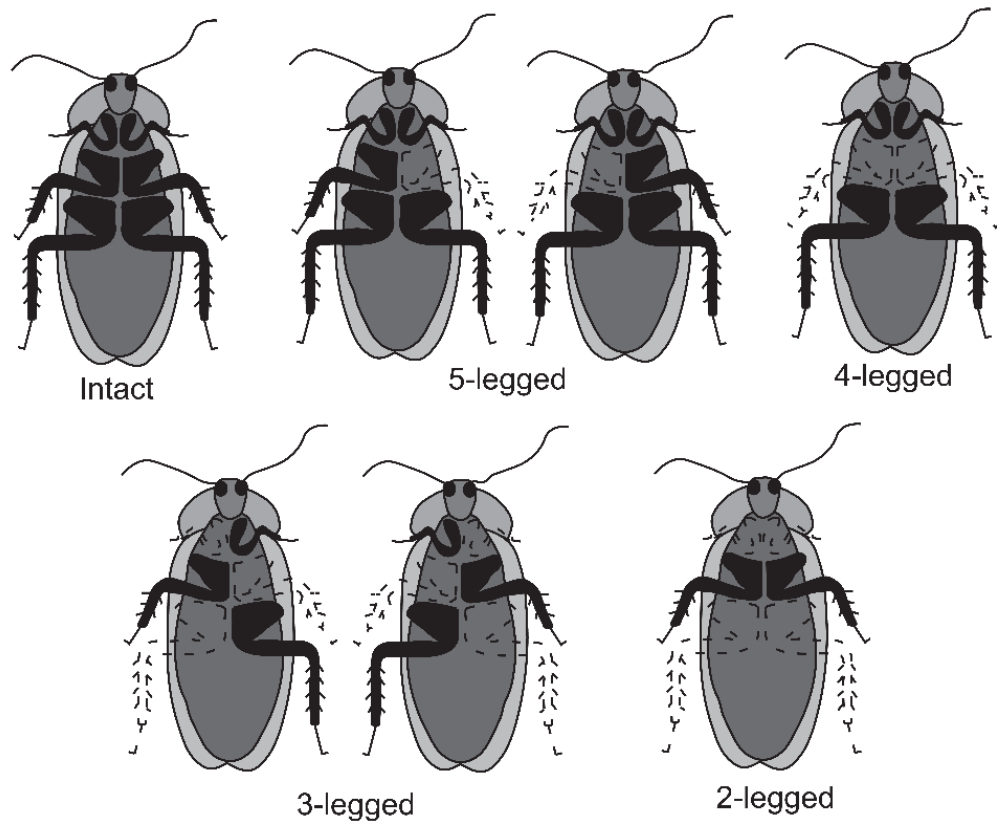
Figure 4.1: The five different leg configurations used to test fault tolerance of cockroaches to the loss of legs. (1) Intact, 6-legged - no manipulation was performed; (2) 5-legged - the middle leg on the left (L2) or right (R2) side was ablated; (3) 4-legged - both middle legs were ablated (L2R2); (4) 3-legged - Right (R1L2R3) or left (L1R2L3) tripod was ablated leaving the other intact; and (5) 2-legged - both front and hind legs on each side were ablated leaving on the middle legs intact (R1R3L1L3).
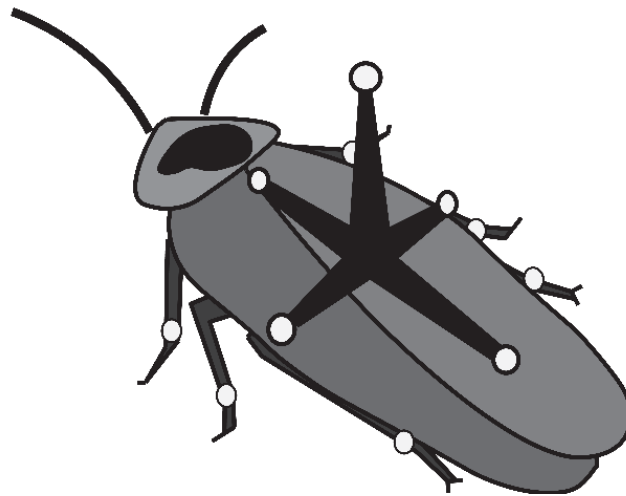
Figure 4.2: Illustration of a cockroach with a cross bearing 5 kinematic markers in addition to the 6 kinematic markers at the intersection of each tibia-tarsus joint. The cross markers enabled us to compute velocity and body attitude, while the leg markers were used to determine stride frequency, length and duty factor.
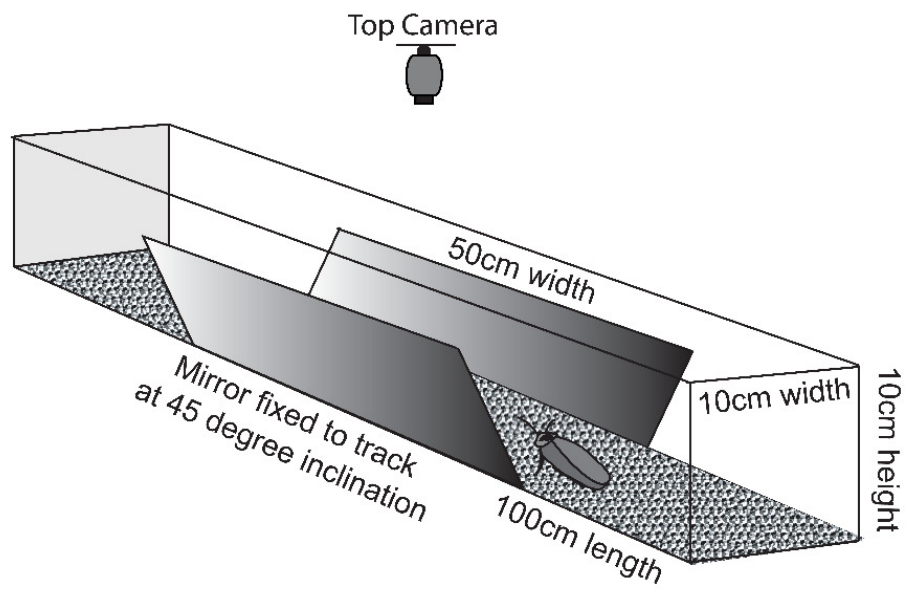
Figure 4.3: Experimental setup for measuring cockroach kinematics using high speed videography. Dual mirrors inclined at 45^0 to the track allowed us to use a single camera from the top to capture multiple views for motion tracking.
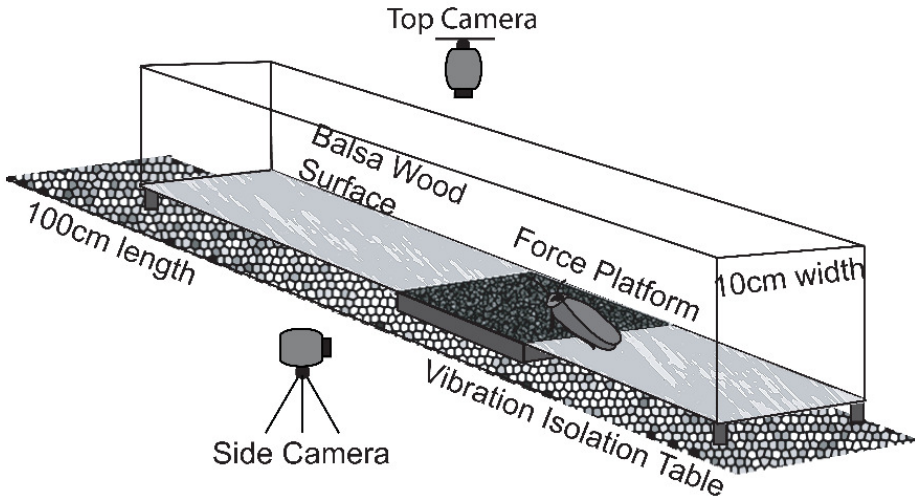
Figure 4.4: Experimental setup for measuring cockroach ground reaction forces using a custom built force platform.
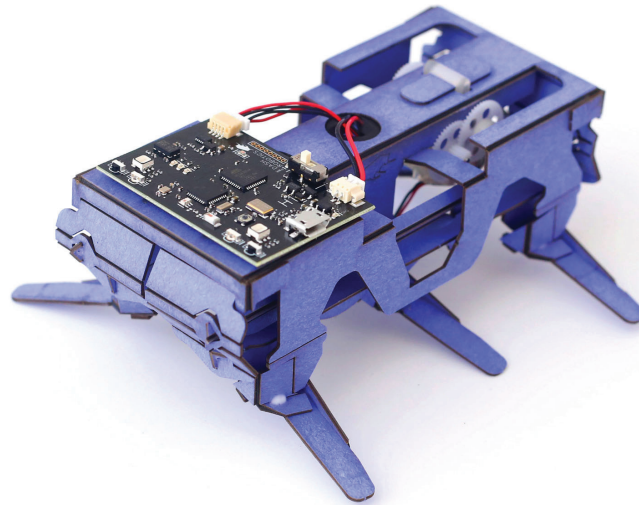
Figure 4.5: Robots used for robustness testing (top) RoboXplorer (bottom) DASH - Dynamic Actuated Sprawled Hexapod.

Figure 4.6: Cockroach gait with 6 legs. Red bars represent the right tripod while the green bars represent the left tripod. Shown on the horizontal axis is time (ms). The colored spaces indicate leg contact with the ground during stance phase, while the white spaces represent legs in the air during swing phase of locomotion. Cockroaches used tripod gait for locomotion in intact condition.
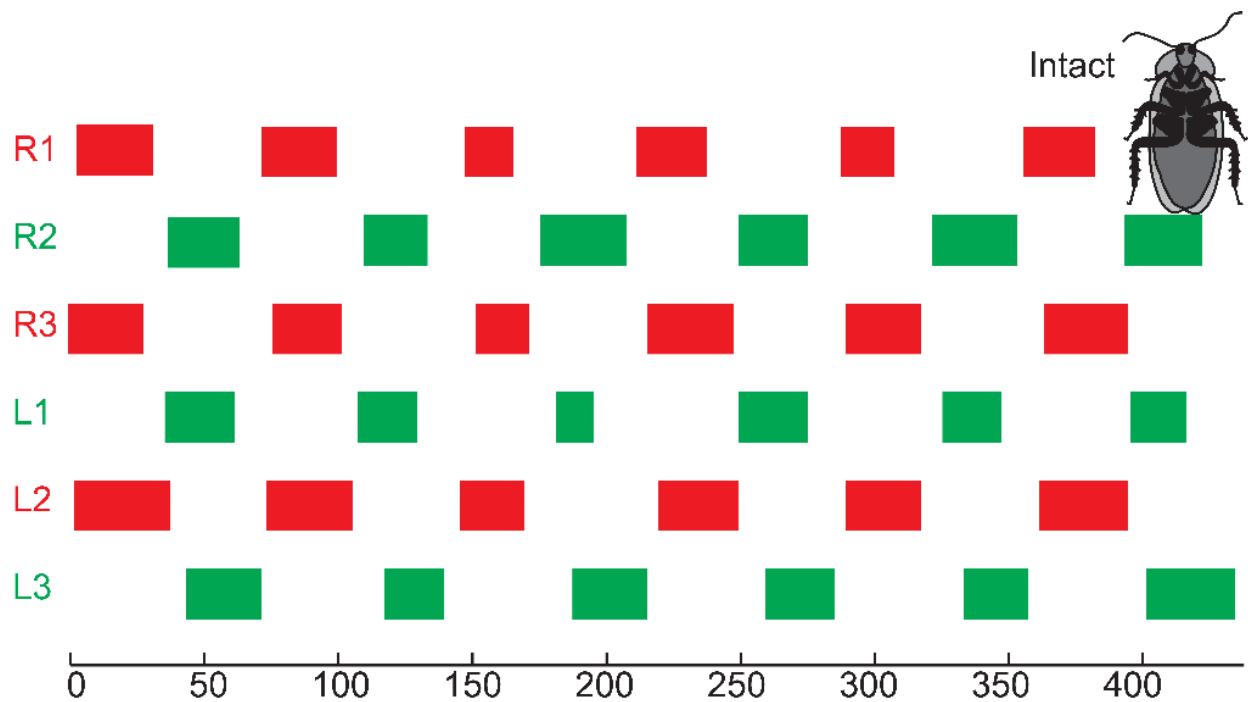
Figure 4.7: Cockroach gait with 5 legs. Red bars represent the right tripod while the green bars represent the left tripod. Shown on the horizontal axis is time (ms). The colored spaces indicate leg contact with the ground during stance phase, while the white spaces represent legs in the air during swing phase of locomotion. Cockroaches used tripod gait for locomotion with one middle leg ablated.

Figure 4.8: Cockroach gait with 4 legs. Red bars represent the right tripod while the green bars represent the left tripod. Shown on the horizontal axis is time (ms). The colored spaces indicate leg contact with the ground during stance phase, while the white spaces represent legs in the air during swing phase of locomotion. Cockroaches used tripod gait for locomotion with both legs ablated.
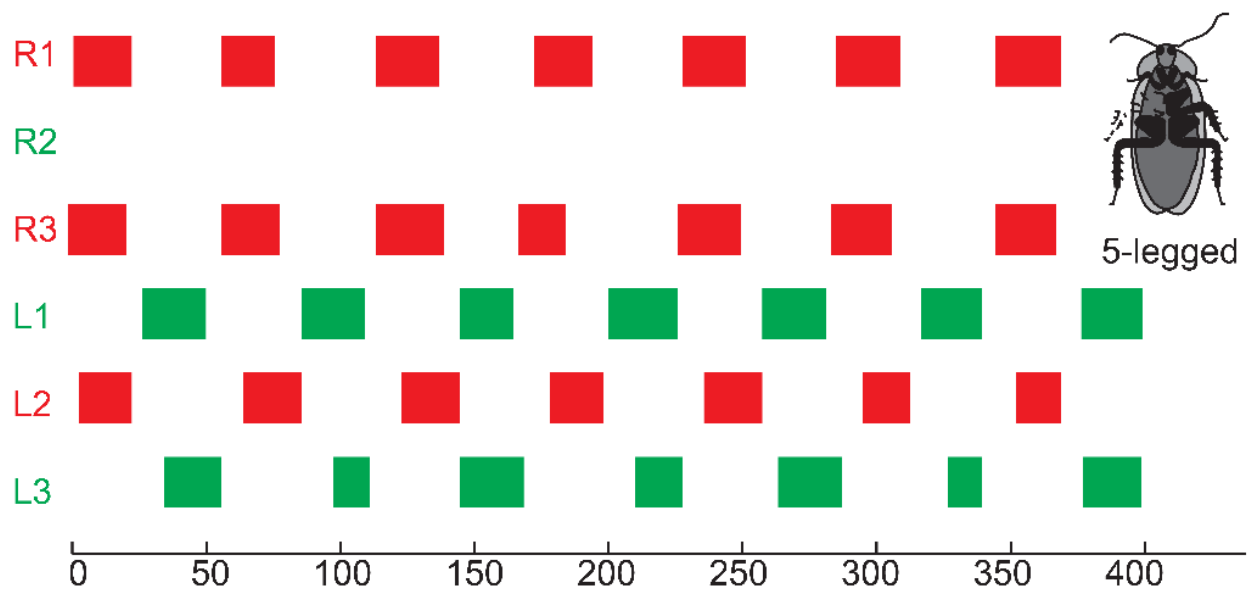
Figure 4.9: Cockroach gait with 3 legs. Red bars represent the right tripod while the green bars represent the left tripod. Shown on the horizontal axis is time (ms). The colored spaces indicate leg contact with the ground during stance phase, while the white spaces represent legs in the air during swing phase of locomotion. Cockroaches used tripod gait for locomotion with the entire tripod ablated, the left one in this case producing a hopping like motion.
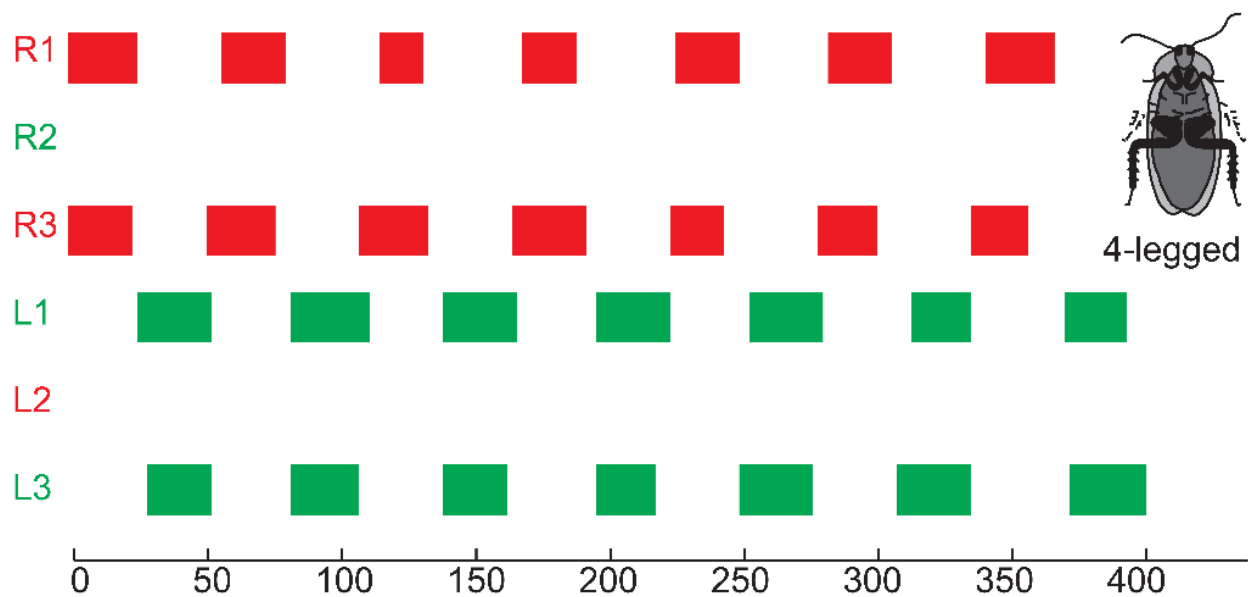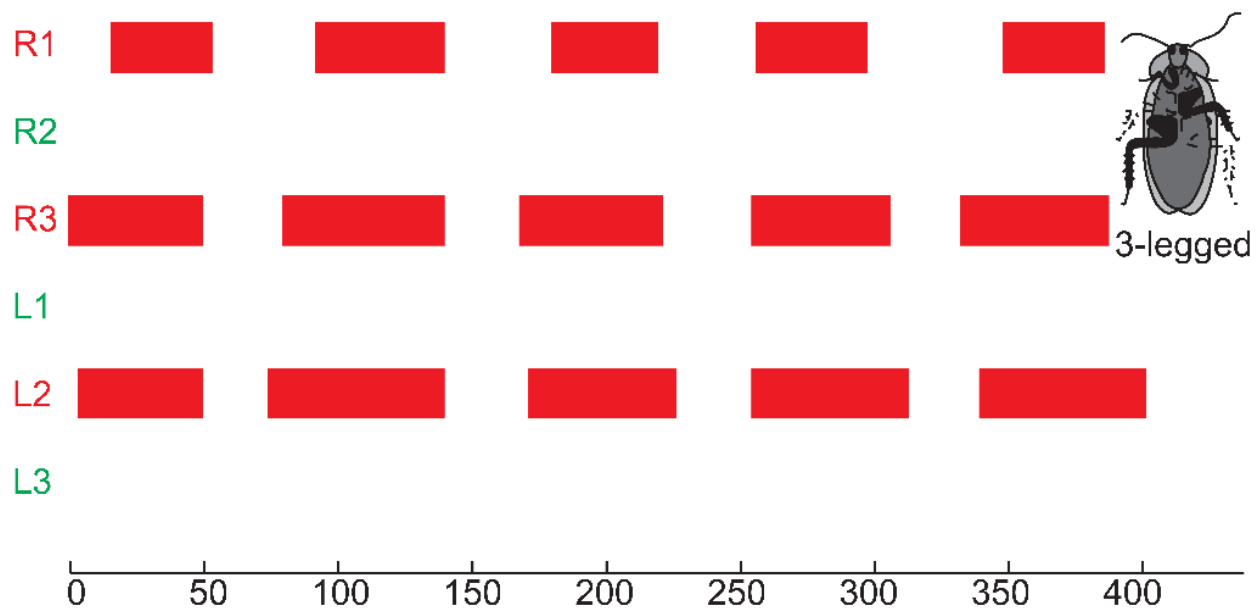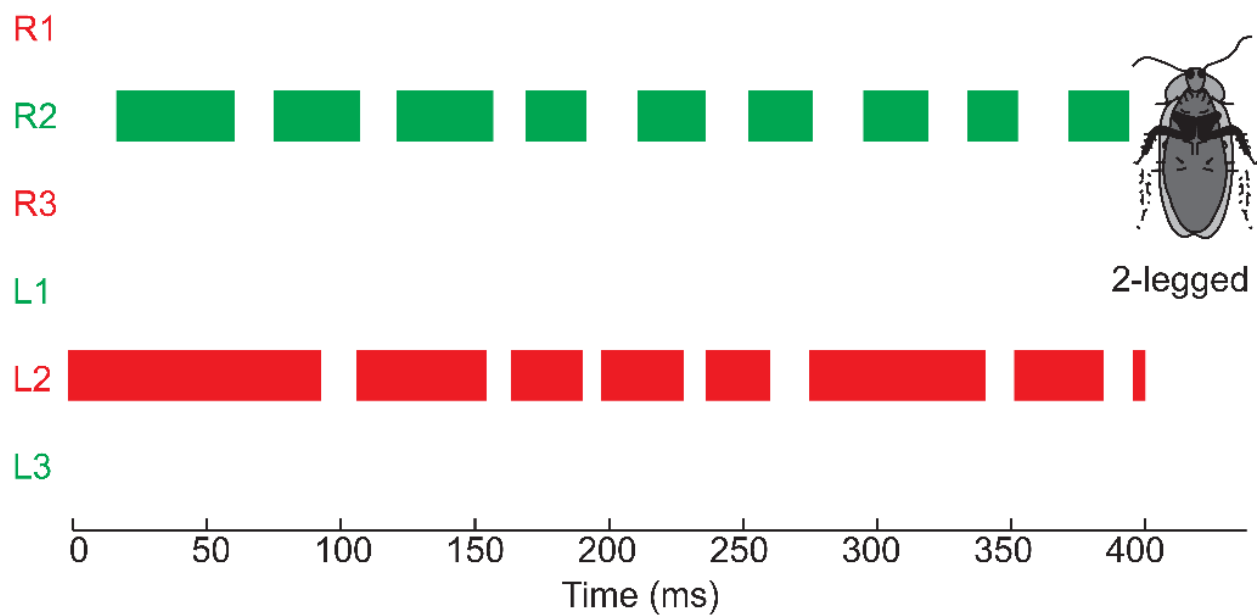
Figure 4.10: Cockroach gait with 2 legs. Red bars represent the right tripod while the green bars represent the left tripod. Shown on the horizontal axis is time (ms). The colored spaces indicate leg contact with the ground during stance phase, while the white spaces represent legs in the air during swing phase of locomotion. Cockroaches used tripod gait for locomotion with just two middle legs left after ablation of all front and hind legs.

Figure 4.11: Variation of velocity (cm s^{-1}) after successive leg loss for the five leg configurations. The column with the error bars represent mean $\pm$ 1 s.d. Cockroaches do not significantly change their running velocity across intact, 5-legged or 4-legged states but significantly reduce when in 3-legged and 2-legged states.

Figure 4.12: Variation of stride frequency (Hz) after successive leg loss for the five leg configurations. The column with the error bars represent mean ± 1 s.d. Cockroaches do not significantly change their stride frequency across intact, 5-legged or 4-legged states but significantly reduce when in 3-legged and 2-legged states.

Figure 4.13: Variation of stride length (cm) after successive leg loss for the five leg configurations. The column with the error bars represent mean $\pm$ 1 s.d. Cockroaches do not significantly change their stride length across intact, 5-legged or 4-legged states but significantly reduce when in 3-legged and 2-legged states.

Figure 4.14: Variation of duty factor after successive leg loss for the five leg configurations. The column with the error bars represent mean ± 1 s.d. Cockroaches do not significantly change their duty factor across intact, 5-legged, 4-legged or 3-legged states but significantly increase when in 2-legged state.
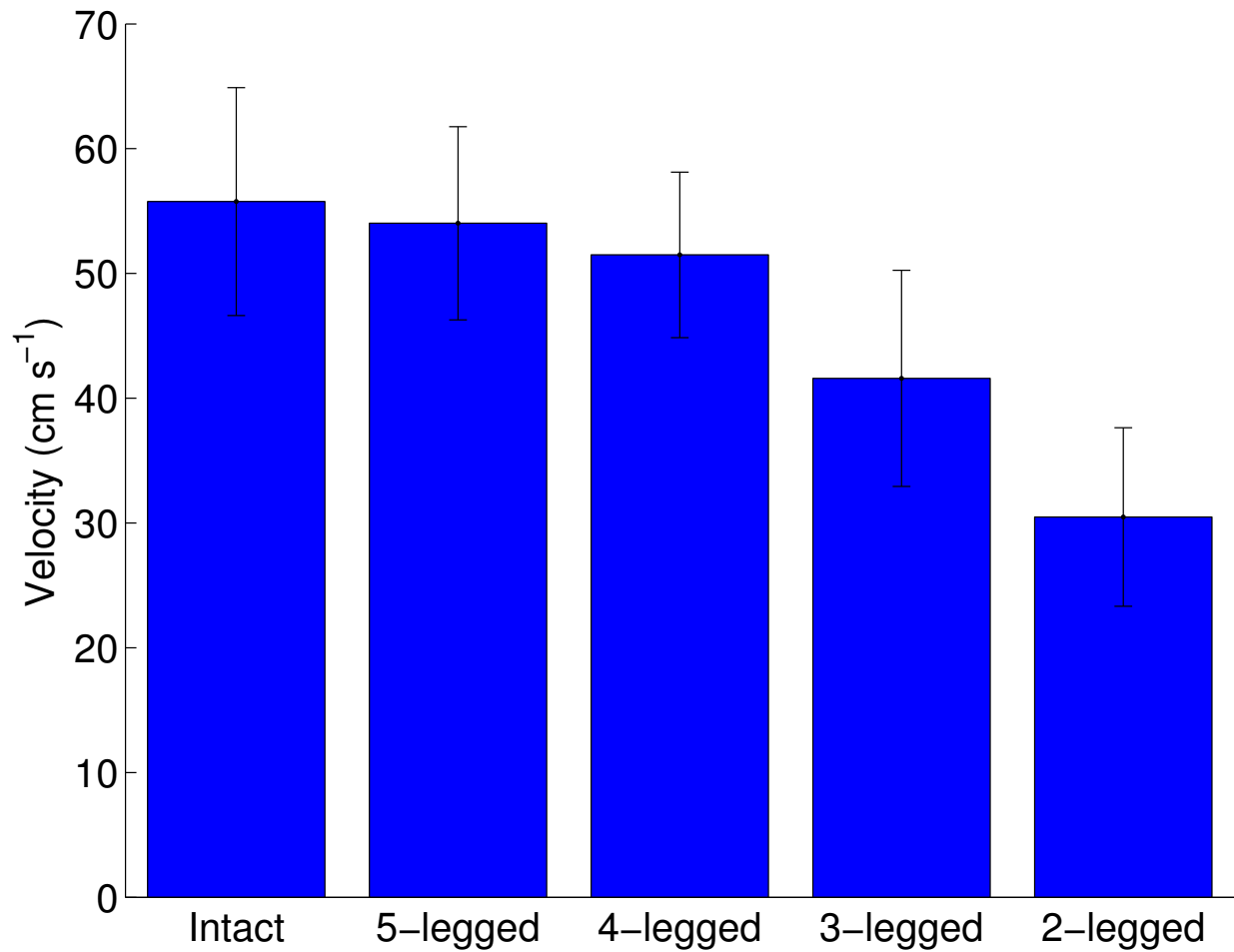
Figure 4.15: Variation of roll angle (^{0}) after successive leg loss for the five leg configurations. The column with the error bars represent mean $\pm$ 1 s.d. Cockroaches increase peak-peak roll angle from intact to 5-legged to 4-legged running, but seem to restore their intact magnitude during 3-legged and 2-legged locomotion.
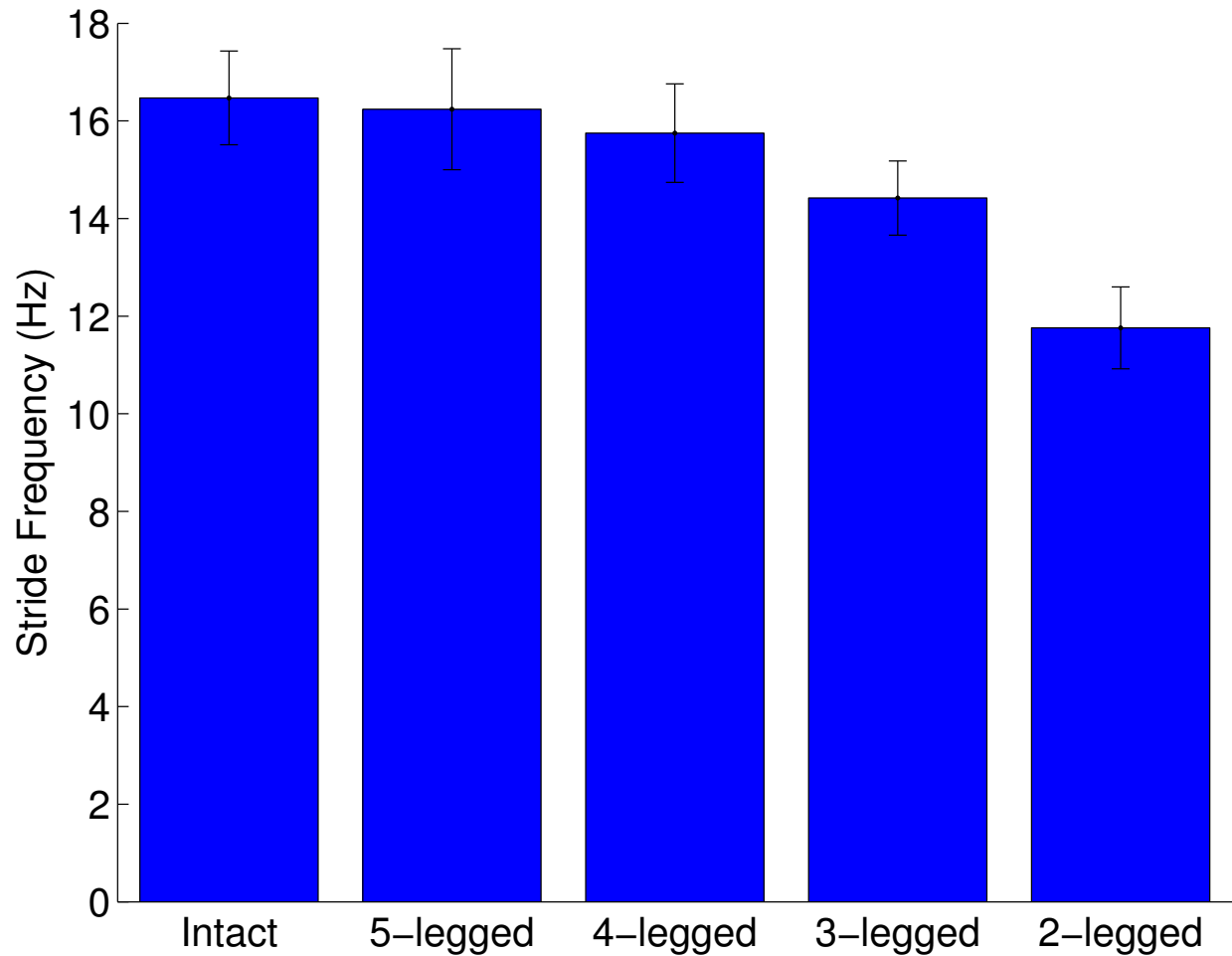
Figure 4.16: Variation of pitch angle (^{0}) after successive leg loss for the five leg configurations. The column with the error bars represent mean $\pm$ 1 s.d. Cockroaches increase their body pitch when running with a single tripod of legs compared to other leg manipulations.
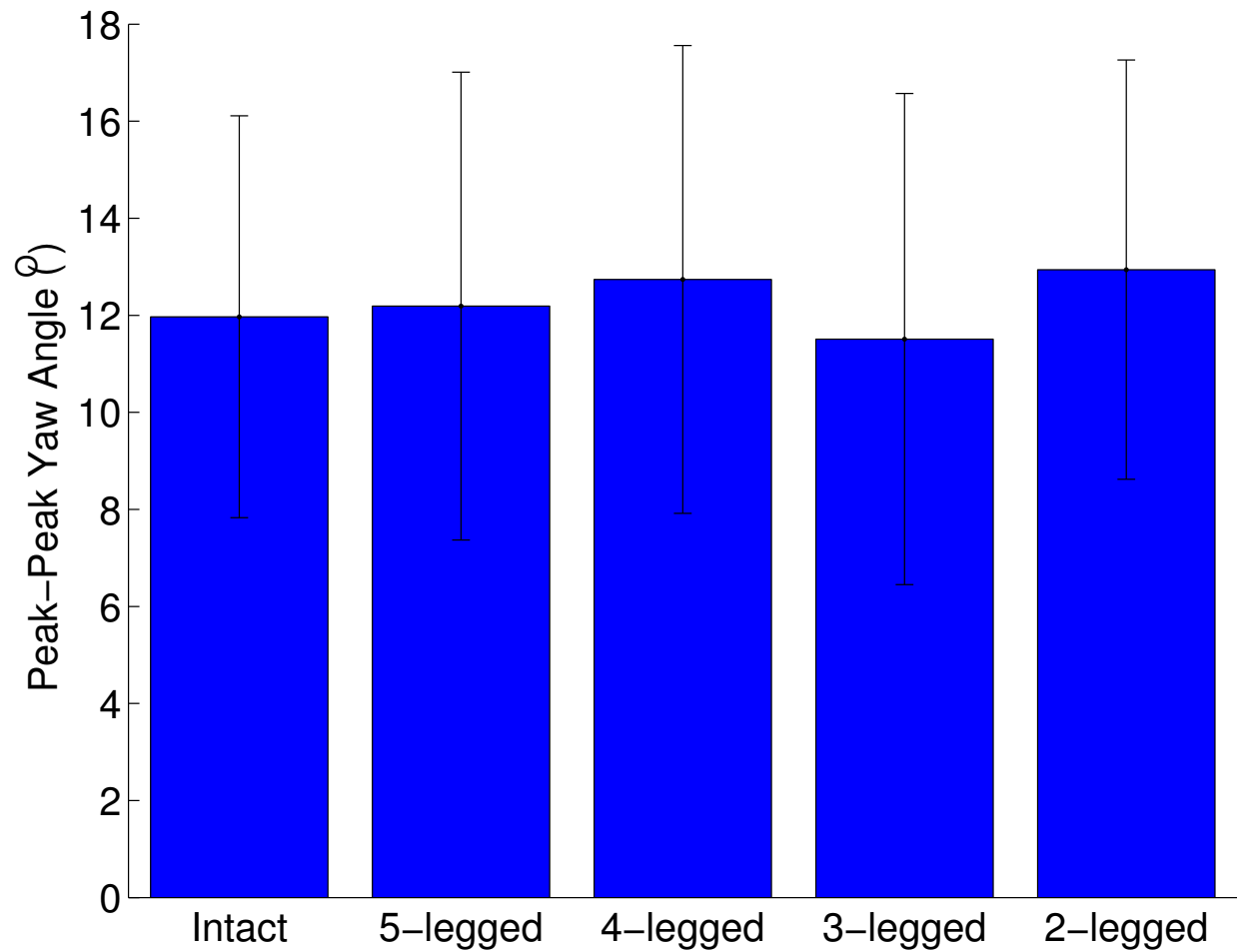
Figure 4.17: Variation of yaw angle (^{0}) after successive leg loss for the five leg configurations. The column with the error bars represent mean $\pm$ 1 s.d. Cockroaches do not change their peak-peak yaw angle across leg manipulations.
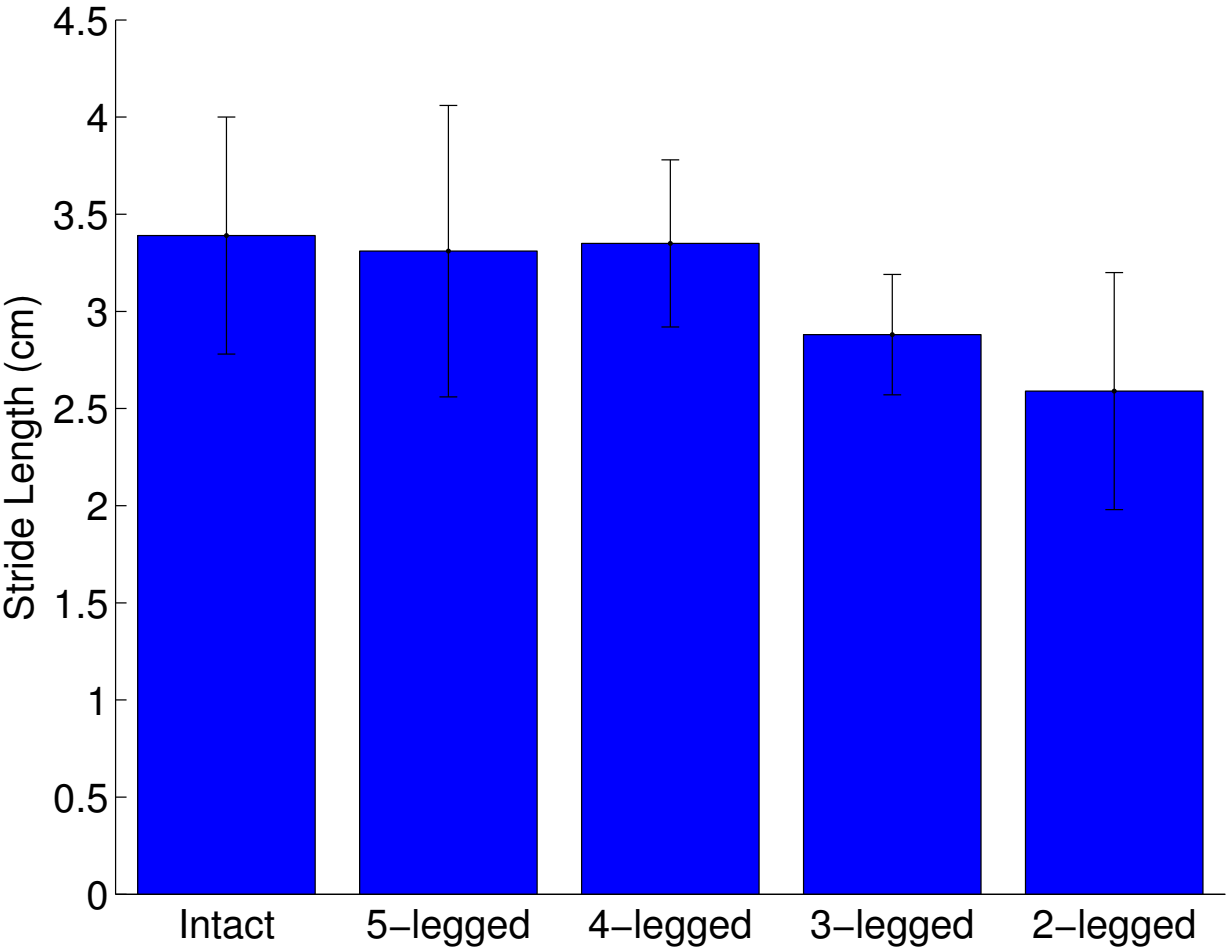
Figure 4.18: Variation of vertical force (mN) after successive leg loss for the five leg configurations. The column with the error bars represent mean ± 1 s.d. Cockroaches seem to maintain leg force across leg manipulations except when running on just two middle legs where the forces generated are significantly lower.
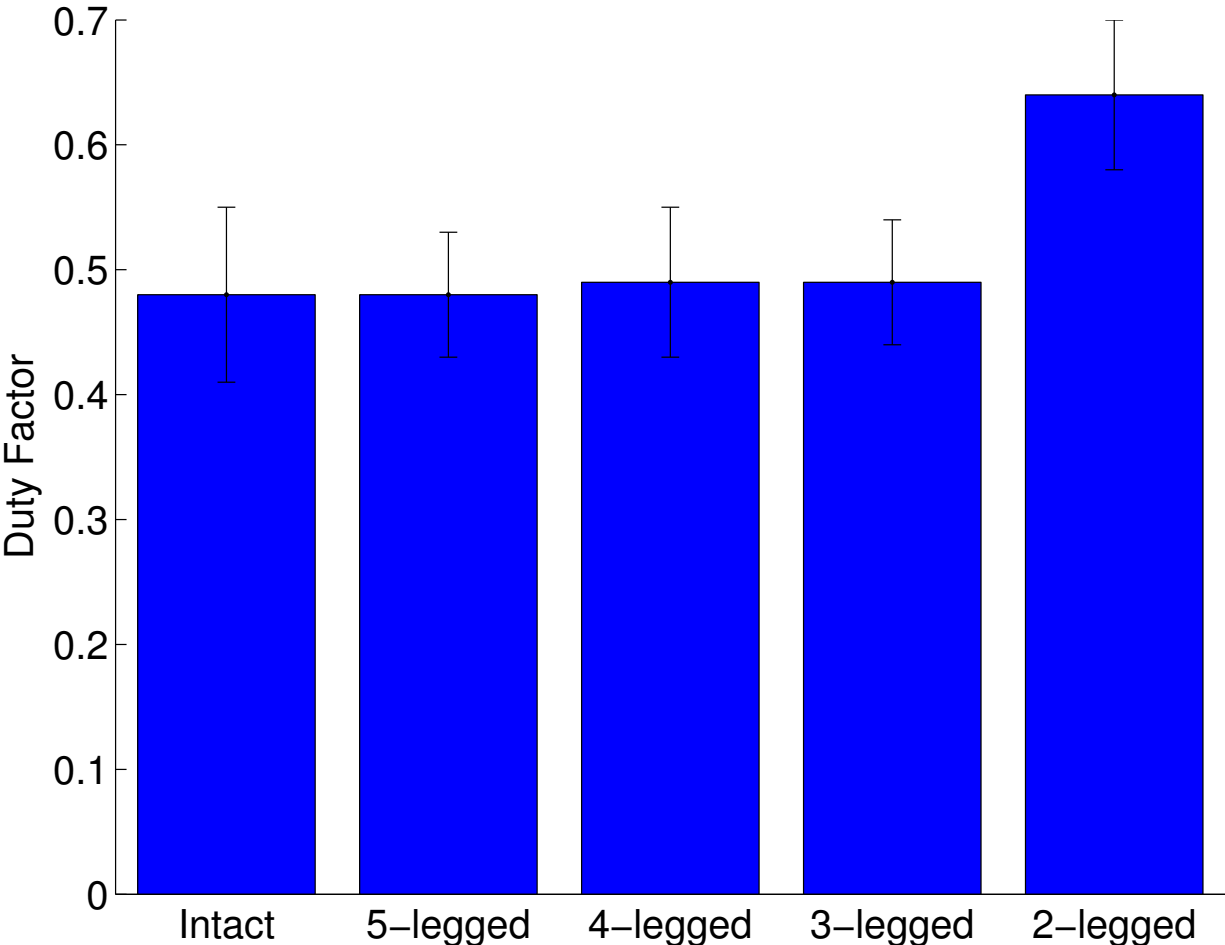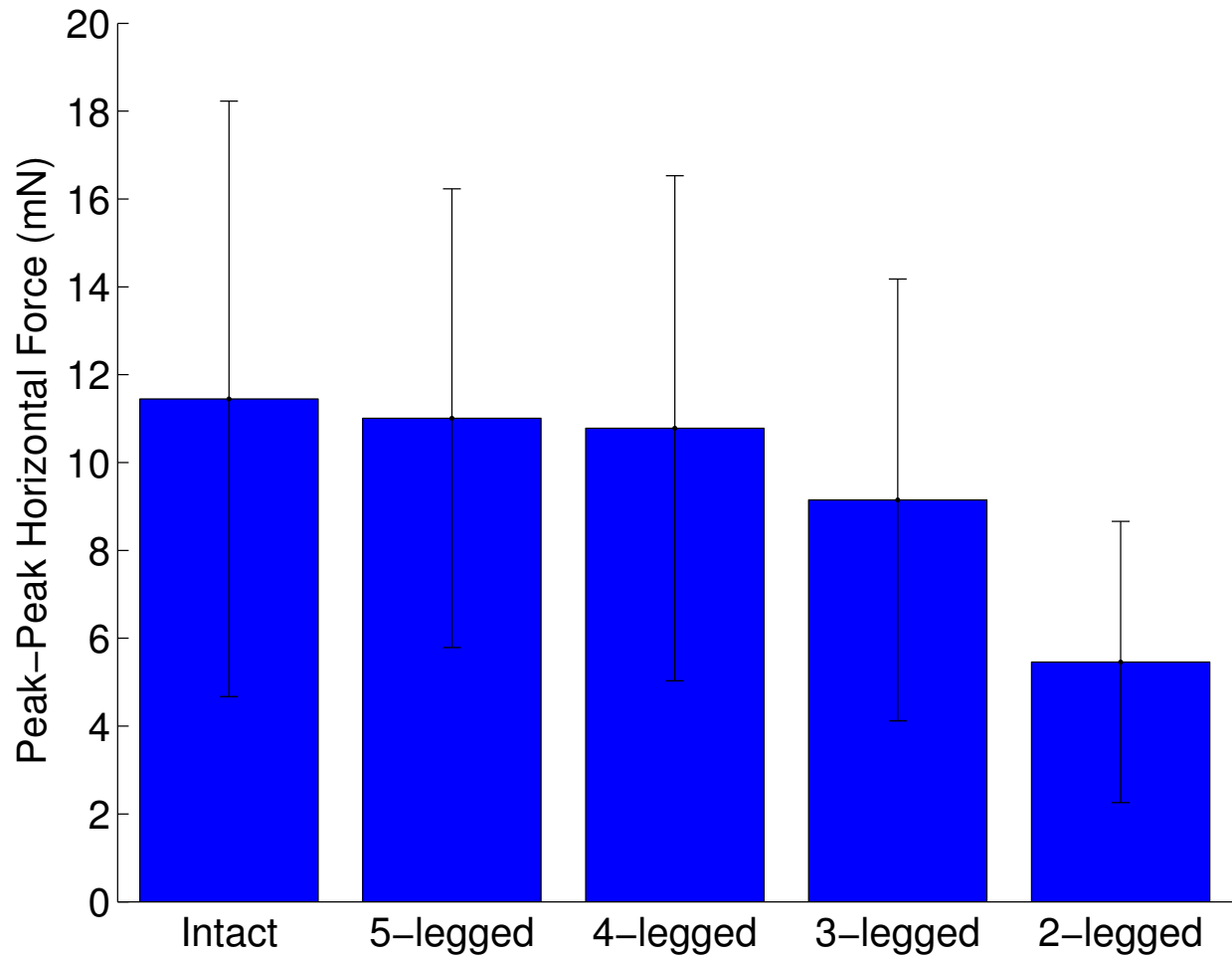
Figure 4.19: Variation of horizontal force (mN) after successive leg loss for the five leg configurations. The column with the error bars represent mean ± 1 s.d. Cockroaches produce similar horizontal forces in intact, 5-legged and 4-legged conditions but reduce it during 3-legged and 2-legged running.
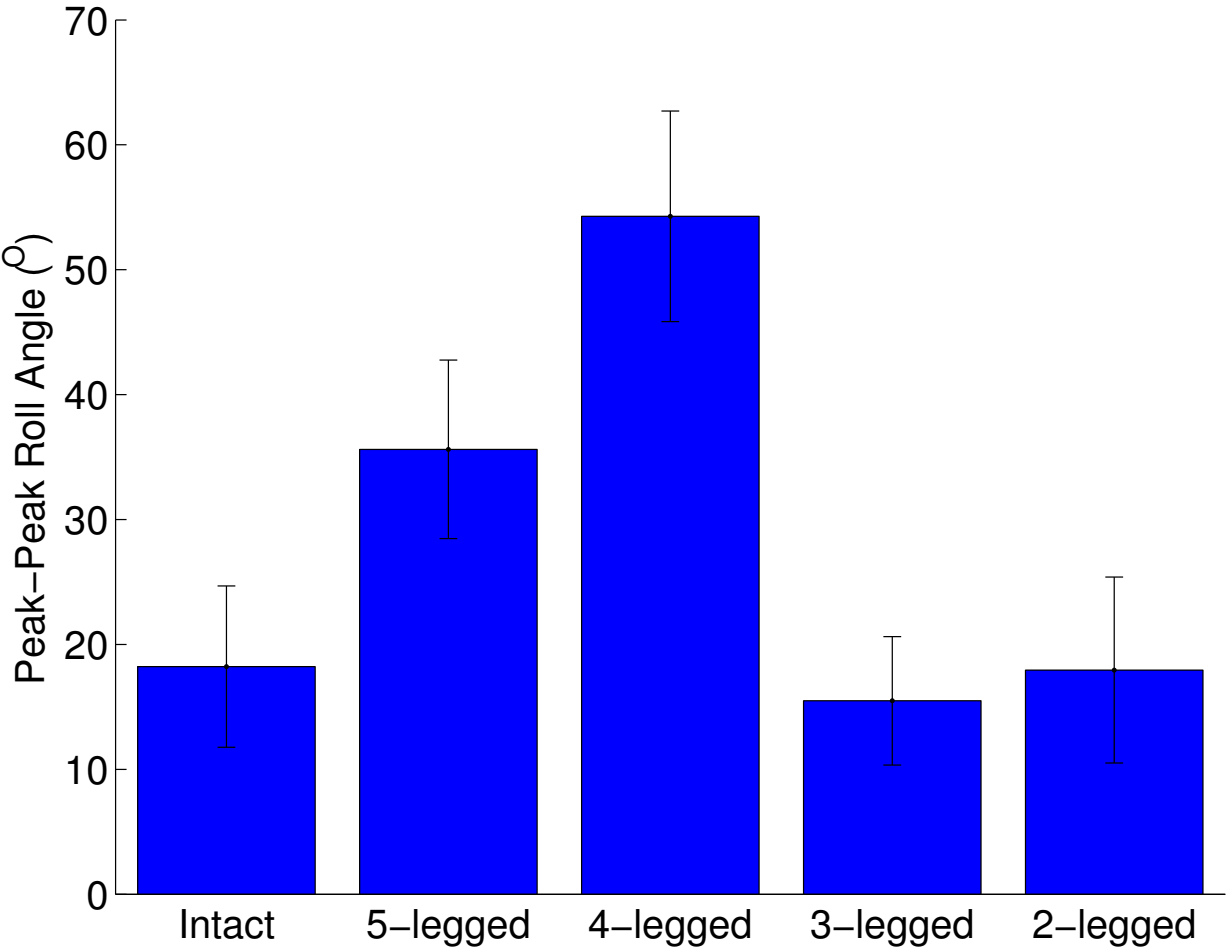
Figure 4.20: Variation of lateral force (mN) after successive leg loss for the five leg configurations. The column with the error bars represent mean $\pm$ 1 s.d. Cockroaches are unable to produce the same level of forces after leg ablation as they would in their intact state. The loss of both middle legs results in the lowest magnitude of lateral force.

Figure 4.21: Variation of velocity (cm s^{-1}) of RoboXplorer after successive leg loss for the five leg configurations. The column with the error bars represent mean $\pm$ 1 s.d. RoboXplorer performance is reduced after the loss of a leg but maintained despite further leg ablations. However even with two legs, can run at about 70% for its speed.
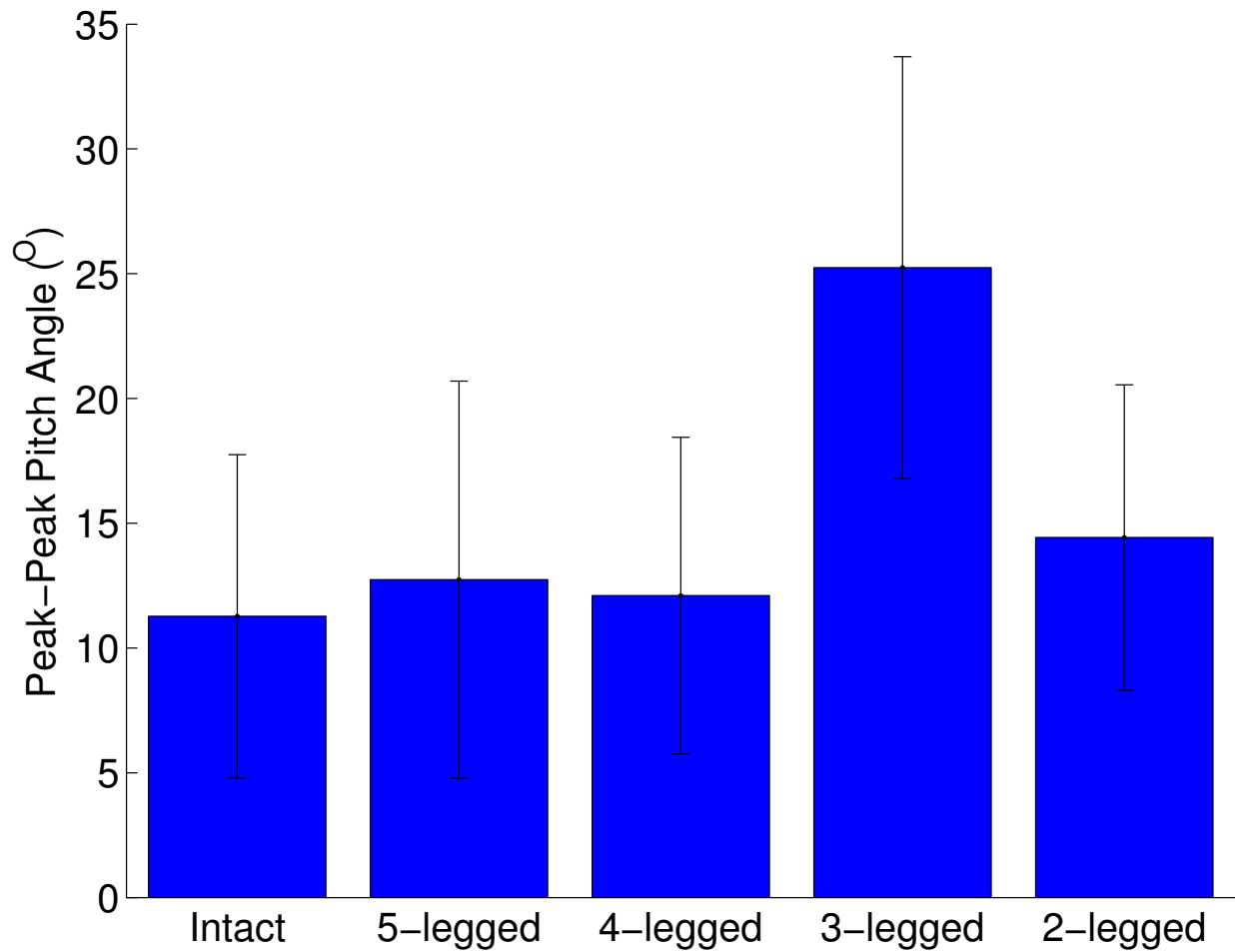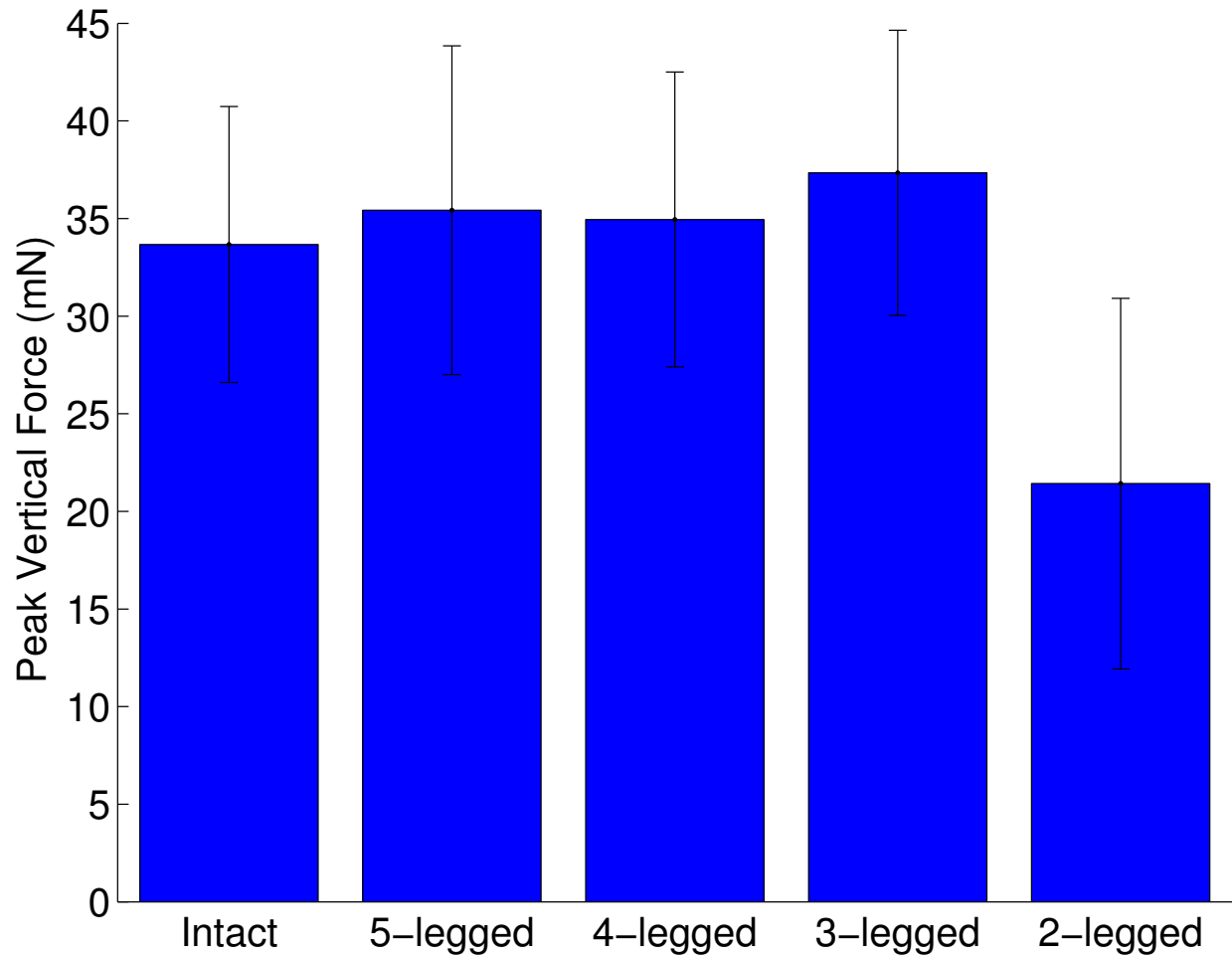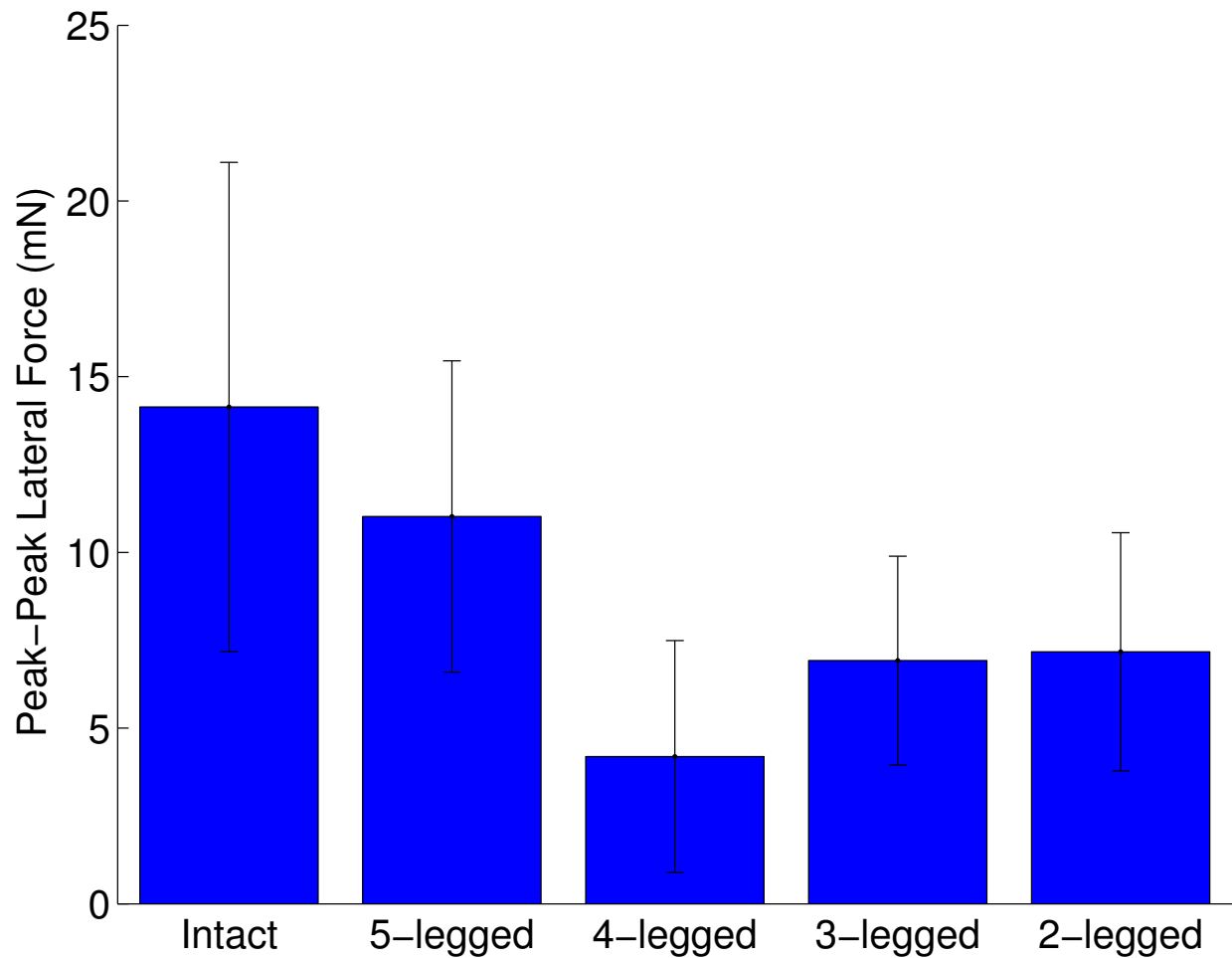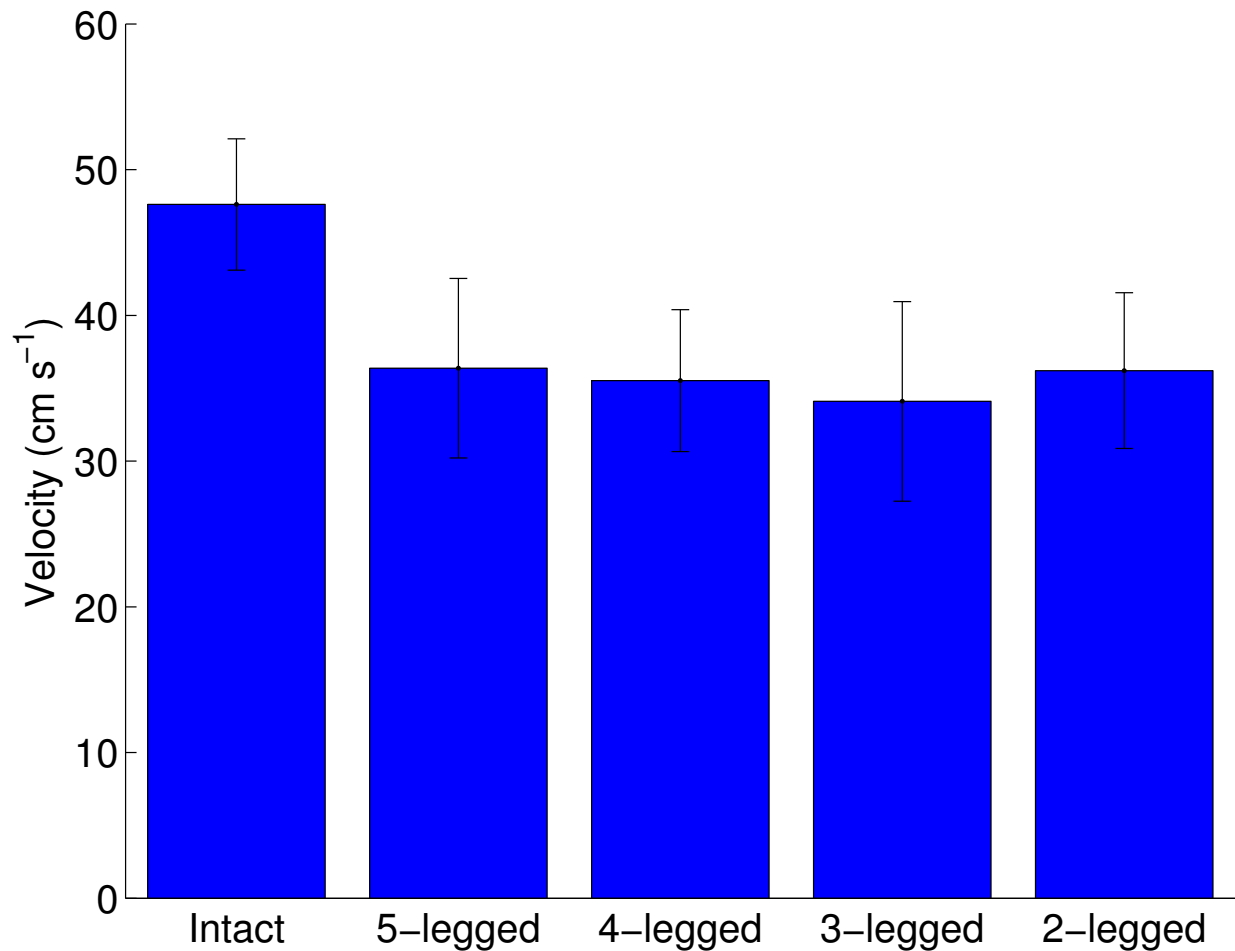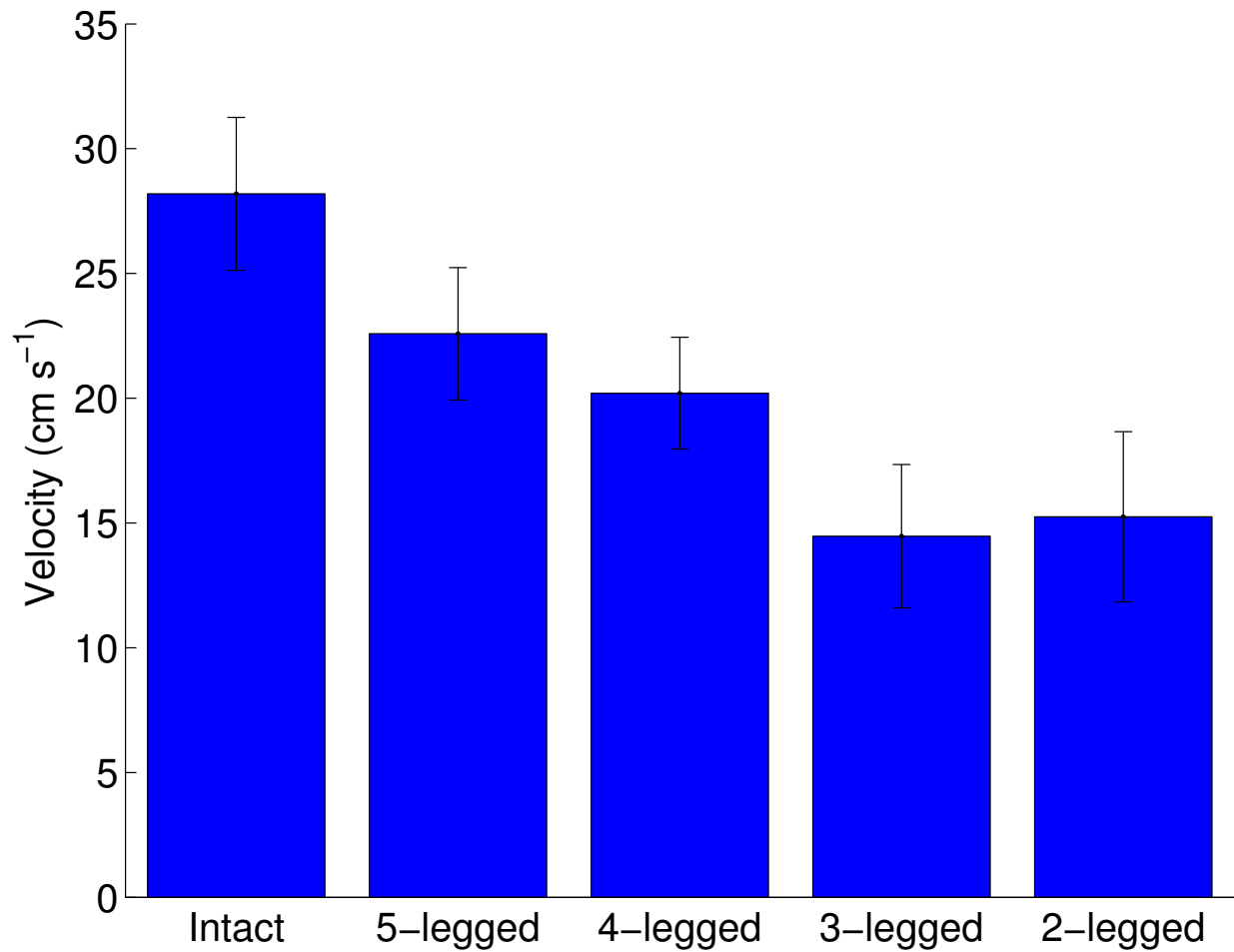
Figure 4.22: Variation of velocity (cm s^{-1}) of DASH after successive leg loss for the five leg configurations. The column with the error bars represent mean $\pm$ 1 s.d. DASH's velocity reduces with successive loss of legs. However even with two legs, can run at about 50% for its speed.

Bibliography

(1) Li, C.; Zhang, T.; Goldman, D. I. *Science* **2013**, *339*, 1408–1412.

(2) Dickinson, M. H.; Farley, C. T.; Full, R. J.; Koehl, M.; Kram, R.; Lehman, S. *Science* **2000**, *288*, 100–106.

(3) Sponberg, S; Full, R. *Journal of Experimental Biology* **2008**, *211*, 433–446.

(4) Valdastri, P.; Webster III, R. J.; Quaglia, C.; Quirini, M.; Menciassi, A.; Dario, P. *Robotics, IEEE Transactions on* **2009**, *25*, 1047–1057.

(5) Spagna, J. C.; Goldman, D. I.; Lin, P.-C.; Koditschek, D. E.; Full, R. J. *Bioinspiration & biomimetics* **2007**, *2*, 9.

(6) Maladen, R. D.; Ding, Y.; Li, C.; Goldman, D. I. *science* **2009**, *325*, 314–318.

(7) Maladen, R. D.; Ding, Y.; Umbanhowar, P. B.; Goldman, D. I. *The International Journal of Robotics Research* **2011**, *30*, 793–805.

(8) Marvi, H.; Gong, C.; Gravish, N.; Astley, H.; Travers, M.; Hatton, R. L.; Mendelson, J. R.; Choset, H.; Hu, D. L.; Goldman, D. I. *Science* **2014**, *346*, 224–229.

(9) Mazouchova, N.; Umbanhowar, P. B.; Goldman, D. I. *Bioinspiration & biomimetics* **2013**, *8*, 026007.

(10) Li, C.; Pullin, A. O.; Haldane, D. W.; Lam, H. K.; Fearing, R. S.; Full, R. J. *Bioinspiration & biomimetics* **2015**, *10*, 046003.

(11) Hosoi, A.; Goldman, D. I. *Annual Review of Fluid Mechanics* **2015**, *47*, 431–453.

(12) Goldman, D. I.; Chen, T. S.; Dudek, D. M.; Full, R. J. *Journal of Experimental Biology* **2006**, *209*, 2990–3000.

(13) Autumn, K.; Sitti, M.; Liang, Y. A.; Peattie, A. M.; Hansen, W. R.; Sponberg, S.; Kenny, T. W.; Fearing, R.; Israelachvili, J. N.; Full, R. J. *Proceedings of the National Academy of Sciences* **2002**, *99*, 12252–12256.

(14) Autumn, K; Dittmore, A; Santos, D; Spenko, M; Cutkosky, M *Journal of Experimental Biology* **2006**, *209*, 3569–3579.

(15) Dai, Z. D.; Gorb, S. N.; Schwarz, U. *J. Experimental Biol.* **2002**, *205*, 2479–2488.

(16) Spagna, J. . C.; Goldman, D. . I.; Lin, P. C.; Koditschek, D. . E.; Full, R. J. *Bioinspiration & Biomimetics* **2007**, *2*, 9–18.

(17) Dorgan, K. M.; Jumars, P. A.; Johnson, B.; Boudreau, B.; Landis, E. *Nature* **2005**, *433*, 475–475.

(18) Dorgan, K. M. *The Journal of experimental biology* **2015**, *218*, 176–183.

(19) Gravish, N.; Monaenkova, D.; Goodisman, M. A.; Goldman, D. I. *Proceedings of the National Academy of Sciences* **2013**, *110*, 9746–9751.

(20) Dorgan, K. *Experimental Mechanics* **2010**, *50*, 1373–1381.

(21) Calisti, M.; Giorelli, M.; Levy, G.; Mazzolai, B.; Hochner, B; Laschi, C.; Dario, P. *Bioinspiration & biomimetics* **2011**, *6*, 036002.

(22) Reichman, O.; Smith, S. C. *Current mammalogy* **1990**, *2*, 197–244.

(23) Trueman, E. R., *locomotion of soft-bodied animals*; Edward Arnold: 1975.

(24) Trimmer, B.; Lin, H.-t. *Integrative and comparative biology* **2014**, *54*, 1122–1135.

(25) Winter, A.; Deits, R.; Dorsch, D.; Slocum, A.; Hosoi, A., et al. *Bioinspiration & biomimetics* **2014**, *9*, 036009.

(26) Kim, S.; Laschi, C.; Trimmer, B. *Trends in biotechnology* **2013**, *31*, 287–294.

(27) Trivedi, D.; Rahn, C. D.; Kier, W. M.; Walker, I. D. *Applied Bionics and Biomechanics* **2008**, *5*, 99–117.

(28) Shepherd, R. F.; Ilievski, F.; Choi, W.; Morin, S. A.; Stokes, A. A.; Mazzeo, A. D.; Chen, X.; Wang, M.; Whitesides, G. M. *Proceedings of the National Academy of Sciences* **2011**, *108*, 20400–20403.

(29) Laschi, C.; Cianchetti, M. *Frontiers in bioengineering and biotechnology* **2014**, *2*.

(30) Lipson, H. *Soft Robotics* **2014**, *1*, 21–27.

(31) Full, R. J.; Tu, M. S. *Journal of Experimental Biology* **1991**, *156*, 215–231.

(32) Goldman, D. I.; Chen, T. S.; Dudek, D. M.; Full, R. J. *J. Experimental Biol.* **2006**, *209*, 2990–3000.

(33) Tullis, A.; Full, R. J. *The Journal of experimental biology* **1990**.

(34) Larsen, G.; Frazier, S.; Fish, S.; Zill, S. *Journal of Comparative Physiology A* **1995**, *176*, 229–238.

(35) Mongeau, J.-M.; McRae, B.; Jusufi, A.; Birkmeyer, P.; Hoover, A. M.; Fearing, R.; Full, R. J. *PloS one* **2012**, *7*, e38003.

(36) Vincent, J. F. *Composites Part A: Applied Science and Manufacturing* **2002**, *33*, 1311–1315.

(37) Vincent, J. F.; Wegst, U. G. *Arthropod Structure & Development* **2004**, *33*, 187–199.

(38) Fabritius, H.; Sachs, C; Raabe, D; Nikolov, S; Friák, M; Neugebauer, J In *Chitin*; Springer: 2011, pp 35–60.

(39) Lin, H.-T.; Dorfmann, A. L.; Trimmer, B. A. *Journal of theoretical biology* **2009**, *256*, 447–457.

(40) Wootton, R. J. *Journal of Experimental Biology* **1999**, *202*, 3333–3345.

(41) Delcomyn, F. *Journal of Experimental Biology* **1971**, *54*, 443–452.

(42) Ding, Y.; Sharpe, S. S.; Masse, A.; Goldman, D. I. **2012**.

(43) Clark, A. J.; Triblehorn, J. D. *PeerJ* **2014**, *2*, e501.

(44) Hoover, A. M.; Fearing, R. S. In *Robotics and Automation, 2008. ICRA 2008. IEEE International Conference on*, 2008, pp 886–892.

(45) Hoover, A. M.; Burden, S.; Fu, X.-Y.; Sastry, S. S.; Fearing, R. S. In *Biomedical Robotics and Biomechatronics (BioRob), 2010 3rd IEEE RAS and EMBS International Conference on*, 2010, pp 869–876.

(46) Wood, R.; Avadhanula, S; Sahai, R; Steltz, E; Fearing, R. *Journal of Mechanical Design* **2008**, *130*, 052304.

(47) Harley, C.; English, B.; Ritzmann, R. *Journal of Experimental Biology* **2009**, *212*, 1463–1476.

(48) Full, R; Yamauchi, A; Jindrich, D *The Journal of experimental biology* **1995**, *198*, 2441–2452.

(49) Quillin, K. *Journal of Experimental Biology* **2000**, *203*, 2757–2770.

(50) Sharpe, S. S.; Kuckuk, R.; Goldman, D. I. *Physical biology* **2015**, *12*, 046009.

(51) Full, R; Ahn, A *The journal of experimental biology* **1995**, *198*, 1285–1298.

(52) Horner, A. M.; Biknevicius, A. R. *Zoology* **2010**, *113*, 189–197.

(53) Bobbert, M. F. *Journal of Applied Physiology* **2012**, *112*, 1975–1983.

(54) Gorb, S. N.; Beutel, R. G.; Gorb, E. V.; Jiao, Y.; Kastner, V.; Niederegger, S.; Popov, V. L.; Scherge, M.; Schwarz, U.; Vötsch, W. *Integrative and Comparative Biology* **2002**, *42*, 1127–1139.

(55) Clemente, C. J.; Dirks, J.-H.; Barbero, D. R.; Steiner, U.; Federle, W. *Journal of Comparative Physiology A* **2009**, *195*, 805–814.

(56) Arzt, E.; Gorb, S.; Spolenak, R. *Proceedings of the National Academy of Sciences* **2003**, *100*, 10603–10606.

(57) Federle, W.; Brainerd, E. L.; McMahon, T. A.; Hölldobler, B. *Proceedings of the National Academy of Sciences* **2001**, *98*, 6215–6220.

(58) Federle, W.; Riehle, M.; Curtis, A. S.; Full, R. J. *Integrative and Comparative Biology* **2002**, *42*, 1100–1106.

(59) Qian, F; Zhang, T; Korff, W; Umbanhowar, P.; Full, R.; Goldman, D In *INTEGRATIVE AND COMPARATIVE BIOLOGY*, 2015; Vol. 55, E148–E148.

(60)   Ahn, A. N.; Full, R. J. *Journal of Experimental Biology* **2002**, *205*, 379–389.

(61)   Dirks, J.-H.; Taylor, D. *The Journal of experimental biology* **2012**, *215*, 1502–1508.

(62)   Seok, S.; Onal, C. D.; Wood, R.; Rus, D.; Kim, S. In *Robotics and Automation (ICRA), 2010 IEEE International Conference on*, 2010, pp 1228–1233.

(63)   Tolley, M. T.; Shepherd, R. F.; Mosadegh, B.; Galloway, K. C.; Wehner, M.; Karpelson, M.; Wood, R. J.; Whitesides, G. M. *Soft Robotics* **2014**, *1*, 213–223.

(64)   Bartlett, N. W.; Tolley, M. T.; Overvelde, J. T.; Weaver, J. C.; Mosadegh, B.; Bertoldi, K.; Whitesides, G. M.; Wood, R. J. *Science* **2015**, *349*, 161–165.

(65)   Umedachi, T.; Vikas, V.; Trimmer, B., et al. In *Intelligent Robots and Systems (IROS), 2013 IEEE/RSJ International Conference on*, 2013, pp 4590–4595.

(66)   Umedachi, T.; Trimmer, B., et al. In *Robotics and Automation (ICRA), 2014 IEEE International Conference on*, 2014, pp 2874–2879.

(67)   *Nonlinear Dynamics* **2014**, *78*, 2811–2821.

(68)   Rus, D.; Tolley, M. T. *Nature* **2015**, *521*, 467–475.

(69)   Birkmeyer, P.; Peterson, K.; Fearing, R. S. In *Intelligent Robots and Systems, 2009. IROS 2009. IEEE/RSJ International Conference on*, 2009, pp 2683–2689.

(70)   Haldane, D. W.; Fearing, R. S.

(71)   Cully, A.; Clune, J.; Tarapore, D.; Mouret, J.-B. *Nature* **2015**, *521*, 503–507.

(72)   Carlson, J.; Murphy, R. R. *Robotics, IEEE Transactions on* **2005**, *21*, 423–437.

(73)   Spence, A. J.; Revzen, S.; Seipel, J.; Mullens, C.; Full, R. J. *The Journal of experimental biology* **2010**, *213*, 1907–1920.

(74)   Goetzke, H. . H. .; Federle, W. . *Integrative Comparative Biol.* **2013**, *53*, E79–E79.

(75)   Carey, J. R.; Liedo, P.; Mueller, H.-G.; Wang, J.-L.; Yang, W.; Molleman, F. *EXPERIMENTAL GERONTOLOGY* **2009**, *44*, 541–545.

(76)   Miura, K.; Ohsaki, N. *ECOLOGICAL RESEARCH* **2015**, *30*, 33–39.

(77)   Jen, E., *Robust Design: A Repertoire of Biological, Ecological, and Engineering Case Studies. Studies in the Sciences of Complexity*; Oxford University Press, USA: 2005.

(78)   Watson, J. T.; Ritzmann, R. E.; Pollack, A. J. *J. Comparative Physiology A-neuroethology Sensory Neural Behavioral Physiology* **2002**, *188*, 55–69.

(79)   Nishikawa, K.; Biewener, A. A.; Aerts, P.; Ahn, A. N.; Chiel, H. J.; Daley, M. A.; Daniel, T. L.; Full, R. J.; Hale, M. E.; Hedrick, T. L., et al. *Integrative and Comparative Biology* **2007**, *47*, 16–54.

(80)   Haldane, J. B. *HarperÕs Magazine* **1926**, *152*, 424–427.

(81)   Brown, I. E.; Loeb, G. E. In *Biomechanics and neural control of posture and movement*; Springer: 2000, pp 148–163.

(82)   Dudek, D. M.; Full, R. J. *Journal of Experimental Biology* **2007**, *210*, 3209–3217.

(83)   Carrier, D. R.; Walter, R. M.; Lee, D. V. *Journal of Experimental Biology* **2001**, *204*, 3917–3926.

(84)   Gruhn, M.; Zehl, L.; Bueschges, A. *JOURNAL OF EXPERIMENTAL BIOLOGY* **2009**, *212*, 194–209.

(85)   Ugo Rosano, H.; arbara Webb, B. *Biological Cybernetics* **2007**, *97*, 229–246.

(86)   Full, R. J.; Koditschek, D. E. *Journal of Experimental Biology* **1999**, *202*, 3325–3332.

(87)   Jindrich, D. L.; Full, R. J. *Journal of Experimental Biology* **2002**, *205*, 2803–2823.

(88)   Revzen, S.; Burden, S. A.; Moore, T. Y.; Mongeau, J.-M.; Full, R. J. *Biological cybernetics* **2013**, *107*, 179–200.

(89)   Oshichika Baba, Y.; kira Tsukada, A.; hristopher M. . Comer, C. *J. Experimental Biol.* **2010**, *213*, 2294–2302.

(90)   Watson, J. T.; Ritzmann, R. E.; Zill, S. N.; Pollack, A. J. *J. Comparative Physiology A-neuroethology Sensory Neural Behavioral Physiology* **2002**, *188*, 39–53.

(91)   Dickinson, M. H. *Integrative and comparative biology* **2005**, *45*, 274–281.

(92)   Jankowski, R. *Earthquake engineering & structural dynamics* **2006**, *35*, 517–524.

(93)   Cowan, N. J.; Lee, J.; Full, R. *Journal of Experimental Biology* **2006**, *209*, 1617–1629.

(94)   Giinther, B *Physiol. Rev* **1975**, *55*, 659–699.

(95)   Garland, T. *Journal of Zoology* **1983**, *199*, 157–170.

(96)   Vincent, J., *Structural biomaterials*; Princeton University Press: 2012.

(97)   Ismail, K.; Stronge, W. *Journal of Applied Mechanics* **2008**, *75*, 061011.

(98)   Ye, K.; Li, L.; Zhu, H. *Earthquake Engineering and Engineering Vibration* **2009**, *8*, 433–446.

(99)   Schwager, T.; Pöschel, T. *Granular Matter* **2007**, *9*, 465–469.

(100)   Full, R. J. *Comprehensive Physiology* **1997**.

(101)   Ashby, M.; Gibson, L.; Wegst, U; Olive, R In *Proceedings of the Royal Society of London A: Mathematical, Physical and Engineering Sciences*, 1995; Vol. 450, pp 123–140.

(102)   Vogel, S., *Life's devices: the physical world of animals and plants*; Princeton University Press: 1988.

(103)   Ridgel, A. L.; Ritzmann, R. E.; Schaefer, P. L. *J. Experimental Biol.* **2003**, *206*, 4453–4465.

(104)   Baba, Y.; Tsukada, A.; Comer, C. M. *The Journal of experimental biology* **2010**, *213*, 2294–2302.

(105) Camhi, J.; Johnson, E. *The Journal of experimental biology* **1999**, *202*, 631–643.

(106) Okada, J; Kanamaru, Y; Toh, Y *ZOOLOGICAL SCIENCE* **2002**, *19*, 1201–1210.

(107) Okada, J.; Toh, Y. *J. Comparative Physiology A-sensory Neural Behavioral Physiology* **2000**, *186*, 849–857.

(108) Stierle, I.; Getman, M; Comer, C. *Journal of Comparative Physiology A* **1994**, *174*, 1–11.

(109) Schaefer, P.; Ritzmann, R. *JOURNAL OF NEUROBIOLOGY* **2001**, *49*, 9–28.

(110) Chen, C.-T.; Quinn, R. D.; Ritzmann, R. E. In *Robotics and Automation, 1997. Proceedings., 1997 IEEE International Conference on*, 1997; Vol. 3, pp 2007–2012.

(111) Went, F. *American Scientist* **1968**, 400–413.

(112) Guiler, R. W.; Wentworth, P. L.; Vaneck, T. W. In *6th AIAA Theoretical Fluid Mechanics Conference*, 2011, p 3117.

(113) Klaptocz, A.; Boutinard-Rouelle, G.; Briod, A.; Zufferey, J.-C.; Floreano, D. In *Robotics and Automation (ICRA), 2010 IEEE International Conference on*, 2010, pp 3349–3354.

(114) Briod, A. *Observation of insect collisions*; tech. rep.; 2008.

(115) Schmitt, J; Holmes, P *BIOLOGICAL CYBERNETICS* **2003**, *89*, 43–55.

(116) Holmes, P.; Full, R. J.; Koditschek, D.; Guckenheimer, J. *Siam Review* **2006**, *48*, 207–304.

(117) Biewener, A. A.; Daley, M. A. *Journal of Experimental Biology* **2007**, *210*, 2949–2960.

(118) Zajac, F. E. *Critical reviews in biomedical engineering* **1988**, *17*, 359–411.

(119) Biewener, A. A.; Gillis, G. B. *Journal of Experimental Biology* **1999**, *202*, 3387–3396.

(120) Kohlsdorf, T; Biewener, A. *Journal of Zoology* **2006**, *270*, 359–371.

(121) Altendorfer, R.; Moore, N.; Komsuoglu, H.; Buehler, M.; Brown Jr, H. B.; McMordie, D.; Saranli, U.; Full, R; Koditschek, D. E. *Autonomous Robots* **2001**, *11*, 207–213.

(122) Saranli, U.; Buehler, M.; Koditschek, D. E. *The International Journal of Robotics Research* **2001**, *20*, 616–631.

(123) Schilling, M.; Hoinville, T.; Schmitz, J.; Cruse, H. *BIOLOGICAL CYBERNETICS* **2013**, *107*, 397–419.

(124) Schilling, M.; Cruse, H.; Arena, P. *BIOLOGICAL CYBERNETICS* **2007**, *96*, 323–340.

(125) Kovač, M.; Schlegel, M.; Zufferey, J.-C.; Floreano, D. In *Intelligent Robots and Systems, 2009. IROS 2009. IEEE/RSJ International Conference on*, 2009, pp 583–588.

(126) Cham, J. G.; Bailey, S. A.; Clark, J. E.; Full, R. J.; Cutkosky, M. R. *The International Journal of Robotics Research* **2002**, *21*, 869–882.

(127) Carlson, J. M.; Doyle, J. *Proceedings of the National Academy of Sciences* **2002**, *99*, 2538–2545.

(128) Roth, L. M.; Willis, E. R. *J. Experimental Zoology* **1952**, *119*, 483–517.

(129) Mytro Gladun, D.; tanislav N. . Gorb, S. *Arthropod-plant Interactions* **2007**, *1*, 77–91.

(130) Dai, Z.; Gorb, S. N.; Schwarz, U. *Journal of Experimental Biology* **2002**, *205*, 2479–2488.

(131) Bullock, J. M. R.; Federle, W. *J. Experimental Biol.* **2009**, *212*, 1876–1888.

(132) Hilipp Busshardt, P.; tanislav N. . Gorb, S. *J. Experimental Biol.* **2013**, *216*, 319–328.

(133) Hilipp Busshardt, P.; tanislav N. . Gorb, S. *J. Comparative Physiology A-neuroethology Sensory Neural Behavioral Physiology* **2014**, *200*, 385–398.

(134) Newland, P. L. *J. Experimental Biol.* **1991**, *155*, 487–503.

(135) Duch, C.; Pfluger, H. J. *J. Experimental Biol.* **1995**, *198*, 1963–1976.

(136) Tanaka, A.; Akahane, H.; Ban, Y. *J. Experimental Zoology* **1992**, *262*, 61–70.

(137) Frazier, S. F.; Larsen, G. S.; Neff, D.; Quimby, L.; Carney, M.; DiCaprio, R. A.; Zill, S. N. *J. Comparative Physiology A-sensory Neural Behavioral Physiology* **1999**, *185*, 157–172.

(138) Niederegger, S.; Gorb, S. *J. Insect Physiology* **2003**, *49*, 611–620.

(139) Niederegger, S.; Gorb, S. N. *J. Comparative Physiology A-neuroethology Sensory Neural Behavioral Physiology* **2006**, *192*, 1223–1232.

(140) Avid Labonte, D.; alter Federle, W. *Plos One* **2013**, *8*, e81943.

(141) Federle, W.; Baumgartner, W.; Holldobler, B. *J. Experimental Biol.* **2004**, *207*, 67–74.

(142) Federle, W.; Endlein, T. *Arthropod Struct. & Development* **2004**, *33*, 67–75.

(143) Drechsler, P.; Federle, W. *J. Comparative Physiology A-neuroethology Sensory Neural Behavioral Physiology* **2006**, *192*, 1213–1222.

(144) Endlein, T.; Federle, W. *J. Comparative Physiology A-neuroethology Sensory Neural Behavioral Physiology* **2008**, *194*, 49–60.

(145) Fleming, P. A.; Bateman, P. W. *Journal of Experimental Biology* **2007**, *210*, 1446–1454.

(146) Clemente, C. J.; Federle, W. *Proc. Royal Soc. B-biological Sciences* **2008**, *275*, 1329–1336.

(147) Arnold, J. W. *International Journal Of Insect Morphology And Embryology* **1974**, *3*, 317–334.

(148) French, A. S. *Biological Cybernetics* **1980**, *38*, 115–123.

(149) French, A. S.; Sanders, E. J. *Cell Tissue Research* **1981**, *219*, 53–68.

(150) Zill, S. N.; Keller, B. R.; Duke, E. R. *J. Neurophysiology* **2009**, *101*, 2297–2304.

(151) Larsen, G. S.; Frazier, S. F.; Zill, S. N. *J. Comparative Physiology A-sensory Neural Behavioral Physiology* **1997**, *180*, 683–700.

(152) Asha N. . Zill, S.; ridget R. . Keller, B.; umaiya Chaudhry, S.; lizabeth R. . Duke, E.; avid Neff, D.; oger Quinn, R.; lay Flannigan, C. *J. Comparative Physiology A-neuroethology Sensory Neural Behavioral Physiology* **2010**, *196*, 407–420.

(153) Frantsevich, L.; Gorb, S. *Arthropod Struct. & Development* **2004**, *33*, 77–89.

(154) Jusufi, A.; Goldman, D. I.; Revzen, S.; Full, R. J. *Proceedings of the National Academy of Sciences* **2008**, *105*, 4215–4219.

(155) Mongeau, J.-M.; Demir, A.; Lee, J.; Cowan, N. J.; Full, R. J. *The Journal of experimental biology* **2013**, *216*, 4530–4541.

(156) Chapman, K. M. *J. Experimental Biol.* **1965**, *42*, 191–.

(157) Broussegaury, P. *Annales Des Sciences Naturelles-zoologie Et Biologie Animale* **1981**, *3*, 69–94.

(158) Ichael Guenther, M.; om Weihmann, T. *J. Theoretical Biol.* **2012**, *293*, 82–86.

(159) Kim, S.; Clark, J. E.; Cutkosky, M. R. *The International Journal of Robotics Research* **2006**, *25*, 903–912.

(160) Birkmeyer, P.; Gillies, A. G.; Fearing, R. S. In *Intelligent Robots and Systems (IROS), 2011 IEEE/RSJ International Conference on*, 2011, pp 5087–5093.

(161) Lee, J. S.; Fearing, R. S. In *Robotics and Automation (ICRA), 2015 IEEE International Conference on*, 2015, pp 4547–4553.

(162) Autumn, K.; Buehler, M.; Cutkosky, M.; Fearing, R.; Full, R. J.; Goldman, D.; Groff, R.; Provancher, W.; Rizzi, A. A.; Saranli, U., et al. In *Defense and Security*, 2005, pp 291–302.

(163) Spenko, M.; Haynes, G. C.; Sanders, J.; Cutkosky, M. R.; Rizzi, A. A.; Full, R. J.; Koditschek, D. E. *Departmental Papers (ESE)* **2008**, 397.

(164) Asbeck, A. T.; Kim, S.; McClung, A.; Parness, A.; Cutkosky, M. R. In *IEEE ICRA*, 2006.

(165) Birkmeyer, P.; Gillies, A. G.; Fearing, R. S. In *Intelligent Robots and Systems (IROS), 2012 IEEE/RSJ International Conference on*, 2012, pp 286–292.

(166) Siciliano, B.; Khatib, O., *Springer handbook of robotics*; Springer Science & Business Media: 2008.

(167) Nagatani, K.; Kiribayashi, S.; Okada, Y.; Otake, K.; Yoshida, K.; Tadokoro, S.; Nishimura, T.; Yoshida, T.; Koyanagi, E.; Fukushima, M., et al. *Journal of Field Robotics* **2013**, *30*, 44–63.

(168) Li, C.; Hsieh, S. T.; Goldman, D. I. *The Journal of experimental biology* **2012**, *215*, 3293–3308.

(169) GRAHAM, D *JOURNAL OF COMPARATIVE PHYSIOLOGY* **1977**, *116*, 91–116.

(170) DELCOMYN, F *JOURNAL OF EXPERIMENTAL BIOLOGY* **1991**, *156*, 503–517.

(171) Blanke, M.; Schröder, J., *Diagnosis and fault-tolerant control*; Springer: 2006; Vol. 2.

(172) Federici, D.; Ziemke, T. In *From Animals to Animats 9*; Springer: 2006, pp 449–460.

(173) SHIMIZU, T; MASAKI, S *JOURNAL OF INSECT PHYSIOLOGY* **1993**, *39*, 1021–1027.

(174) BOHN, H *DEVELOPMENTAL BIOLOGY* **1976**, *53*, 285–293.

(175) TANAKA, A; AKAHANE, H; BAN, Y *JOURNAL OF EXPERIMENTAL ZOOLOGY* **1992**, *262*, 61–70.

(176) Guffey, C. *Canadian journal of zoology* **1999**, *77*, 824–830.

(177) Brueseke, M. A.; Rypstra, A. L.; Walker, S. E.; Persons, M. H. *The American Midland Naturalist* **2001**, *146*, 153–160.

(178) Blickhan, R.; Ernst, M.; Koch, M.; Mueller, R. *HUMAN MOVEMENT SCIENCE* **2013**, *32*, 971–983.

(179) Cruse, H. *Journal of Comparative Physiology* **1976**, *112*, 235–262.

(180) Gorb, S. N.; Niederegger, S.; Hayashi, C. Y.; Summers, A. P.; Voetsch, W.; Walther, P. *Nature* **2006**, *443*, 407–407.

(181) Asamichi Kanou, M.; hinsuke Morita, S.; etsuya Matsuura, T.; suneo Yamaguchi, T. *Zoological Science* **2007**, *24*, 945–952.

(182) Wilson, D. M. *Annual review of entomology* **1966**, *11*, 103–122.

(183) Hughes, G. *Journal of Experimental Biology* **1952**, *29*, 267–285.

(184) Hughes, G. *Journal of Experimental Biology* **1957**, *34*, 306–333.

(185) Cruse, H; Kuhn, S; Park, S; Schmitz, J *JOURNAL OF COMPARATIVE PHYSIOLOGY A-NEUROETHOLOGY SENSORY NEURAL AND BEHAVIORAL PHYSIOLOGY* **2004**, *190*, 983–991.

(186) Anagnostopoulos, S. A. *Earthquake Engineering and Structural Dynamics* **1988**, *16*, 443–456.

(187) Huang, M., *Vehicle crash mechanics*; CRC press: 2002.

(188) Hirota, K.; Fukuda, T., *Soft computing in mechatronics*; Springer Science & Business Media: 1999; Vol. 32.

(189) Alexander, R. M., *Principles of animal locomotion*; Princeton University Press: 2003.

(190) Koditschek, D. E.; Full, R. J.; Buehler, M. *Arthropod structure & development* **2004**, *33*, 251–272.

(191) Walter, R. M.; Carrier, D. R. *Journal of experimental biology* **2002**, *205*, 2135–2141.

(192) Balasubramanian, R.; Rizzi, A.; Mason, M. T., et al. In *Intelligent Robots and Systems, 2003.(IROS 2003). Proceedings. 2003 IEEE/RSJ International Conference on*, 2003; Vol. 1, pp 880–885.

(193) Nichols, E.; Franklin, W., *The Elements of Physics: Mechanics and heat*; The Elements of Physics: A College Text-book; Macmillan: 1898.

(194) Jiao, Y. K.; Gorb, S.; Scherge, M. *J. Experimental Biol.* **2000**, *203*, 1887–1895.

(195) Gorb, S.; Jiao, Y. K.; Scherge, M. *J. Comparative Physiology A-sensory Neural Behavioral Physiology* **2000**, *186*, 821–831.

(196) Harley, C. M.; English, B. A.; Ritzmann, R. E. *J. Experimental Biol.* **2009**, *212*, 1463–1476.

(197) Akay, T.; Haehn, S.; Schmitz, J.; Buschges, A. *J. Neurophysiology* **2004**, *92*, 42–51.

(198) Durr, V. *J. Experimental Biol.* **2001**, *204*, 1589–1604.

(199) Cruse, H.; Dean, J.; Suilmann, M. *J. Comparative Physiology* **1984**, *154*, 695–705.

(200) Nelson, G. M.; Quinn, R. D. *Ieee Control Systems Magazine* **1999**, *19*, 9–14.

(201) Kramer, K.; Markl, H. *J. Insect Physiology* **1978**, *24*, 577–586.

(202) Blaesing, B.; Cruse, H. *J. Experimental Biol.* **2004**, *207*, 1273–1286.

(203) Blasing, B.; Cruse, H. *J. Comparative Physiology A-neuroethology Sensory Neural Behavioral Physiology* **2004**, *190*, 173–183.

(204) Schargott, M.; Popov, V. L.; Gorb, S. *J. Theoretical Biol.* **2006**, *243*, 48–53.

(205) Hooper, S. L.; Guschlbauer, C.; Bluemel, M.; Rosenbaum, P.; Gruhn, M.; Akay, T.; Bueschges, A. *J. Neuroscience* **2009**, *29*, 4109–4119.

(206) Ritzmann, R. E.; Pollack, A. J.; Archinal, J.; Ridgel, A. L.; Quinn, R. D. *J. Comparative Physiology A-neuroethology Sensory Neural Behavioral Physiology* **2005**, *191*, 253–264.

(207) Delcomyn, F.; Nelson, M. E.; Cocatre-Zilgien, J. H. *Int. J. Robotics Research* **1996**, *15*, 113–127.

(208) Nne M. . Peattie, A. *J. Comparative Physiology B-biochemical Systemic Environmental Physiology* **2009**, *179*, 231–239.

(209) Tichy, H.; Barth, F. G. *Microscopy Research Technique* **1992**, *22*, 372–391.

(210) Oris Al Bitar, L.; agmar Voigt, D.; laus P. . W. . Zebitz, C.; tanislav N. . Gorb, S. *J. Insect Physiology* **2009**, *55*, 1029–1038.

(211) Ichael S. . Bartsch, M.; alter Federle, W.; obert J. . Full, R.; homas W. . Kenny, T. *J. Microelectromechanical Systems* **2007**, *16*, 709–718.

(212) French, A. S.; Marmarelis, V. Z. *Biological Cybernetics* **1995**, *73*, 425–430.

(213) French, A. S.; Torkkeli, P. H. *Neuroscience Lett.* **1994**, *178*, 147–150.

(214) Hilipp Busshardt, P.; tanislav N. . Gorb, S.; arald Wolf, H. *J. Experimental Biol.* **2011**, *214*, 1676–1684.

(215) Onas O. . Wolff, J.; tanislav N. . Gorb, S. *Arthropod Struct. & Development* **2012**, *41*, 419–433.

(216) Oy E. . Ritzmann, R.; ynthia M. . Harley, C.; athryn A. . Daltorio, K.; rian R. . Tietz, B.; lan J. . Pollack, A.; ohn A. . Bender, J.; eiyuan Guo, P.; udra L. . Horomanski, A.; icholas D. . Kathman, N.; laudia Nieuwoudt, C.; my E. . Brown, A.; oger D. . Quinn, R. *Frontiers In Neuroscience* **2012**, *6*, UNSP 97.

(217) French, A. S.; Torkkeli, P. H. *News In Physiological Sciences* **1994**, *9*, 158–161.

(218) French, A. S.; Klimaszewski, A. R.; Stockbridge, L. L. *J. Neurophysiology* **1993**, *69*, 669–673.

(219) Ndrew S. . French, A. *Biological Cybernetics* **2009**, *100*, 417–426.

(220) Looft, F. J.; Baltensperger, C. M. *Ieee Transactions On Biomedical Engineering* **1990**, *37*, 565–573.

(221) Frantsevich, L. I.; Cruse, H. *J. Insect Physiology* **2005**, *51*, 1092–1104.

(222) French, A. S.; Patrick, S. K. *Biological Cybernetics* **1994**, *70*, 435–441.

(223) Llen Wohlfart, E.; onas O. . Wolff, J.; duard Arzt, E.; tanislav N. . Gorb, S. *J. Experimental Biol.* **2014**, *217*, 222–224.

(224) Homas Endlein, T.; alter Federle, W. *Proc. Royal Soc. B-biological Sciences* **2013**, *280*, 20122868.

(225) Onas O. . Wolff, J.; tanislav N. . Gorb, S. *Scientific Reports* **2013**, *3*, 1101.

(226) Oris Al Bitar, L.; agmar Voigt, D.; laus P. . W. . Zebitz, C.; tanislav N. . Gorb, S. *J. Insect Physiology* **2010**, *56*, 1966–1972.

(227) Iroshi Yoshida, H.; unihiko Kaneko, K. *Developmental Dynamics* **2009**, *238*, 1974–1983.

(228) Horsten Jeck, T.; olk Cruse, H. *J. Insect Physiology* **2007**, *53*, 724–733.

(229) Eslie M. . Theunissen, L.; olker Duerr, V. *Plos One* **2013**, *8*, e85321.

(230) Endlein, T. .; Federle, W. . *Comparative Biochem. Physiology A-molecular & Integrative Physiology* **2007**, *146*, S121–S122.

(231) Onas O. . Wolff, J.; tanislav N. . Gorb, S. *Zoology* **2015**, *118*, 1–7.

(232) Anmin Zhou, Y.; dam Robinson, A.; llrich Steiner, U.; alter Federle, W. *J. Royal Soc. Interface* **2014**, *11*, 20140499.

(233) Asha N. . Zill, S.; umaiya Chaudhry, S.; nnelie Exter, A.; nsgar Bueschges, A.; osef Schmitz, J. *Arthropod Struct. & Development* **2014**, *43*, 441–455.

(234) Ichael Guenther, M.; om Weihmann, T. *Archive Appl. Mechanics* **2011**, *81*, 1269–1287.

(235) Dam van Casteren, A.; onathan R. . Codd, J. *J. Insect Science* **2010**, *10*, 40.

(236) L. uther R. ., I. I. I. P.; ric Diller, E.; oger D. . Quinn, R. *Ieee-asme Transactions On Mechatronics* **2015**, *20*, 631–640.

(237) Zhou, W. Y.; Robinson, A. .; Steiner, U. .; Federle, W. . *Journal Of The Royal Society Interface* **2014**, *11*, 20140499 (12 pp.)–20140499 (12 pp.)

(238) Liu, W. Y.; Sun, W. S.; Wu, W. X.; Mei, W. T. *2013 Ieee International Conference On Robotics And Biomimetics (robio)* **2013**, 1819–24.

(239) Oger D. . Quinn, R.; lexander Boxerbaum, A.; uther Palmer, L.; illel Chiel, H.; ric Diller, E.; lexander Hunt, A.; ichard Bachmann, R. *Unmanned Systems Technology Xiii* **2011**, *8045*, 804511.

(240) L. uther R. ., I. I. I. P.; ric D. . Diller, E.; oger D. . Quinn, R. *2010 Ieee Int. Conference On Robotics Automation (icra)* **2010**, 2810–2815.

(241) Bullock, J. . M. . R. .; Federle, W. . *Integrative Comparative Biol.* **2009**, *49*, E23–E23.

(242) Federle, W.; Clemente, C.; Endlein, T. *Comparative Biochem. Physiology A-molecular & Integrative Physiology* **2008**, *150*, S87–S87.

(243) Pollack, A. J.; Ritzmann, R. E.; Ridgel, A. L.; Archinal, J. *Society For Neuroscience Abstract Viewer And Itinerary Planner* **2003**, *2003*, Abstract No. 606.5–Abstract No. 606.5.

(244) Zill, S. .; Noah, J. .; Quimby, L. .; Ridgel, A. .; Neff, D. .; Frazier, S. .; Harshbarger, D. . *Society For Neuroscience Abstracts* **2001**, *27*, 1364–1364.

(245) Gorb, S. N.; Scherge, M. *Biona Report* **2000**, *14*, 28–30.

(246) Noah, J. . A. .; Ridgel, A. . L. .; Frazier, S. . F. .; Zill, S. . N. . *Society For Neuroscience Abstracts* **2000**, *26*, Abstract No.–643.13.

(247) Wyttenbach, R. . A. .; Nelson, M. . C. .; Buschbeck, E. . K. .; Hoy, R. . R. . *Society For Neuroscience Abstracts* **2000**, *26*, Abstract No.–368.17.

(248) Ridgel, A. . L.; Frazier, S. F.; Zill, S. N. *Society For Neuroscience Abstracts* **1999**, *25*, 364–364.

(249) Zarrouk, D.; Haldane, D. W.; Fearing, R. S. In *SPIE Defense+ Security*, 2015, 94671S–94671S.

(250) Haldane, D. W.; Peterson, K. C.; Garcia Bermudez, F. L.; Fearing, R. S. In *Robotics and Automation (ICRA), 2013 IEEE International Conference on*, 2013, pp 3279–3286.

(251) Matsuura, T; Kanou, M; Yamaguchi, T *JOURNAL OF COMPARATIVE PHYSIOLOGY A-NEUROETHOLOGY SENSORY NEURAL AND BEHAVIORAL PHYSIOLOGY* **2002**, *187*, 987–995.

(252) TOBIAS, M.; RITZMANN, R. *JOURNAL OF COMPARATIVE PHYSIOLOGY* **1984**, *154*, 641–647.

(253) Hayot, C. M.; Enders, S.; Zera, A.; Turner, J. A. *JOURNAL OF MATERIALS RESEARCH* **2013**, *28*, 2650–2659.

(254) Niven, J. E.; Buckingham, C. J.; Lumley, S.; Cuttle, M. F.; Laughlin, S. B. *CURRENT BIOLOGY* **2010**, *20*, 86–91.

(255) Li, C.; Umbanhowar, P. B.; Komsuoglu, H.; Koditschek, D. E.; Goldman, D. I. *PROCEEDINGS OF THE NATIONAL ACADEMY OF SCIENCES OF THE UNITED STATES OF AMERICA* **2009**, *106*, 3029–3034.

(256) Ritzmann, R.; Quinn, R. In *WALKING: BIOLOGICAL AND TECHNOLOGICAL ASPECTS*, ed. by Pfeiffer, F and Zielinska, T; CISM Course on Walking - Biological and Technological Aspects, Udine, ITALY, SEP 08-12, 2003, 2004, 31–49.

(257) Nishii, J *BIOLOGICAL CYBERNETICS* **2000**, *83*, 435–442.

(258) Ridgel, A.; Frazier, S.; DiCaprio, R.; Zill, S. *JOURNAL OF NEUROPHYSIOLOGY* **1999**, *81*, 1432–1437.

(259) Bassler, D; Rathmayer, W *JOURNAL OF EXPERIMENTAL BIOLOGY* **1996**, *199*, 2369–2382.

(260) MACHIN, J; SMITH, J.; LAMPERT, G. *JOURNAL OF EXPERIMENTAL BIOLOGY* **1994**, *192*, 83–94.

(261) Tan, L.-F.; Zhao, Y.; Lei, C.-L. *BULLETIN OF INSECTOLOGY* **2013**, *66*, 173–180.

(262) Szabo, R.; Ferrier, D. E. K. *JOURNAL OF EXPERIMENTAL ZOOLOGY PART B-MOLECULAR AND DEVELOPMENTAL EVOLUTION* **2014**, *322*, 257–268.

(263) Nakamura, T.; Mito, T.; Bando, T.; Ohuchi, H.; Noji, S. *CELLULAR AND MOLECULAR LIFE SCIENCES* **2008**, *65*, 64–72.

(264) Morrey, J.; Lambrecht, B; Horchler, A.; Ritzmann, R.; Quinn, R. In *IROS 2003: PROCEEDINGS OF THE 2003 IEEE/RSJ INTERNATIONAL CONFERENCE ON INTELLIGENT ROBOTS AND SYSTEMS, VOLS 1-4*; IEEE/RSJ International Conference on Intelligent Robots and Systems, LAS VEGAS, NV, OCT 27-31, 2003, 2003, 82–87.

(265) Yan, Z.; JunXia, Z.; LuQuan, R. *SCIENCE CHINA-TECHNOLOGICAL SCIENCES* **2015**, *58*, 999–1006.

(266) Wang, S.; Tan, X. L.; Michaud, J. P.; Shi, Z. K.; Zhang, F. *BULLETIN OF ENTO-MOLOGICAL RESEARCH* **2015**, *105*, 245–252.

(267) Berendes, V.; Duebbert, M.; Bockemuehl, T.; Schmitz, J.; Bueschges, A.; Gruhn, M. *JOURNAL OF NEUROSCIENCE METHODS* **2013**, *215*, 224–233.

(268) Wosnitza, A.; Bockemuehl, T.; Duebbert, M.; Scholz, H.; Bueschges, A. *JOURNAL OF EXPERIMENTAL BIOLOGY* **2013**, *216*, 480–491.

(269) Grabowska, M.; Godlewska, E.; Schmidt, J.; Daun-Gruhn, S. *JOURNAL OF EXPERIMENTAL BIOLOGY* **2012**, *215*, 4255–4266.

(270) Al-Homsy, A.; Hartmann, J.; Maehle, E. In *ADAPTIVE MOBILE ROBOTICS*, ed. by Azad, AKM and Cowan, NJ and Tokhi, MO and Virk, GS and Eastman, RD; 15th International Conference on Climbing and Walking Robots and the Support Technologies for Mobile Machines, Baltimore, MD, JUL 23-26, 2012, 2012, 173–182.

(271) Nakamura, T.; Mito, T.; Miyawaki, K.; Ohuchi, H.; Noji, S. *DEVELOPMENTAL BIOLOGY* **2008**, *319*, 46–55.

(272) Auf, A. E. S.; Litza, M.; Maehle, E. In *BIOLOGICALLY-INSPIRED COLLABORATIVE COMPUTING*, ed. by Hinchey, M and Pagnoni, A and Rammig, FJ and Schmeck, H; 2nd International Conference on Biologically-Inspired Collaborative Computing held at the 20th World Computer Congress, Milan, ITALY, SEP 08-09, 2008, 2008; Vol. 268, 115–124.

(273) Carey, J. R.; Pinter-Wollman, N.; Wyman, M.; Mueller, H.-G.; Molleman, F.; Zhang, N. *EXPERIMENTAL GERONTOLOGY* **2007**, *42*, 166–172.

(274) Zaitoun, S.; Al-Ghzawi, A.; Shannag, H. *JOURNAL OF APPLIED ENTOMOLOGY-ZEITSCHRIFT FUR ANGEWANDTE ENTOMOLOGIE* **2001**, *125*, 85–87.

(275) ZOLLIKOFER, C. *JOURNAL OF EXPERIMENTAL BIOLOGY* **1994**, *192*, 95–106.

(276) KIMURA, S; YANO, M; SHIMIZU, H *BIOLOGICAL CYBERNETICS* **1994**, *70*, 505–512.

(277) DEAN, J *JOURNAL OF EXPERIMENTAL BIOLOGY* **1991**, *159*, 449–471.

(278) DELCOMYN, F *JOURNAL OF EXPERIMENTAL BIOLOGY* **1991**, *156*, 483–502.

(279) Schmitz, J.; Gruhn, M.; Bueschges, A. *JOURNAL OF NEUROPHYSIOLOGY* **2015**, *113*, 2309–2320.

(280) Zill, S. N.; Chaudhry, S.; Exter, A.; Bueschges, A.; Schmitz, J. *ARTHROPOD STRUCTURE & DEVELOPMENT* **2014**, *43*, 441–455.

(281) Theunissen, L. M.; Vikram, S.; Duerr, V. *JOURNAL OF EXPERIMENTAL BIOLOGY* **2014**, *217*, 3242–3253.

(282) Calas-List, D.; Clare, A. J.; Komissarova, A.; Nielsen, T. A.; Matheson, T. *JOURNAL OF NEUROSCIENCE* **2014**, *34*, 7509–7521.

(283) Theunissen, L. M.; Duerr, V. *PLOS ONE* **2013**, *8*, DOI: {10.1371/journal.pone.0085321}.

(284) Mongeau, J.-M.; Demir, A.; Lee, J.; Cowan, N. J.; Full, R. J. *JOURNAL OF EXPERIMENTAL BIOLOGY* **2013**, *216*, 4530–4541.

(285) Krause, A. F.; Winkler, A.; Duerr, V. *JOURNAL OF PHYSIOLOGY-PARIS* **2013**, *107*, 116–129.

(286) Zill, S. N.; Schmitz, J.; Chaudhry, S.; Bueschges, A. *JOURNAL OF NEUROPHYSIOLOGY* **2012**, *108*, 1453–1472.

(287) Pflueger, H.-J.; Field, L. H.; Nishino, H.; Currie, M. J. *JOURNAL OF INSECT PHYSIOLOGY* **2011**, *57*, 1420–1430.

(288) Simon, M. A.; Trimmer, B. A. *JOURNAL OF EXPERIMENTAL BIOLOGY* **2009**, *212*, 1021–1031.

(289) Hooper, S. L.; Guschlbauer, C.; Bluemel, M.; Rosenbaum, P.; Gruhn, M.; Akay, T.; Bueschges, A. *JOURNAL OF NEUROSCIENCE* **2009**, *29*, 4109–4119.

(290) Baessler, U.; Wolf, H.; Stein, W. *JOURNAL OF COMPARATIVE PHYSIOLOGY A-NEUROETHOLOGY SENSORY NEURAL AND BEHAVIORAL PHYSIOLOGY* **2007**, *193*, 1151–1168.

(291) Kanou, M.; Morita, S.; Matsuura, T.; Yamaguchi, T. *ZOOLOGICAL SCIENCE* **2007**, *24*, 945–952.

(292) Akay, T.; Ludwar, B. C.; Goeritz, M. L.; Schmitz, J.; Bueschges, A. *JOURNAL OF NEUROSCIENCE* **2007**, *27*, 3285–3294.

(293) Ausborn, J; Wolf, H; Mader, W; Kayser, H *JOURNAL OF EXPERIMENTAL BIOLOGY* **2005**, *208*, 4451–4466.

(294) Akay, T; Haehn, S; Schmitz, J; Buschges, A *JOURNAL OF NEUROPHYSIOLOGY* **2004**, *92*, 42–51.

(295) Noah, J.; Quimby, L; Frazier, S.; Zill, S. *JOURNAL OF COMPARATIVE PHYSIOLOGY A-NEUROETHOLOGY SENSORY NEURAL AND BEHAVIORAL PHYSIOLOGY* **2004**, *190*, 217–231.

(296) Blaesing, B; Cruse, H *JOURNAL OF EXPERIMENTAL BIOLOGY* **2004**, *207*, 1273–1286.

(297) Frantsevich, L; Gorb, S *ZOOLOGY* **2002**, *105*, 225–237.

(298) Akay, T; Bassler, U; Gerharz, P; Buschges, A *JOURNAL OF NEUROPHYSIOLOGY* **2001**, *85*, 594–604.

(299) Frazier, S.; Larsen, G.; Neff, D; Quimby, L; Carney, M; DiCaprio, R.; Zill, S. *JOURNAL OF COMPARATIVE PHYSIOLOGY A-SENSORY NEURAL AND BEHAVIORAL PHYSIOLOGY* **1999**, *185*, 157–172.

(300) Williams, D.; Shepherd, D *JOURNAL OF NEUROBIOLOGY* **1999**, *39*, 275–286.

(301) BASSLER, U *BIOLOGICAL CYBERNETICS* **1993**, *69*, 305–317.

(302) DEAN, J; SCHMITZ, J *PHYSIOLOGICAL ENTOMOLOGY* **1992**, *17*, 331–341.

(303) BASSLER, U; ROHRBACHER, J; KARG, G; BREUTEL, G *BIOLOGICAL CYBERNETICS* **1991**, *65*, 507–514.

(304) KARG, G; BREUTEL, G; BASSLER, U *BIOLOGICAL CYBERNETICS* **1991**, *64*, 329–335.

(305) Wohlfart, E.; Wolff, J. O.; Arzt, E.; Gorb, S. N. *JOURNAL OF EXPERIMENTAL BIOLOGY* **2014**, *217*, 222–224.

(306) Zarrouk, D.; Fearing, R. S. In *2013 IEEE INTERNATIONAL CONFERENCE ON ROBOTICS AND AUTOMATION (ICRA)*; IEEE International Conference on Robotics and Automation (ICRA), Karlsruhe, GERMANY, MAY 06-10, 2013, 2013, 2548–2553.

(307) Tajiri, R.; Misaki, K.; Yonemura, S.; Hayashi, S. *DEVELOPMENT* **2011**, *138*, 4621–4626.

(308) Prud'homme, B.; Minervino, C.; Hocine, M.; Cande, J. D.; Aouane, A.; Dufour, H. D.; Kassner, V. A.; Gompel, N. *NATURE* **2011**, *473*, 83–86.

(309) Sutton, G. P.; Burrows, M. *JOURNAL OF EXPERIMENTAL BIOLOGY* **2010**, *213*, 1406–1416.

(310) Toegel, J. P.; Wimmer, E. A.; Prpic, N.-M. *DEVELOPMENT GENES AND EVOLUTION* **2009**, *219*, 53–58.

(311) Harwood, J. F.; Vargas, R. I.; Carey, J. R. *ENTOMOLOGIA EXPERIMENTALIS ET APPLICATA* **2013**, *147*, 73–81.

(312) Mitten, E. K.; Jing, D.; Suzuki, Y. *INSECT BIOCHEMISTRY AND MOLECULAR BIOLOGY* **2012**, *42*, 854–864.

(313) Cruse, H; Dean, J; Kindermann, T; Schmitz, J; Schumm, M *ZEITSCHRIFT FUR NATURFORSCHUNG SECTION C-A JOURNAL OF BIOSCIENCES* **1998**, *53*, Workshop on Natural Organisms, Artificial Organisms, and Their Brains, UNIV BIELEFELD, BIELEFELD, GERMANY, MAR 08-12, 1998, 628–638.

(314) Manoonpong, P.; Parlitz, U.; Woergoetter, F. *FRONTIERS IN NEURAL CIRCUITS* **2013**, *7*, DOI: {10.3389/fncir.2013.00012}.

(315) Dirks, J.-H.; Taylor, D. *JOURNAL OF EXPERIMENTAL BIOLOGY* **2012**, *215*, 1502–1508.

(316) Ren, G.; Chen, W.; Kolodziejski, C.; Woergoetter, F.; Dasgupta, S.; Manoonpong, P. In *2012 IEEE/RSJ INTERNATIONAL CONFERENCE ON INTELLIGENT ROBOTS AND SYSTEMS (IROS)*; 25th IEEE\RSJ International Conference on Intelligent Robots and Systems (IROS), Algarve, PORTUGAL, OCT 07-12, 2012, 2012, 2756–2761.

(317) Rivera, A.; Perez, F.; Andres, J. *ODONATOLOGICA* **2002**, *31*, 117–128.

(318) NORMAN, A. *JOURNAL OF EXPERIMENTAL BIOLOGY* **1995**, *198*, 1341–1350.

(319) Guffey, C. *Journal of Arachnology* **1998**, 296–302.